

https://dspace.org/

Review of geotechnical challenges experienced within a weak kimberlite zone: a case study at Cullinan diamond mine

Banjwa, Phumza

2022
https://hdl.handle.net/10539/35733

Downloaded from a DSpace repository. https://dspace.org/

School of Mining Engineering



UNIVERSITY OF THE
WITWATERSRAND,
JOHANNESBURG

REVIEW OF GEOTECHNICAL CHALLENGES EXPERIENCED WITHIN A WEAK KIMBERLITE ZONE – A CASE STUDY AT CULLINAN DIAMOND MINE

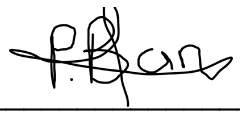
Phumza Banjwa

A research report submitted to the Faculty of Engineering and the Built Environment, University of the Witwatersrand, Johannesburg, in partial fulfilment of the requirements for the degree of Master of Science in Engineering.

Johannesburg, 2022

DECLARATION

I declare that this report is my own, unaided work. I have read the University Policy on Plagiarism and hereby confirm that no plagiarism exists in this report. I also confirm that there is no copying nor is there any copyright infringement. I willingly submit to any investigation in this regard by the School of Mining Engineering and I undertake to abide by the decision of any such investigation.



16/11/2022

Signature of Candidate

Date

ABSTRACT

The centenary cut is a mechanised block cave with an advanced undercut at Cullinan Diamond Mine. About 25% of the C-Cut block was at risk of not being recoverable following an unplanned pillar on uncaved material that was left on the initiation horizon (undercut). The layout design had to be modified leading to increased drawpoint spacing in an attempt to maintain stable pillars on the extraction horizon. Uncertainty on drawpoint interaction triggered the need for research to be conducted. The consequences of poor draw interaction are often severe and irreversible, evident through early dilution entry and point loading on the extraction level. The research examined the deformation rates experienced as a result of high stresses exerted by the uncaved material on the undercut horizon. Monitoring methods included the use of ZEB-HORIZON 3D mobile scanner, drone, borehole camera and observations using laser technology. In addition, a finite difference model (FLAC3D) was employed to assess stability of a weak zone on the extraction horizon. Preconditioning by blast was one of the tools employed to initiate caving of the ore material around the weakzone or the unplanned pillar. The PC/BC model was used to understand the interaction of the drawzones in the area where the spacing has been increased. The finding of the investigation showed that there was little interaction (the cave propagates upwards in silos leaving solid rock between the drawbells) which agreed with the FLAC3D results**.** The deformation rates at 75% undercutting were influenced by the geometry of the footprint and the strength of the rock mass relative to the abutment

stresses at the end construction phase. The deformation rates from the inelastic model compared well with underground measurements though slightly underestimated. Empirical methods suggest that drawpoints should not be spaced 24 m apart which is also greater than 1.5 times the width of the drawzone even in weaker rock types where local instability prevails.

In memory of my loving mother Nomangesi Banjwa. We miss you dearly Makhulu.

ACKNOWLEDGMENTS

I would like to extend my utmost gratitude to the people who have supported me, cheering me on in difficult times. The following individuals/companies have created the opportunity to conduct this research:

- Professor Bryan Watson as supervisor of this research study.
- Mr. Kevin Le Bron and MLB Consulting for their assistance with inelastic modelling.
- Cullinan Diamond Mine for allowing me to undertake this study and providing the necessary tools and funding and to my former colleagues for the never-ending assistance.
- Katinka Cartes and Groundwork Consulting for assistance with the FLAC3D software and the *ITASCA* key.
- My family and friends who allowed me time away from them while I completed this research.

TABLE OF CONTENTS

DECLARATION i

ABSTRACT ii

ACKNOWLEDGMENTS v

LIST OF FIGURES ix

LIST OF TABLES xiv

APPENDIX LIST OF FIGURES xiv

APPENDIX LIST OF TABLES xiv

LIST OF SYMBOLS xvi

1. INTRODUCTION 1

    1.1 Mine Setting 6

    1.2 Regional Geology 7

    1.3 Local Geology 10

    1.4 Brief history of blocks above the C-Cut 13

    1.5 Problem Statement 17

    1.6 Justification for Research 20

    1.7 Research Methods 21

    1.8 Purpose and Objectives 22

    1.9 Sources of Data 23

    1.10 Structure of the Research Report 24

2. LITERATURE REVIEW 25

2.1 Introduction 25

2.2 Drawzone interaction and drawpoint spacing 28

2.3 Drawpoint Spacing 31

2.4 Preconditioning 32

2.5 Implications of spacing drawpoints too far apart 33

2.6 PC/BC model 33

2.7 Recompaction Theory 34

2.8 Rock Mass Strength 35

2.8.1 Hoek-Brown Failure Criterion 35

2.8.2 Mohr-Coulomb Failure Criterion 37

3. BECK ENGINEERING METHOD OF ANALYSING THE STABILITY OF DRAWPOINTS AND PILLARS 38

3.1 Modelling the Old Collapses - AUC Results 40

3.2 Prediction of Collapse - C-Cut Results (Undercut) 43

3.3 Prediction of Collapse - C-Cut Results (Extraction Horizon) 45

4. CAVE INITIATION USING PRECONDITIONING AND RELATED UNDERGROUND MONITORING 47

4.1 Preconditioning 48

4.1.1 Drone Footage 52

4.1.2 Review of the PC/BC Input Parameters 54

4.1.3 Recompaction at the Weakzone 57

4.2 Zeb Laser Scanner Results 58

5. STABILITY ASSESSMENT USING THE FLAC3D NUMERICAL MODELLING SOFTWARE 66

5.1 Strength Criterion 68

5.2 Failure Criterion 68

5.3 Model set-up 68

5.4 FLAC3D Results and Analysis 75

6. DISCUSSION 91

7. CONCLUSION 94

8. RECOMMENDATIONS 97

9. SUGGESTIONS FOR FURTHER WORK 97

REFERENCES 98

APPENDICES 105

LIST OF FIGURES

Figure 1.1: Plan view showing the extraction level layouts as widely used in BC 5

Figure 1.2: Mine Locality 6

Figure 1.3: Top view of the mining (green) and farm boundary at which the Mine is situated 7

Figure 1.4: Illustrating the regional geology surrounding CDM 9

Figure 1.5: Litho-stratigraphy of the Pretoria group, Transvaal supergroup 10

Figure 1.6: Example of the various Cullinan country rock and kimberlite rock types A: Transvaal Metasediment B: Bushveld Igneous Complex Gabbro-norite C: Waterberg Quartzite D: 1060 Pale Grey kimberlite E: Black Transitional kimberlite and F: Calcite Dyke. 12

Figure 1.7: Plan (A) and 3D section (B) view of geological kimberlite boundaries 13

Figure 1.8: Mining blocks exploited at CDM 14

Figure 1.9: Illustrating the slot initiation position and the face shape for the undercut 17

Figure 1.10: A not to scale Illustration showing block caving with specific focus on the collapsed area at the undercut level 19

Figure 2.1: The draw and movement ellipsoids 27

Figure 2.2: Classical approach to the flow ellipsoid concept 29

Figure 2.3: Cave Draw Ellipsoid 30

Figure 2.4: Excessive drawpoint spacing with non-overlapping zones and interactive draw zones 32

Figure 3.1: Showing rock mass damage at the extraction horizon of the AUC block cave 38

Figure 3.2: Prediction of failure using Abaqus 40

Figure 3.3: Illustrating rock mass damage at AUC block cave (the grey area represents the undercut front – retreated zone) 43

Figure 3.4: Rock mass damage at 75% undercutting 44

Figure 3.5: Rock mass damage on the extraction horizon at (75% undercutting) 46

Figure 4.1: Section view showing drilled holes and sequence of mining (Not drawn to scale) 48

Figure 4.2: Depicting the grout holes during the precondition process 50

Figure 4.3: Isometric view illustrating the pillar left in the undercut in relation to the extraction level with drilled holes depicted 50

Figure 4.4: Schematic illustration of the cave back and the blast conditioned section of the undercut 51

Figure 4.5: Illustrating the ring designs (a) 824L Undercut (b) 839L Extraction horizon 52

Figure 4.6: View of draw bell void scans showing a lack of interaction across the major apex 53

Figure 4.7: View of draw bell void scans showing a lack of interaction across the minor apex (between DB90 & DB77) 53

Figure 4.8: An example comparison of drawzone interaction size between DP spaced 16 m and those spaced 24 m (plan view) 55

Figure 4.9: Illustrating the tonnes extracted at the C-Cut footprint and the HOD achieved at the NE corner..... 56

Figure 4.10: Illustrating drilled borehole positions and related footage 57

Figure 4.11: Geoslam Zeb Horizon 3D Instrumentation 59

Figure 4.12: Sections showing sidewall bulging from the Mobile scanner and Images taken underground around the Pillar/1060 Grey Kimberlite area 60

Figure 4.13: Showing T41 rock mass damage as measured by the Zeb Horizon scanner and underground observations 61

Figure 4.14: Showing T36 rock mass damage and underground tunnel closure 62

Figure 4.15: An example of the weekly scans conducted at the weak zone 63

Figure 4.16: Depicting tunnel convergence at T41 and the correlation to the activity taking place..... 64

Figure 4.17: Depicting tunnel convergence at T36 and the correlation to the activity taking place..... 64

Figure 4.18: Comparison between the Zeb Horizon Scanner and Laser Technology 65

Figure 5.1: Snapshot from the FLAC3D Software illustrating an example of the Extrude file 70

Figure 5.2: Showing the schematic diagram of the boundary conditions and model set up - note that the open pit excavation was included in the model and was simulated as a separate mining step between the pre-mining phase, and the underground development phase 71

Figure 5.3: Showing an Illustration of the Hosting Rock and different Kimberlite Facies 72

Figure 5.4: Illustrating Sequencing of the Weakzone 73

Figure 5.5: Snapshot from FLAC3D model showing excavations relative to each other and relative to the undercut – note that 18 mining steps were scheduled in the FLAC3D model to simulate the development sequence and cave retreat 75

Figure 5.6: showing increasing stress with depth 76

Figure 5.7: Illustrating mining steps and an increasing cave propagation with each step (ideal/strong kimberlite throughout the footprint of the C-Cut block cave) 77

Figure 5.8: Illustrating damage at the weakzone (mining step 5 of the C-Cut cave still on strong/Black kimberlite) 78

Figure 5.9: Showing shear failure on the extraction level at 75% undercutting (MS6) 79

Figure 5.10: Illustrating and unbalanced force for MS1 to MS4 80

Figure 5.11: Illustrating unbalanced forces for MS5 to MS7 81

Figure 5.12: Displacement depicted at the weak zone for MS1 and MS2 82

Figure 5.13: Showing contours of displacement for MS3 and MS4 for the weak zone..... 83

Figure 5.14: High displacement at the end construction phase (MS6)..... 84

Figure 5.15*:* Contours of displacement – Long section along T41 Showing X/Cuts at the weak zone (MS1 and MS2) 85

Figure 5.16: Contours of displacement Long section along T41 at the weak zone (MS3 and MS4) 85

Figure 5.17: Contours of displacement (Left – Long section along T41 at the weak zone, Right – section along X/Cuts showing Tunnels)..... 86

Figure 5.18: Depicting contours of displacement – Long section along T41 at MS6 87

Figure 5.19: Depicting contour of displacement – Long section along T41 at MS7 89

Figure 5.20: Deformation Measured using FLAC3D 90

Figure 6.1: Deformation Results Comparing underground measurements and FLAC3D Results. 92

LIST OF TABLES

Table 1.1: Advantages and disadvantages of the different undercutting strategies 3

Table 5.1: FLAC3D input parameters 67

Table 5.2: Section Along X/cuts Showing Tunnels (T32, T36 & T41) 88

Table 5.3: Section Along the T41 Showing X/Cuts (DP89, DP90 & T91) 88

APPENDIX LIST OF FIGURES

Figure B-1: Ring Designs for the extraction horizon weak zone 106

Figure C-1: Scan Results for Individual Tunnels 112

Figure C-2: Laser technology results for individual tunnels..... 113

Figure E-1: Presence of water at the weak zone 115

Figure E-2:Tunnel conditions showing extensive localized closure..... 116

APPENDIX LIST OF TABLES

Table A-1: Revenue locked up in the weak zone drawpoints..... 105

Table C-1: Manual Laser technology results for T41 108

Table C-2: Manual Laser technology cumulative results for T41 109

Table C-3: Manual Laser technology results for T36 110

Table C-4: Manual Laser technology cumulative results for T36 111

Table D-1: CDM RMR Database..... 114

Table F-1 : Grey Kimberlite..... 117

Table F-2 : Brown Kimberlite..... 118

Table F-3 : Metasediment Host Rock..... 119

Table F-4: Black Kimberlite..... 120

LIST OF SYMBOLS

σ_{ci}	Intact Rock Uniaxial Compressive Strength (MPa)
σ_1	Major Principal Stress (MPa)
σ_2	Intermediate Principal Stress (MPa)
σ_3	Minor Principal Stress (MPa)
E	Modulus of Elasticity (GPa)
v	Poisson's ratio
o	Degrees
ϕ	Angle of friction
c	Cohesion (MPa)
m_b	Parameter for rock mass
m_i, S	Hoek-Brown Parameters for intact rock
a_N, b_N	Major and Minor Semi-axes of the Ellipsoid of Motion
ε	Eccentricity of an Ellipsoid
τ	Shear strength of a rock (MPa)

1. INTRODUCTION

Block caving (BC) has been used for many years in the mining industry as a preferred mass mining method that is capable of maximising net present value from large, low-grade orebodies (Woo, et.al., 2013). In this mining method, drilling and explosives cost are minimised in that caving of rock material is driven by gravity with the assistance of stresses and geological structures. Compared to other mining methods, BC can be regarded as being capital intensive due to the extensive development that is required before production commences.

Butcher (1999) states that the correct size and spacing of the draw points is essential for efficient extraction. Stability in the draw horizon is also essential for the full life of a block if the BC operation is to be successful. Some of the features that make a BC are described below:

- Draw horizon/extraction level/production level which is characterised by draw points, draw bells, production drifts and ore passes from which the caved ore is drawn and transported
- An undercut level where the cave initiates. The main purpose of the undercut is to create a void above the draw horizon to induce the caving process (Butcher, 1999)
- Draw bells are developed from the production level to connect to the undercut level such that caved ore may be collected and

transported to ore passes, crushers conveyor belts and ultimately to the plant located on surface.

The undercut may be created using three undercutting strategies namely- post-, pre-, and advance undercutting from which other added variants can arise. Brown (2003) describes each method with its advantages and disadvantages as shown in Table 1.1. The strategy chosen by the mine (advanced undercut) has resulted in rehabilitation requirements on the extraction level as well as cave propagation challenges.

Table 1.1: Advantages and disadvantages of the different undercutting strategies

Advantages	**Disadvantages**
Pre – Undercut	
1. Extraction level is developed in a de-stressed environment	Need for a separate ore handling facility on the undercut level
2. Undercut can be mined independently of the extraction level	Draw bells are developed into broken ore on the undercut level
3. Lower support requirements than post undercut	Possible re-compaction of blasted ore on the undercut level
	High stress remnants (resulting from re-compaction)
	Draw point hang-ups (resulting from re-compaction)
Advance – Undercut	
1. Extraction level damage is reduced compared to post undercut	Cave comes into production later than in post undercut
2. The cave is brought into production much quicker than in pre-undercut	Escalated rehabilitation costs associated with the extraction level
Post – undercut	
1. Blocks are brought into production much quicker than the above-mentioned strategies	Not suitable for high stressed environments. Butcher (2000a) suggests that at depths greater than 500 m, the use of post undercut should be critically assessed
2. No separate ore handling facility required on the undercut level	
3. Very little possibility of ore re-compaction	

In the pre-undercut strategy, the undercut is mined ahead of the extraction level development. This means that all development including production drifts, draw point cross cuts/ stubs and draw bells are mined in de-stressed ground. Two variants of this method exist, one where the undercut is completed before any development on the extraction level and the other carried out with lead/lags. In most cases the latter maintains the 45-degree rule where the lagging of the extraction level development from the undercut is the separation distance between the two levels.

Where the advanced undercut method is used, the undercut level is drilled and blasted above a partially developed extraction level (production drifts only or with draw point stubs). However, draw bells are always developed in de-stressed ground lagging behind the undercut and adhering to the 45-degree rules.

Post undercut is also referred to as the conventional undercutting strategy where the drilling and blasting of the undercut takes place after completing the development of the underlying extraction level. In this strategy the draw bells are drilled and blasted in stressed ground and are ready to receive broken rock from the undercut. The extraction level comprises of several layouts widely used in the mining industry and these are described below and shown in Figure 1.1:

- Henderson – The opposite drawpoints are in line but inclined to the production drift. The minor apices are in line and at right angles to the major apex.
- El Teniente – The drawpoint drifts/stubs are developed in straight lines and 60° to the production drifts. The minor apices are inclined relative to the major apices.
- Herringbone – In this layout, the minor apices are in line with each other and at right angles to the major apex.
- Offset herringbone – This is a variation of the herringbone extraction level layout with opposite drawpoints staggered. Compared to the original Herringbone design, this variation results in improved stability conditions.

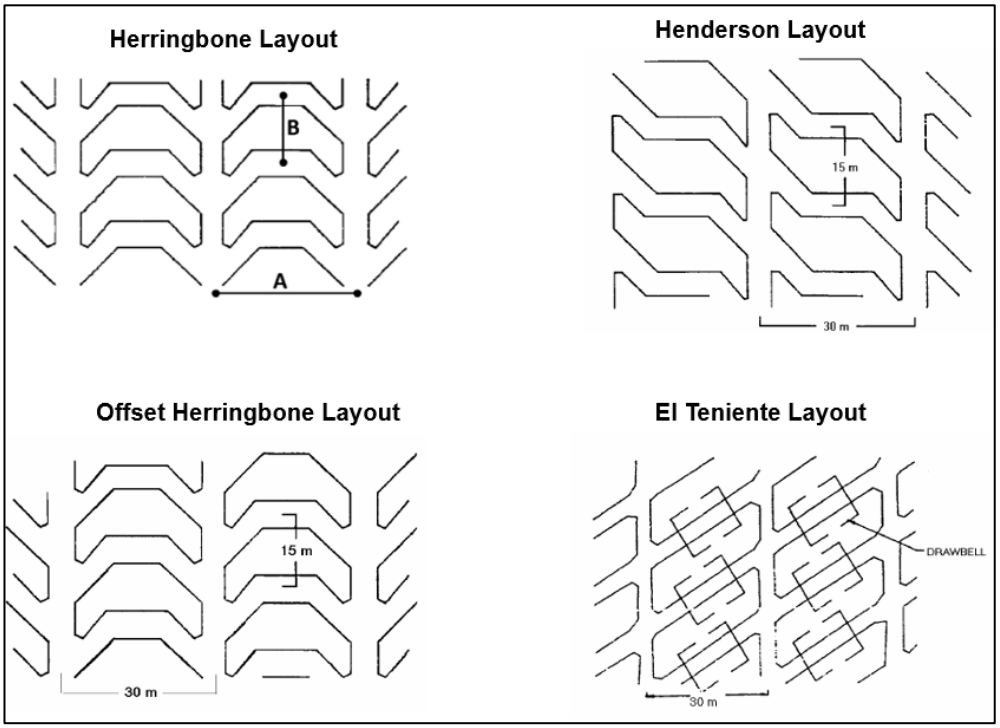


Figure 1.1: Plan view showing the extraction level layouts as widely used in BC (Ugarte et al, 2017)

1.1 Mine Setting

The Cullinan Diamond Mine (CDM) is an underground BC mine situated 40 km east of Pretoria in Gauteng Province, South Africa (Figures 1.2 and 1.3). CDM is known as a source of large, rare blue and high-quality diamonds. The mine started operating in 1903 when it was still called Premier mine. Petra Diamonds Limited purchased the mine from De Beers Consolidated Mines in 2008. The current life of mine extends to 2030, however, new developments for further prospective blocks are currently underway, which will take the life of mine beyond 2030. The mine's output currently operates at 4.0 Mt as of Financial Year (FY) 2020 with an annual target of 5.2Mt when the mine is in full production.

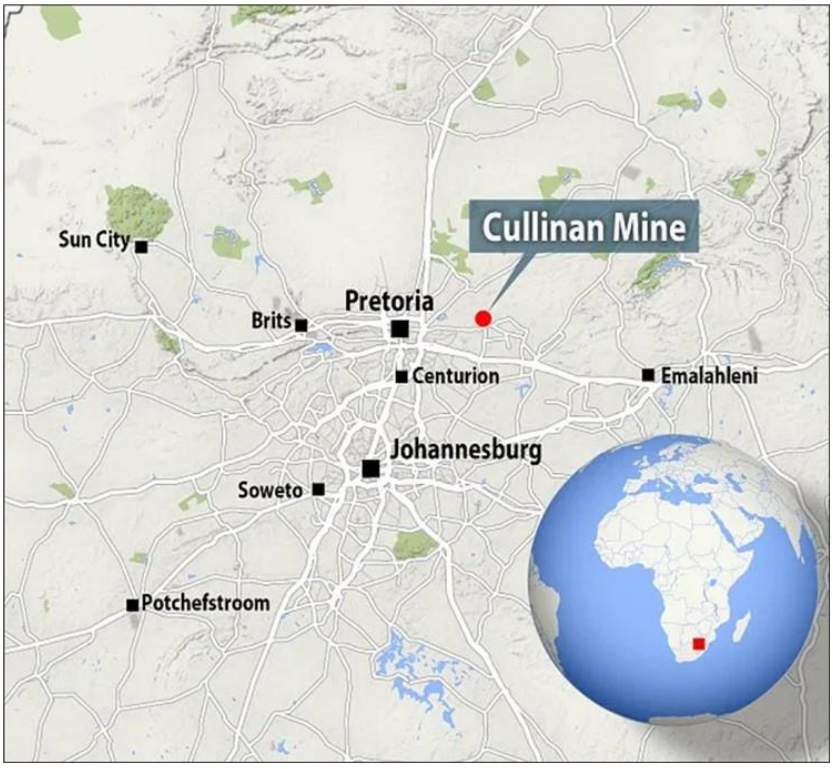


Figure 1.2: Mine Locality (CDM, 2005)

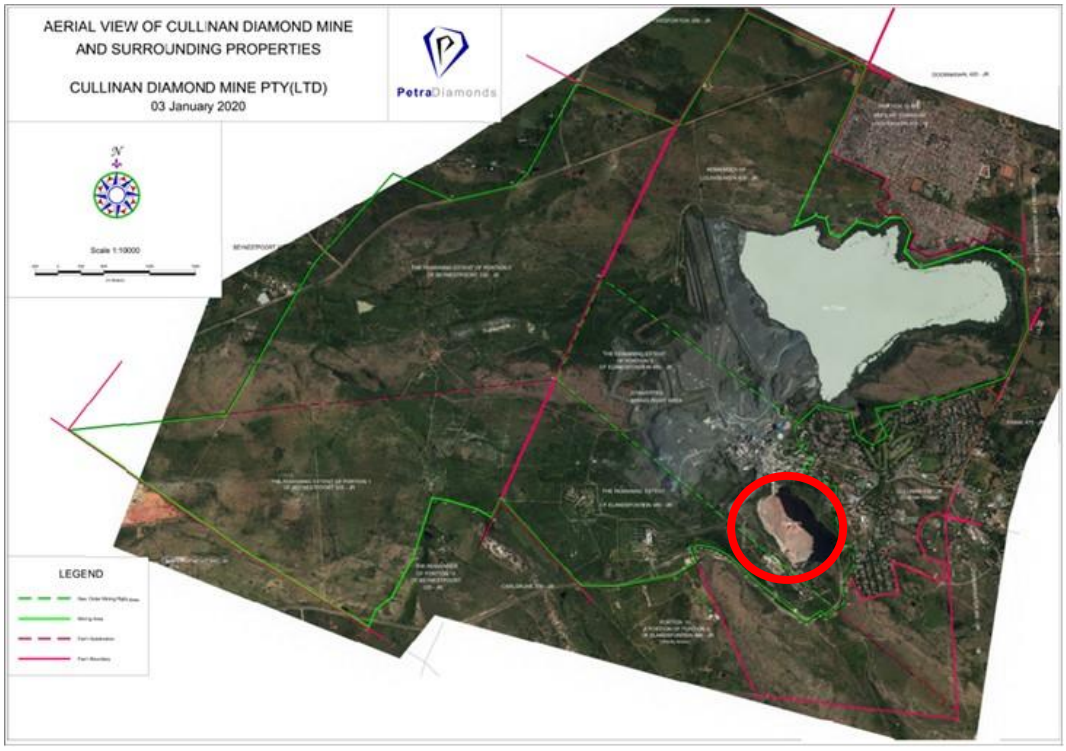


Figure 1.3: Top view of the mining (green) and farm boundary at which the Mine is situated (Code of Practice, 2019)

1.2 Regional Geology

CDM's Kimberlite pipe is the largest known intrusion in South Africa and one of the eleven kimberlite diatremes located in the Cullinan-Rayton region. The Cullinan pipe has three types of kimberlites, namely brown, grey, and black (hyperbyssal). The Cullinan kimberlite pipe is situated within the stable 3-billion-year-old Kaap-Vaal Craton (Anhaeusser & Burger, 1982). Van Zyl (1973, cited in COP 2019) describes the deposition and ages for the subgroups found within and surrounding the Cullinan pipe. The pipe intruded through an estimated 300 m of 1700 million-year-old sediments of the Waterberg Supergroup (now eroded away) overlying sediments of the Transvaal Supergroup (Rayton Formation). The Transvaal Supergroup sediments were originally laid down in a shallow marine environment 2200

million years ago. The Transvaal Supergroup sediments were intruded 2000 million years ago by a 350 m thick felsite and numerous norite sills ranging in thickness from 2 m to 300 m.

Bartlett, 1998 describes the country rock surrounding the Cullinan Kimberlite pipe. The norite sills have been correlated with the lower part of the critical zone of the Bushveld Complex. The intrusion of the norite sills has resulted in varying degrees of metamorphism of the sediments into which they were intruded. Below 800 m depth, the geological column is made up of norite sills ranging in thickness from 5 m to 100 m. The sills have intruded into sediments of the Rayton Formation. The Rayton Formation consists of hard quartzites intercalated with metasediments, which include carbonates, cherts, and mudstone horizons (Figure 1.4).

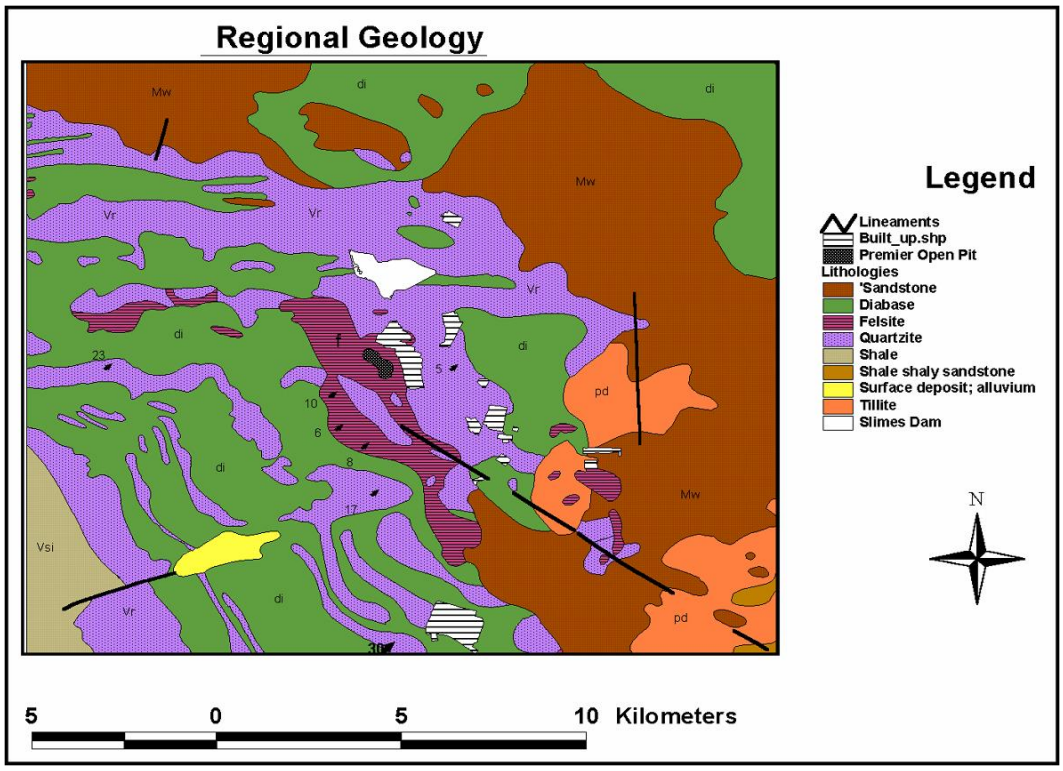


Figure 1.4: Illustrating the regional geology surrounding CDM (Code of Practice, 2019)

Geologically, the region has been subjected to little tectonic activity since the intrusion of the pipe with neither folding nor faulting affecting the orebody.

The Cullinan pipe has an elongated, kidney-shaped exposure on surface with the east-west axis 880 m long and the north-south axis 450 m long at maximum. The pipe had a surface area of 32 ha decreasing progressively to 22 ha at 500 m below surface and 12.9 ha at 1 082 m below surface. The geology is typical of the diatreme zone of a kimberlite pipe. The geological model shows that it remains consistent with depth and shows little evidence of the geological complexities that characterise a root zone. The contacts between the pipe and surrounding country rock are sharp and dip inwards

at an average angle of 85°, the pipe decreases in size by 6.9% for every 100 m of increasing depth (Code of Practice, 2019). The geological sequence of the surrounding country rock is shown is Figure 1.5.

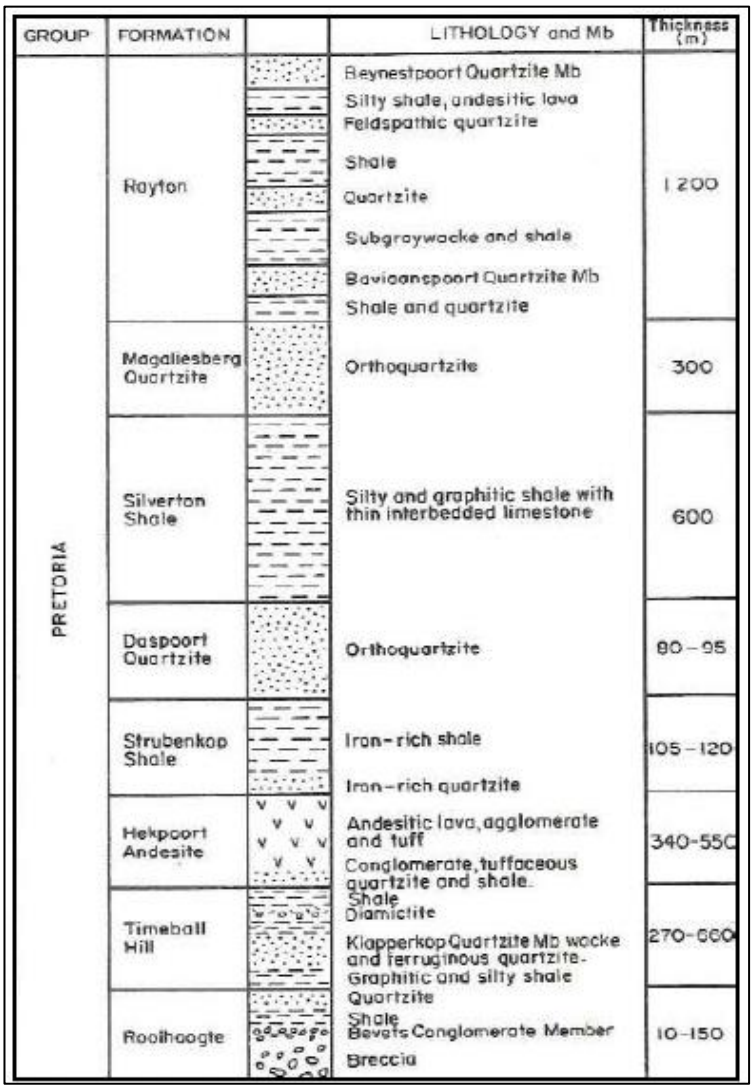


Figure 1.5: Litho-stratigraphy of the Pretoria group, Transvaal supergroup (Code of Practice, 2019)

1.3 Local Geology

The kimberlite pipe is comprised of three types of kimberlites, namely, Grey, Brown, and black kimberlite. The project is focused on 1060 pale grey kimberlite described in this section. The 1060 Pale Grey kimberlite facie

(1060 PG) was first identified on 1010 level, in the Cullinan kimberlite and, is sub-divided into two rock-variants. The first variant of the 1060 PG is characterized as a predominantly light brown to greyish in colour, medium to coarse grained, olivine rich, volcaniclastic kimberlite. This kimberlite phase is characterized by sub-rounded, mostly microcrystic, serpentinized olivine xenocryts, which often makes up above 40% of a rock specimen. However, in some instances, it can be as much as 70% of a sample. In most cases, olivine has been completely serpentinized into montmorillonite clay. Other mantle minerals observed include fresh to altered, sub-rounded chrome diopside, with kelyphitic rims; sub-rounded ilmenite and fresh to altered orthopyroxene. Garnets are rare. Country rock xenoliths observed include Bushveld Igneous Complex norite and metasediments of the Transvaal Supergroup, including quartzite and carbonaceous shale. All these components are set in medium to fine grained serpentinized pale greenish-grey matrix. Contacts with other kimberlite phases is gradational over about a 1 m zone. The rock is characterized by sub-vertical joint sets (four joint sets), and very minor sub-horizontal features. There are two variants of the rock type. The first variant swells and disintegrates when immersed in water. Internal experiments show that a 50 mm diameter sample will completely disintegrate within about 12 hours, after having been immersed in water. The second variant is similar, except most lithic xenoliths have been altered into calcsilicate xenoliths and, all components, i.e., xenoliths, xenocrysts and phenocrysts are set in a medium to fine grained pale greenish-grey matrix. The second variant is usually more

competent than the first variant. The 1060 PG kimberlite (Figure 1.6) is a diatreme facies unit which is sporadically distributed throughout the Cullinan kimberlite. The unit is often hosted as a mega xenolith in various kimberlite units of the Cullinan kimberlite.



Figure 1.6: Example of the various Cullinan country rock and kimberlite rock types A: Transvaal Metasediment B: Bushveld Igneous Complex Gabbro-norite C: Waterberg Quartzite D: 1060 Pale Grey kimberlite E: Black Transitional kimberlite and F: Calcite Dyke.

The plan view and 3D model of the geology that forms the CDM kimberlite pipe is shown in Figure 1.7. The eastern side of the block is predominantly characterized by the Brown Kimberlite while the centre and west are characterized by Grey waste and grey kimberlite, respectively. The 1060 PG Kimberlite is indicated on the plan view in Figure 1.7 found within the Grey kimberlite on the Northeast corner of the C-Cut footprint.

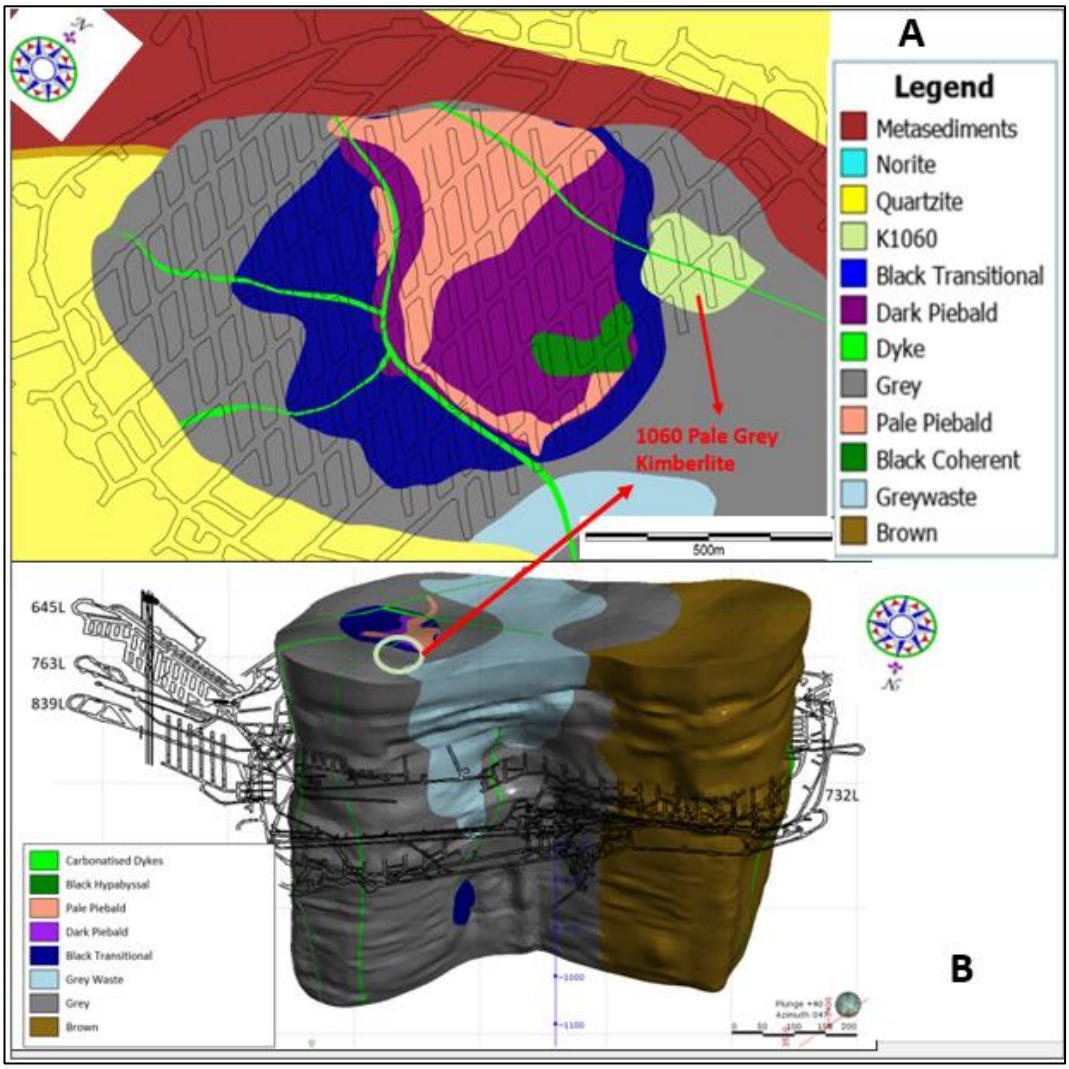


Figure 1.7: Plan (A) and 3D section (B) view of geological kimberlite boundaries (Code of Practice, 2019)

1.4 Brief history of blocks above the C-Cut

CDM utilises a BC mining method with an advance undercutting strategy. The kimberlite orebody is currently exploited by mining blocks CC1 - East (a sub-level cave nearing depletion) and the centenary cut (C-cut) block cave that recently came to full production (Figure 1.8).

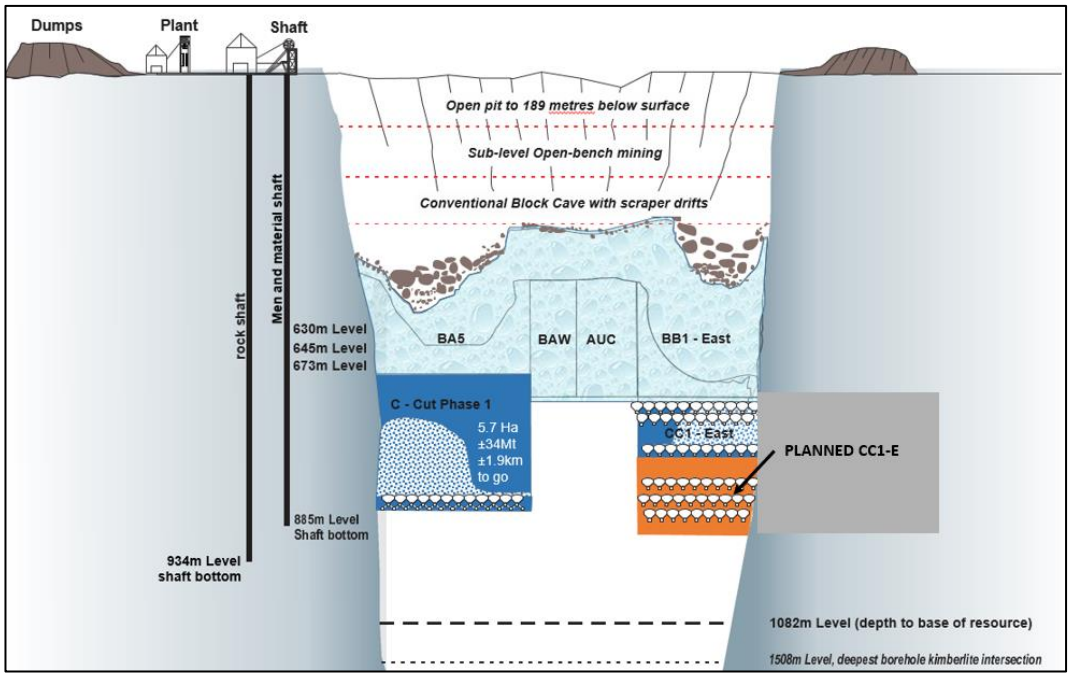


Figure 1.8: Mining blocks exploited at CDM

The project was conducted at CDM's C-Cut. The production level is situated 839 m below surface while the undercut level is situated 15 m above it (824L). The extraction level utilizes an El Teniente layout which is more stable than the Herringbone or Henderson layouts (Brown, 2003). Draw bells (DB) connect the extraction and undercut level and serve as a place for caving rock to fall into. Soon, a 3-level sublevel cave will come into production (shown as the orange block in Figure 1.8), and development into this block is currently underway.

The BB1E and AUC mining blocks (Figure 1.8) that lie within the soft eastern Brown and Grey kimberlites, respectively, experienced massive tunnel failures early in their lives and a recovery level on 747 mbs had to be established to recover the remaining BB1 - East resource tons.

The BA5 and BB1 - East blocks (Figure 1.8) were changed from post-undercut panel retreat caves to advance undercut block caves to reduce the tunnel deformation and failures caused by high abutment stresses on the production level infrastructure, which was developed and constructed ahead of the undercut face. Tukker et al (2016) state that “The BA5 block cave can be considered a success, with high extractions achieved, especially in the hard western Hypabyssal Kimberlite, albeit with significant tunnel failures in the softer Grey Kimberlite zones close to the contact”. Localised stress failures were encountered in the block and maximum recovery was not realised.

The rock mass conditions of the grey kimberlite close to the southern contact (at the BA5 block) were very poor with Mining Rock Mass Ratings (MRMR) below 35. The draw bell layout was adjusted and the first line of draw bells along the immediate southern contact zone was removed. As a result, large wedges formed along the contact zones causing high static loads on the weak contacts that caused production tunnel collapses. The second failure followed shortly after the undercut face shape was changed from a V-shape to a diagonal shape resulting in several tunnels being located close to the pivot point for a few months (Holder et al, 2020 pg. 9). The pivot point was located close to the eastern internal contact of the BA5 block with poor ground condition prevalent. The overall extraction from the BA5 block was high, but the ventilation level on the 645-elevation had to be converted to a retreat level to recover the areas impacted by the two failures.

The list of changes that were made to the original design of the C-Cut undercut because of the failures experienced in the upper block/panel caves is as follows (illustrated in Figure 1.9):

- The C-Cut block cave utilised an advanced undercut as opposed to post-undercut strategy used in upper blocks.

- The undercut initiation point was positioned in the south-west within the poorer rock mass zone to advance the undercut with a diagonal face from “weak” to “strong” rock mass. The diagonal face-shape was however planned to advance during the final stages through the north-eastern internal contact zone where the C-Cut failure eventually occurred.

- The diagonal face-shape was maintained throughout with strict adherence to advance rates and lead-lags. The traditional advance rates of 3.0 m - 4.5 m per month was increased to 6.0 m - 10 m per month.

- The mapping of the local geology and structures during development to obtain more detailed information is paramount to revising execution strategies.

- The management of internal kimberlite contacts during the undercutting and draw bell construction phase required detailed strategies specific to these zones.

- Provided sufficient space between production level and ground handling elevation to potentially have a recovery level should the need arise.

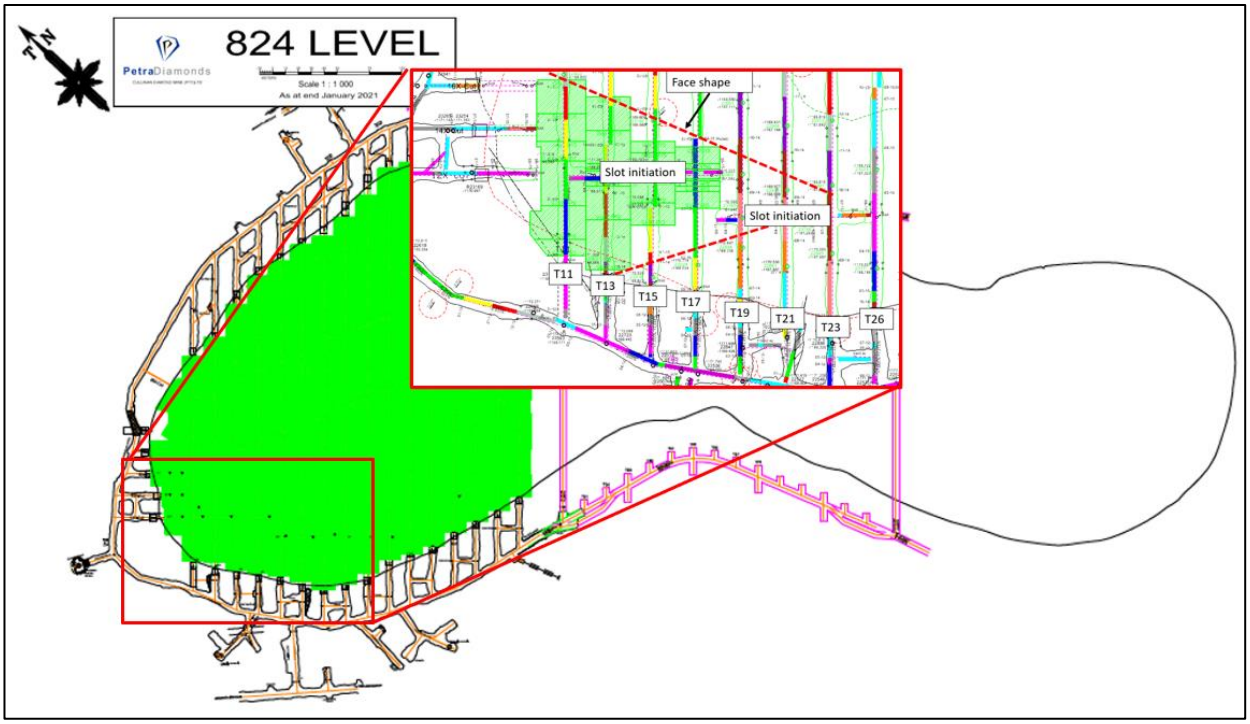


Figure 1.9: Illustrating the slot initiation position and the face shape for the undercut (after MicroStation Mine Software)

1.5 Problem Statement

Arguably, the main goal for a mining company is to realise profit through maximum ore recovery and this must be done safely. In a functional mine,

several departments give service to the production team through their respective expertise. The Geotechnical team at CDM is one such department. This research will focus on the contribution that the Geotechnical personnel had to the success of the Centenary cut (C-Cut) block cave. Of course, the overall success came with geotechnical challenges which are discussed in this report.

The end stage construction phase in an advanced undercutting strategy block cave and weak/soft kimberlite is a unique phenomenon and is not well understood. The deformation rates at CDM have not been well quantified. As the pillar passes through critical minimum dimensions, stress levels and stress fracturing tend to increase. This phenomenon was particularly noticeable in the C-Cut as the block approached completion (both in the undercut and construction of draw bells in the extraction level).

The original geotechnical model did not recognise the weak zone due to the fact that boreholes drilled during the pre-feasibility study did not intersect the weak zone. During the development of the undercut and extraction level, the weak zone was mapped and deemed negligible. However, as the abutment stresses moved closer to the weak zone, the need to update the geological model was recognised and the extent of the affected area due to the weak zone increased.

In general, financial implications are realised when the extraction level draw bell construction cannot be completed due to instabilities brought about by

remnants/stubs point loading into the extraction level. The risk of leaving ore locked up in this last 25% would mean the planned tonnes of approximately 5.2 million Tonnes Per Annum (mtpa) could not be met and additionally this problem could persist into successive blocks below the C-Cut. The immediate dilemma was that the rehabilitation of the Northeast (NE) corner was too costly.

This research reviews the type of mining in hindsight, providing an understanding of what went wrong and recommendations for similar mining conditions elsewhere.

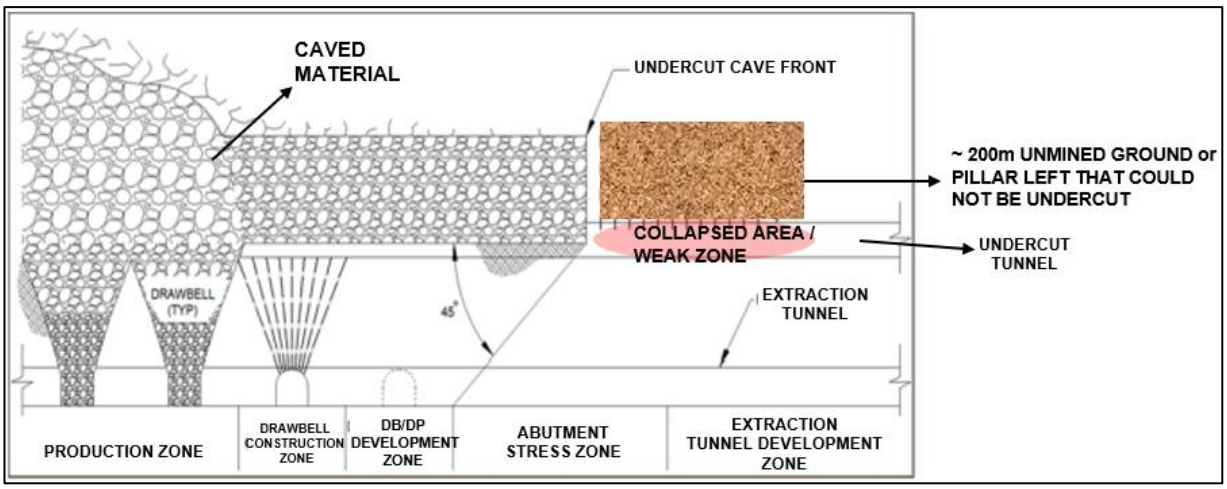


Figure 1.10: A not to scale Illustration showing block caving with specific focus on the collapsed area at the undercut level (after van As, 2017)

1.6 Justification for Research

During the retreat of the last 20-25% of the undercut, elevated stress levels led to a collapse of some of the tunnels such that a significantly large pillar was left unmined. As a remedy, draw point spacing was altered on the production level from 16 m to 24 m. Research was conducted to determine whether there would be draw interaction between drawpoints with the increase in spacing.

Although geotechnical modelling indicated better results compared to older mined out areas, the undercut (and subsequently the extraction horizon) was predicted to suffer stability problems near the end of the life of that level. Such stability problems would be primarily because of the unfavourable geometry of the pipe (orebody footprint). Many factors play a role in the stability of the remaining pillar as completion of the construction phase on the undercut level is approached. These factors may include but are not limited to:

- Geometry between the undercutting mining front and the pipe boundary
- Influence of geological structures
- Expected stress levels (abutment stresses) and
- Implementation of support standards as per the Code of Practice (COP)

1.7 Research Methods

A literature survey was undertaken to give an understanding of how rocks flow in a BC and how that affects the spacing of drawpoints. A trade-off is critical in BC as either spacing drawpoints too far or too close to each other have detrimental effects.

The effects of increasing drawpoint spacing from 16 m to 24 m was analysed and evaluated using a 3D finite difference code (FLAC3D). Practically, underground tunnels, Drawpoints (DPs) & Drawbells (DBs) were monitored using drones, Zeb Horizon scanners and laser technology in conjunction with borehole cameras in order to confirm the possibility of ore re-compaction.

The results from the numerical analysis will be analysed and compared to what was experienced underground with practical evidence of the effects spacing has on weak kimberlite zones. Below is a summary of the methodology followed:

- Review of the current PC/BC model to check for drawzone interaction.
- The use of the Zeb Horizon scanner to measure deformation rates with an accuracy of 10 mm – 30 mm. The scan was conducted over a period of 8 months on a weekly basis.

- Void scanning using drones was conducted after every newly open draw bell particularly when adjacent draw bells were believed to not have connected from the blasting activities.
- Borehole cameras were utilised to assess the possibility of re-compaction and/or lack of drawzone interaction.
- Numerical modelling was utilised to check the stability of tunnels after changing DP spacing to 24m in the weak 1060 PG kimberlite.
- The input parameters used by Beck Engineering in the global geotechnical model were accepted and adopted for use in this report.
- Damage mapping done on upper block caves was also used to calibrate the numerical models (also adopted from Beck Engineering).
- Rock mass classification was carried out using different methods such as the Geomechanics classification system (RMR) and Geological Strength Index (GSI).

1.8 Purpose and Objectives

The uncaved material left on the undercut level comprised of 1060 PG kimberlite which is one of the weakest kimberlites. This material was expected to bring about stability challenges at the extraction level. Throughout the footprint of the C-Cut block, draw points are spaced 16 m apart centre to centre. It was evident that the spacing warranted a review in the weak kimberlite material to maintain stability. It was decided that the spacing would be revised to 24 m centre to centre (draw bell to draw bell along tunnels/drifts). The objective of the study was to understand if that

spacing was ideal, considering that ore recovery must be maximised while maintaining draw zone interaction. Key considerations included:

- Evaluation of drawzone interaction through the review of the PC/BC model in conjunction with drone footage and borehole camera data.
- Determination of specific deformation rates in the weak/soft kimberlite – 1060 PG kimberlite using the Zeb Horizon Scanner as well as laser technology.
- Stability assessment at the weak zone after increasing drawpoint spacing to 24 m using FLAC3D software.

This research describes some of the geotechnical challenges experienced during the last 25% construction phase of the block cave footprint at the C-cut block. Deformation rates experienced at the extraction level are highlighted such that an informed decision can be made when it comes to the type of support to be selected in subsequent blocks.

1.9 Sources of Data

The data used in this research is a combination of field work and historical data available at the CDM's archives**.**

1.10 Structure of the Research Report

The research report has the following chapters:

- Introduction
- Literature review
- Beck engineering method of analysing the stability of drawpoints and pillars
- Cave initiation using preconditioning and related underground monitoring
- Stability assessment using FLAC3D software
- Discussion
- Conclusion
- Recommendations and References

2. LITERATURE REVIEW

2.1 Introduction

In this chapter, the basic understanding of material flow in a block cave will be discussed. Relevant and current guidelines associated with drawpoint spacing will be considered for use in the back analysis in weak/soft kimberlite. The following sub-sections will be expanded on:

- Draw zone interaction
- Drawpoint spacing
- Implications of spacing drawpoints too far apart
- Preconditioning
- PC/BC model
- Re-compaction theory applicable to CDM
- Rock Strength

The ellipsoid of draw concept will be discussed in this section. In the research of flow of broken rock in caving mines, there are two main concepts describing the shapes formed by material moving within the cave (Nedderman, 1995). Different researchers have referred to these using different names for the same concepts.

The first of these is the outline or contour surrounding the original location of material that has been drawn from a drawpoint at any given point in time. This has been defined in various places as the ellipsoid of motion, the ellipsoid of draw, the ellipsoid of extraction, the draw body, the draw area, the draw envelope, or the draw zone. Draw zone will be maintained throughout the report.

The second concept is the outline or contour surrounding the original location of material that has moved from its original location (but not necessarily been removed at the drawpoint) at any given point in time during drawing of a drawpoint. This has been called, amongst other things the limit ellipsoid, the loosening ellipsoid, the ellipsoid of movement, or the movement envelope. The term limit ellipsoid will be maintained in this report. These concepts are shown in Figure 2.1.

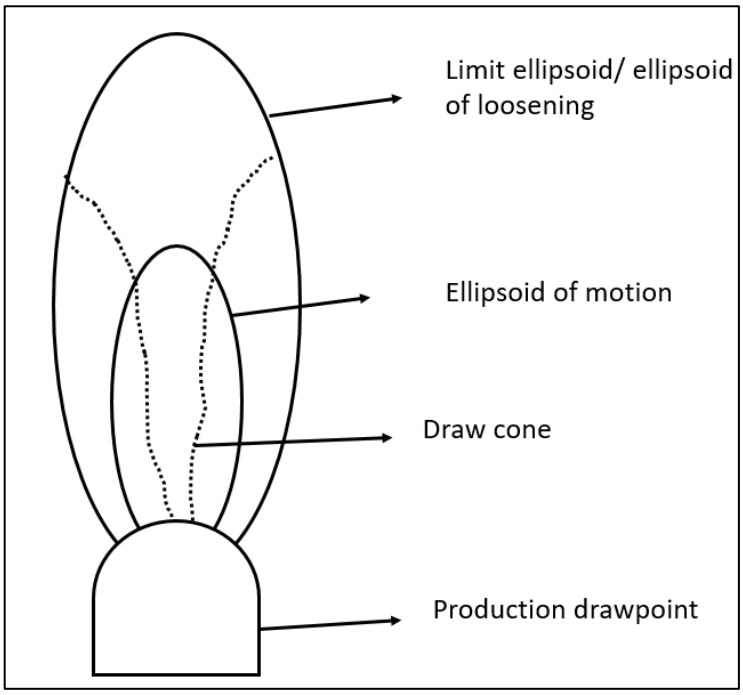


Figure 2.1: The draw and movement ellipsoids (Just, 1981)

The third and fourth concepts as described by Halim (2006) are *interaction* and *overlapping.* Interaction between two or more adjacent drawpoint extraction or movement zones is defined as when these zones expand from their isolated size under the drawing process, as a result of drawing of neighbouring drawpoints. Isolated extraction or movement zones are defined as overlapped when two or more zones are intersecting each other.

Castro and Halim (2008) defined *interactive and isolated draw*. Interactive draw is described as when two or more adjacent drawpoints are drawn concurrently. When only one drawpoint is drawn, it is defined as *isolated draw*.

2.2 Drawzone interaction and drawpoint spacing

Castro et al (2012) described the concept of drawpoint spacing as being based on recovery considering the concept of interaction of draw zones. In this concept, mass flow only occurs when adjacent flow zones are spaced such that there is interaction at a given height.

Gravity flow of caved ore has been extensively studied, although the gravity flow characteristics are still not well understood. In the past, data accumulated through experience from different mines has been used to formulate guidelines and principles for draw point spacing and design though an analytical approach is still not available. The classical approach (first described by Kvapil, 1992) to describing gravity flow involves the concept of the flow ellipsoid shown in Figure 2.2.

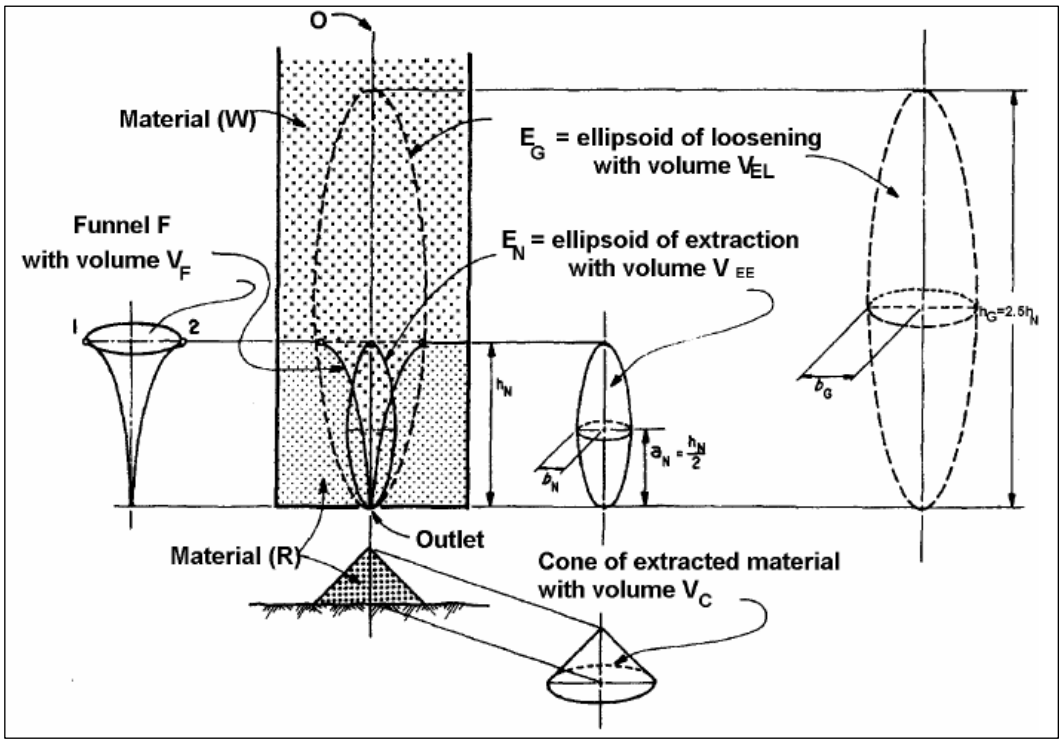


Figure 2.2*:* Classical approach to the flow ellipsoid concept

Kvapil described the ellipsoid of motion, draw or extraction as the area where the material reporting at a drawpoint after a given period would have originated from. The material outside the ellipsoid of motion would have loosened and displaced within the ellipsoid of loosening but would not have reported to the drawpoint. Outside the ellipsoid of loosening, the material would remain stationary. It is on this basis many Sub - Level Caves and block caves have been designed. Rustan, 2000 argued that the ellipsoid is not always the default shape material will choose to flow. Sometimes the classical ellipsoid is a function of particle size within the flow mass and the width of the discharge point (drawpoint opening). In essence the shape of this ellipsoid can be described by its eccentricity looking at the following equation:

$$\varepsilon = \frac{1}{a_N}\sqrt{(a_N^2 - b_N^2)} \quad (1)$$

Where:

a_N and b_N are the major and minor semi-axes of the ellipsoid of motion. Laubscher, 1994 derived a relationship between drawpoint spacing and interaction. Interaction is guaranteed at a maximum spacing of 1.5 times the diameter of the isolated draw (Laubscher refers to this as isolated drawzone or IDZ). Presented in Figure 2.3 is an example of the cave draw ellipsoid.

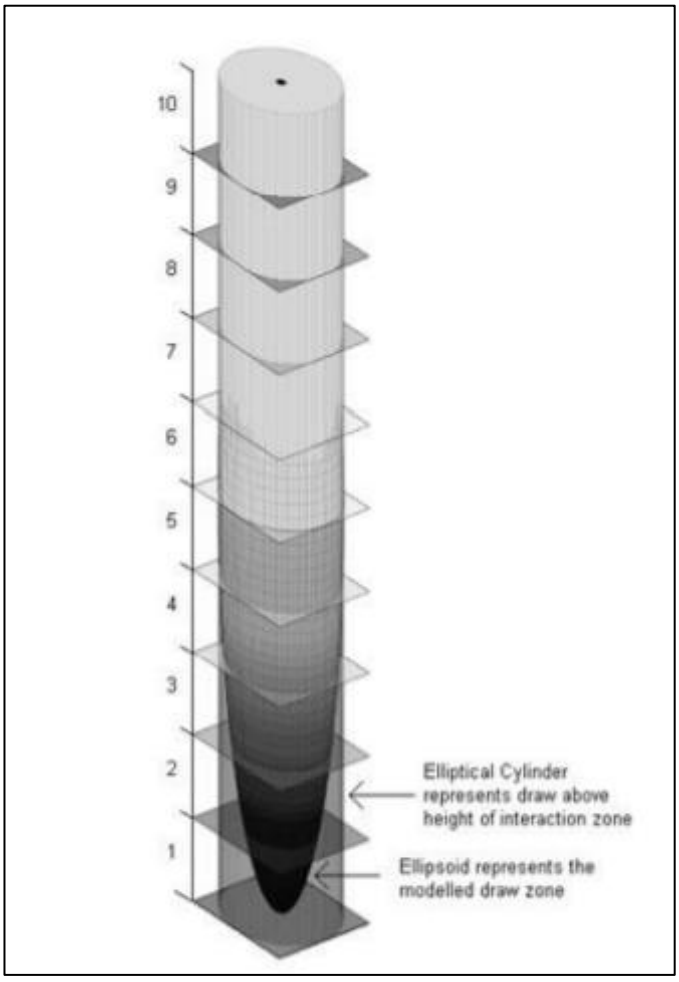


Figure 2.3: Cave Draw Ellipsoid (Steward et al, 2010)

2.3 Drawpoint Spacing

The spacing referred to in this research project is the centre to centre spacing of drawpoints in a direction parallel to the production drifts across the minor apex. Drawpoint spacing is affected by number of factors which include but are not limited to: fragmentation, planned rate of draw, geotechnical factors influencing the strengths of pillars and the number of drawpoints required to achieve the planned production (Brown, 2003). An inverse relationship exists between the drawpoint spacing that must be developed and the cost of development. Increased drawpoint spacing leads to fewer drawpoints being developed thereby decreasing the cost of developing those drawpoints. Other contributing factors ignored, increased drawpoint spacing means that an acceptable level of stability is achieved as the size of pillars would be increased.

However, according to Laubscher (2000), the drawpoint spacing is a function of fragmentation with finer material likely to lead to isolated draw zones while coarse material leads to interactive draw zones. Isolated draw zones develop when draw zones in adjacent drawpoints do not overlap thereby causing pillars of undrawn ore to be left as shown in Figure 2.4. This would potentially result in a loss of ore and an application of load to pillars between excavations on the extraction level.

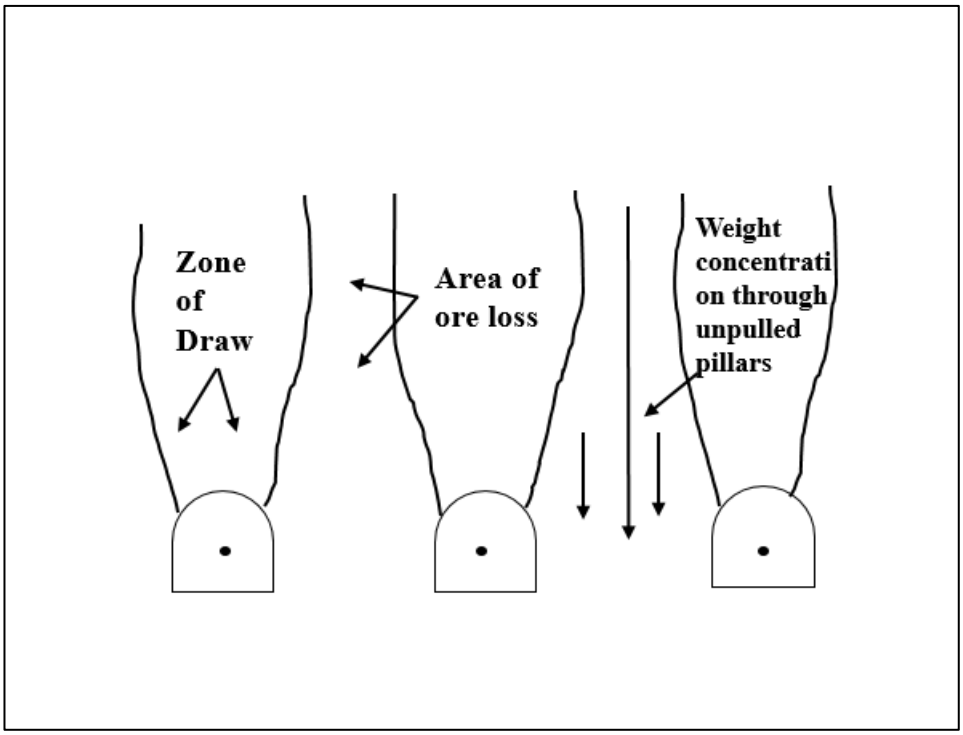


Figure 2.4: Excessive drawpoint spacing with non-overlapping zones (after Richardson, 1981) and interactive draw zones

2.4 Preconditioning

According to Cordova et al (2021), preconditioning involves treating the rock mass prior to caving, under natural confinement conditions, with an appropriate process to generate fractures by activating the *in-situ* structural network, or by explicitly creating a set of new fractures. The main purpose is to weaken the competent rock mass in the primary domain material.

There are three main ways to precondition the rock mass for caving namely:

- Preconditioning with hydraulic fracturing (HF)
- Preconditioning with explosives

- Mixed or intensive preconditioning

While preconditioning is normally applied in block caving to create new fractures in competent rock masses, similar techniques were utilised at CDM to re-create the “cave initiation level” where the undercut could not be mined successfully.

2.5 Implications of spacing drawpoints too far apart

It is well known that in the case of widely spaced drawpoints with no drawzone interaction, the stagnant material between the draw zones consolidates and may act as a ‘stress conduit’ leading to point loading on the extraction level. Thus, a potential consequence of designing large pillars is more frequent damage to the extraction level and ultimately this design could exacerbate the stability problems that it attempted to prevent (Van As & Van Hout, 2008).

2.6 PC/BC model

Gemcom PC-BC is an empirical code for prediction of gravity flow in block caving mines. It is based on understanding developed from sand model experiments, in situ marker trials and back analysis of drawn grades/lithologies from caving operations (Diering, 2000). The code does not claim to predict the evolution and velocity profiles associated with gravity flow; rather, a series of fixed radius “draw cones” are defined ahead of time. Empirical mixing rules are then applied to the material within those cones to account for the mixing caused by non-uniform velocity profiles, fines migration and free surface trickling. It is presumed within the code that

interactive draw is always achieved, which makes it unsuitable for the analysis of recovery and dilution in cases where fine fragmentation (relative to drawpoint spacing) leads to isolated draw and early waste entry. The software requires input parameters such as the height above the extraction level at which uniform drawdown occurs (Height of Interaction Zone, or HIZ), isolated movement zones (IMZ) maximum width, a draw control factor and definition of fines percolation attributes. These inputs require site specific calibration using grades and geological markers from the block caving operation to which it is being applied. While this limits the robustness of the code, it has proven useful at several operations where data was available for calibration (Diering, 2000).

2.7 Recompaction Theory

The re-compaction theory of caved/blasted kimberlite at the undercut level was investigated. The CDM kimberlite re-compaction time guideline was used in determining the construction cycles and resource requirements. The maximum time available to open up a drawbell, from the time the undercut advances over the area, is about 6 months (Tukker et. al, 2016). Two months is required for the undercut moving at 8m per month to create a de-stress shadow, and another four months for development and construction of the drawbells in the extraction level. If this timeline is not adhered to and the undercut “runs” away from the extraction level, the area already undercut might fill up with excessive caved materials and bulking of these materials may ultimately re-compact, transferring stress down onto the 839L extraction level.

2.8 Rock Mass Strength

Numerous criteria describing the strength of rock as a function of applied stresses or strains have found application in practical rock engineering. Both the Hoek-Brown and Mohr-Coulomb failure criteria for rock masses are widely accepted and has been applied in a large number of projects worldwide (Hoek et al, 2002). Saiang et al. (2014) used FLAC3D to compare Mohr-Coulomb and Hoek-Brown to actual underground observations. They found that the Mohr-Coulomb failure criteria with elastic-perfectly-plastic behaviour best represented what was observed in reality.

2.8.1 Hoek-Brown Failure Criterion

The criterion was developed in 1980 with numerous updates over the years. From this study it was stipulated that rock mass fails in shear (Hoek & Brown, 1980). It is common to present the failure criterion in terms of shear and normal stresses on the failure plane. An alternative is to present the failure criterion in terms of major principal stresses (σ_1) and minor principal stresses (σ_3), Hoek and Brown, 2018. This criterion is valid for intact rock and rock masses. The equation below represents the original Hoek-Brown failure criterion (Hoek & Brown, 1980)

$$\sigma_1 = \sigma_3 + \sigma_{ci} \left[m_i \frac{\sigma_3}{\sigma_{ci}} + S \right]^{0.5} \quad (2)$$

Where:

- σ_{ci} is the UCS of intact rock material; and

- “m and s” are material constants, where s = 1 for intact rock.

The generalised Hoek-Brown failure criterion evolved from earlier versions and is also applicable to rock mass. This criterion was developed with the assumption that rocks will have isotropic behaviour. It works well in intact rocks as well as a large range of GSI representing different rock masses. The generalised Hoek-Brown failure criterion introduced by Hoek (1994) and Hoek et al. (1995) is expressed as follows:

$$\sigma_1 = \sigma_3 + \sigma_{ci} \left[\left(m_b \frac{\sigma_3}{\sigma_{ci}}\right) + s\right]^a \quad (3)$$

Where:

- m_b is the parameter for rock masses and can be derived from m_i of intact rocks as:
- $m_b = m_i * e^{\left[\frac{GSI - 100}{28 - 14D}\right]}$ (4)
- where D is the disturbance factor in rock masses due to blasting or stress relief (range between 0-1 for undisturbed to highly disturbed rock masses respectively). GSI is the geological strength index which can be determined from mapping underground or the relationship with rock mass rating (RMR).
- $S = e^{\frac{GSI-100}{9-3D}}$ (5)
- $a = \frac{1}{2} + \frac{1}{6}\left[e^{\frac{-GSI}{15}} - e^{\frac{-20}{3}}\right]$ (6)

2.8.2 Mohr-Coulomb Failure Criterion

The Mohr–Coulomb (M-C) failure criterion is a set of linear equations in principal stress space describing the conditions for which an isotropic material will fail, with any effect from the intermediate principal stress (σ_2) being neglected (Labuz and Zang, 2012). The advantages of the M-C failure criterion are its mathematical simplicity, clear physical meaning of the material parameters, and general level of acceptance. M-C can be written as a function of major and minor principal stresses, or normal stress and shear stress on the failure plane presented as:

$$\tau = c + \sigma tan\phi \quad (7)$$

Where C is the cohesion (MPa), σ is normal stress (MPa) and ϕ is the friction angle (º). The failure criterion can also be expressed in the major and minor principal stress space as follows (Brady & Brown, 2004):

$$\sigma_1 = \frac{2Ccos\phi + \sigma_3(1+sin\phi)}{1 - sin\phi} \quad (8)$$

3. BECK ENGINEERING METHOD OF ANALYSING THE STABILITY OF DRAWPOINTS AND PILLARS

In 2009, Beck Arndt Engineering was contracted to back analyse the AUC failure and use the data to calibrate a numerical model of the C-Cut. A 3D model was developed using the FEM Abaqus Explicit with geotechnical enhancements including an improved constitutive model for underground problems. The strain criterion that Beck (2009) utilised was based on damage mapping done at the Advanced Undercut Block (AUC) block cave. The strain criterion was related to the % rock mass damage and ranges from minor (~0.6%) to significant (~5%) shown in Figure 3.1.

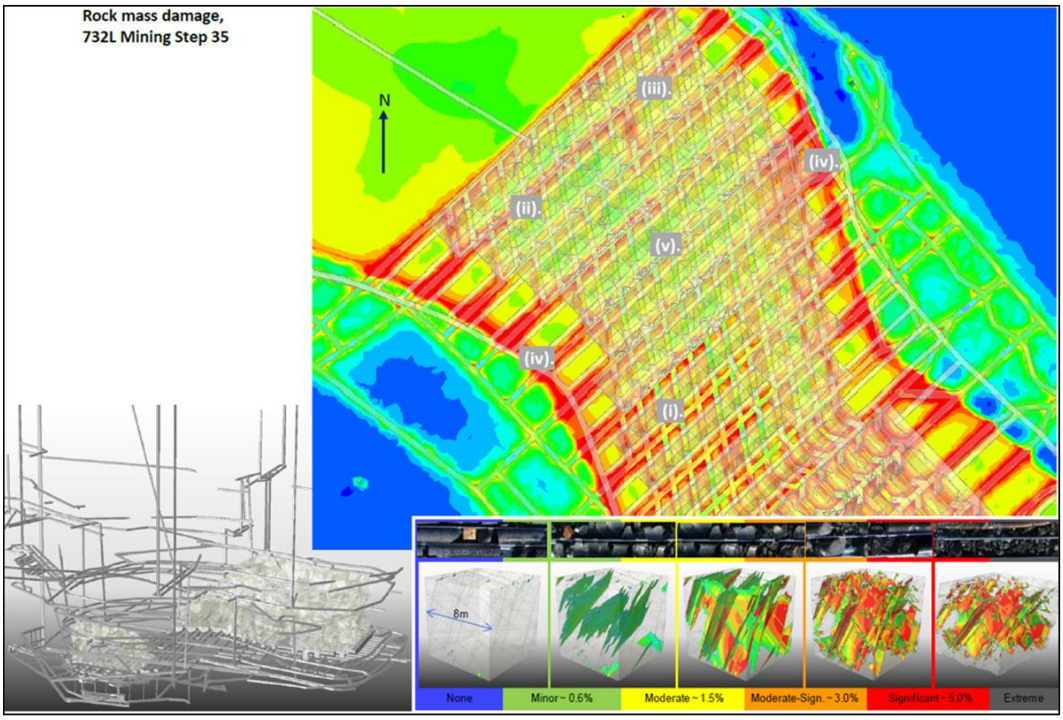


Figure 3.1: Showing rock mass damage at the extraction horizon of the AUC block cave (Beck, 2009)

During the damage mapping, it was concluded that significant damage in a pillar core has a high correlation with extreme closure in adjacent drives. In the sub-sections to follow, the results as modelled by Beck Engineering at the end of the undercutting stage (~75% undercutting) for both the AUC and C-Cut will be discussed.

Beck Engineering (2016) again performed extensive geotechnical modelling focusing only on the C-Cut block. The model was calibrated with deformation data collected during the AUC North collapse (which lies approximately 200 m east and above the C-Cut). One of the main objectives was to model the undercut face-shape (sequence) and the pillar sizes between draw points. From the results, challenges were predicted to start after having retreated 70 – 75% of the footprint and indeed that was the case. The rock mass failure in the south, shown by the yellow lobes in Figure 3.2, is associated with fringe issues due to the difference in rock mass strength of the host rock compared to the kimberlite orebody.

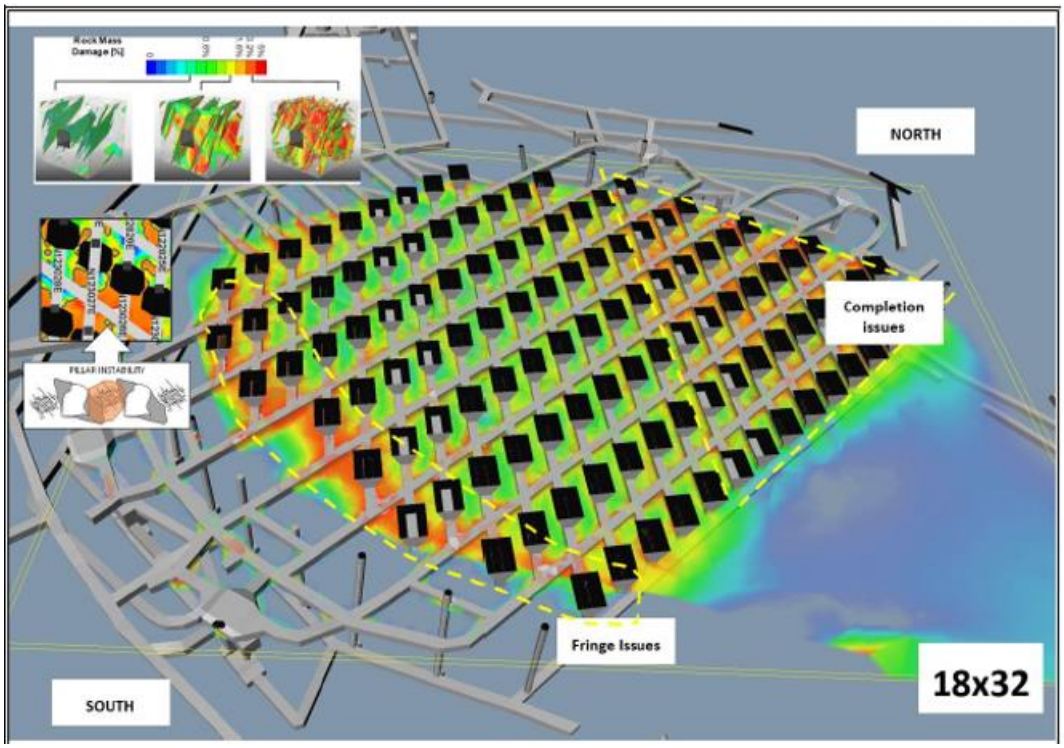


Figure 3.2: Prediction of failure using Abaqus (Beck, 2016)

It was also where the lowest mining rock mass rating (MRMR) was estimated during the pre-feasibility stage. The north lobe was associated with completion issues (possible multiple tunnel failures) due to the geometry of the kimberlite pipe.

3.1 Modelling the Old Collapses - AUC Results

Beck Engineering noted that near the end of the AUC undercut, pillars showed varied degrees of failure (shown in Figure 3.1):

i. Conditions were slightly worse than in the earlier stages, suggesting that extraction level/horizon protection was reduced in this area.

ii. Localised areas or groups of pillars may still collapse. Some pillars at the abutments show moderate-significant damage and may still be

problematic. Pillars that were formed on the extraction level under the northern undercut front appear stable on average at this stage, though damage is slightly higher than for the southern advancing front and the depth of damage in the walls of the development is higher.

iii. This area is under the southern undercut front.

iv. Crosscuts show significant damage at the contacts.

v. The central portion of the AUC footprint is similar to the southern abutment, but with some moderate-significant damage in isolated pillars.

Near the end of undercutting (75% undercutting) of the AUC results are discussed below and shown in Figure 3.3.

i. In the old North collapse area of the AUC, the strain is similar to the earlier steps (say, 20% undercutting).

ii. Damage in the northern access tunnels now extends for the remaining length of undercutting.

iii. Damage in the northern access turnouts remains similar, except adjacent to crosscuts where undercutting is being completed, where there are increases in damage. In the model some sections of the perimeter drive show new or increased damage, primarily where the drive is closer to the contact. This result would be very sensitive to the actual proximity to the contact and the geometry of the model

may be imperfect, so common sense and experience are needed to assess the real level of risk

iv. On the northern undercut front. The pillar core damage averages moderate to moderate-significant (3%) in some crosscuts. At this level conditions similar to the AUC at the time of the collapse should be expected. Some crosscuts show less damage, which is an indicator of the effect of the geometry of the contact relative to the undercut front, the angle is starting to open up and in newer crosscuts there is comparative improvement. The access through the contacts continues to significantly experience damage

v. On the southern undercut front at this stage, pillar core strain ranges on this undercut front remain at minor to moderate levels except at the access through the contact.

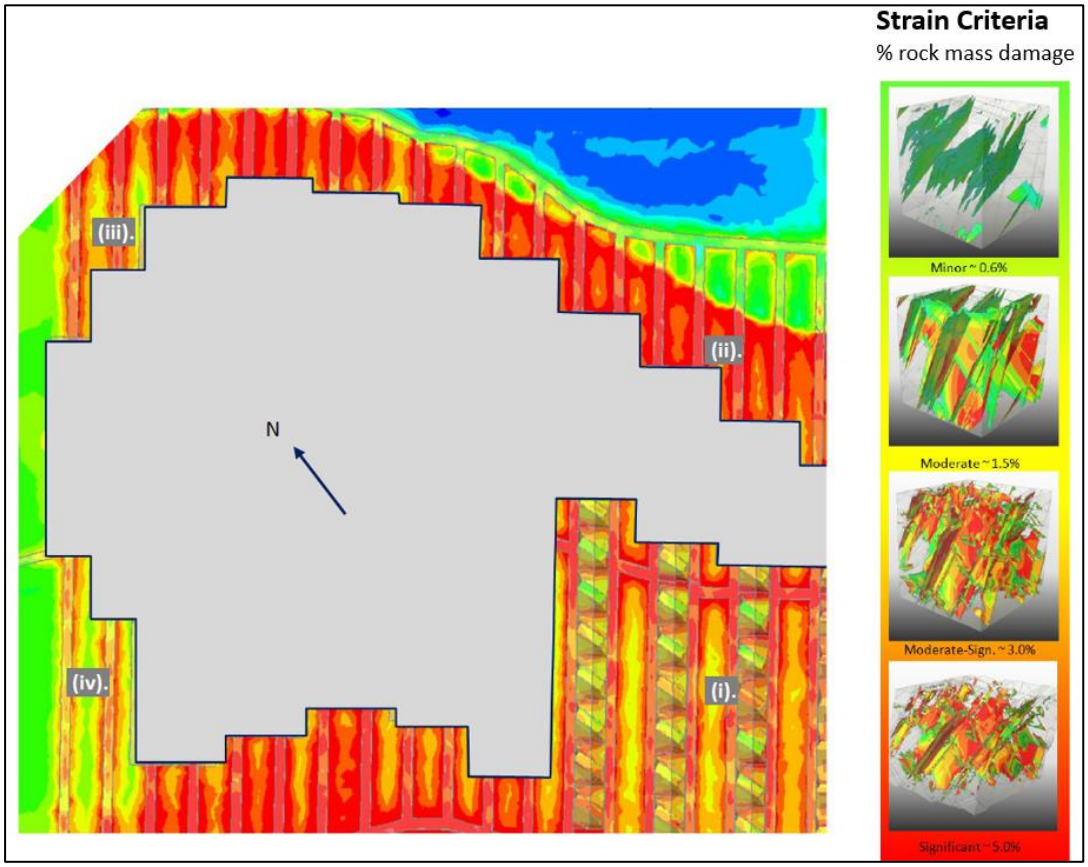


Figure 3.3: Illustrating rock mass damage (Beck, 2009) at AUC block cave (the grey area represents the undercut front – retreated zone)

3.2 Prediction of Collapse - C-Cut Results (Undercut)

The results for the C-Cut block at 75% undercutting are summarised below and illustrated in Figure 3.4.

i. The Northern accesses through the contact are slightly damaged.

ii. The Southern accesses through the contact are slightly damaged (crosscut spacing leads to pillar damage due to tunnels alone)

iii. The centre of the undercut front worsens slightly, though pillar cores are still averaging less than 1.5%.

iv. At the Southern end of the mining front, the angle that the undercut makes with the contact may have improved and the moderately

damaged pillar cores now extend only 20 m or so in advance of the undercut.

v. At the Northern edge of the footprint, damage adjacent to the contact, extending inwards 50 m or so increases.

   a. The level of damage is approaching levels seen on the AUC

   b. The problem is sufficient that it should be addressed. If grade is lower there, this may allow some flexibility in the scheduling. Lessons from the AUC block can also be applied.

   c. A positive is that it is only part of the undercut that is affected, however this may also be a risk. Uncollapsed areas need to be blasted but as the damage occurs at the access to the undercut crosscuts, access to this area would need to be regained to ensure caving is initiated.

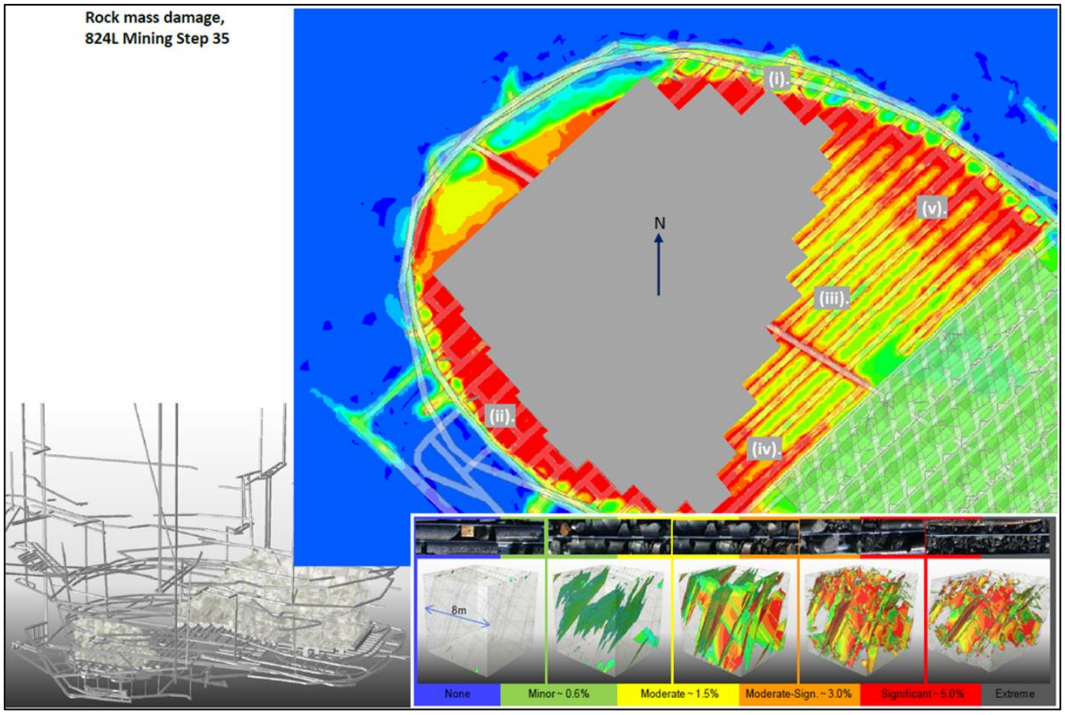


Figure 3.4: Rock mass damage at 75% undercutting (Beck, 2016))

3.3 Prediction of Collapse - C-Cut Results (Extraction Horizon)

The extraction horizon was also analysed to understand how rock behaves at 75% undercutting. The summary of results is listed below and presented in Figure 3.5.

i. Just behind the undercut front, pillar damage is minor/insignificant though wall damage is significant.
ii. The north-west access drives interact significantly causing damage to pillars.
iii. Infrastructure development at the Northern and Southern abutments needs revision, local pillars are too small.
iv. Some pillars in the start-up area show moderate damage, though the problem could possibly be managed using a draw strategy.
v. Very minor rock mass damage extends below the undercut to the extraction horizon.

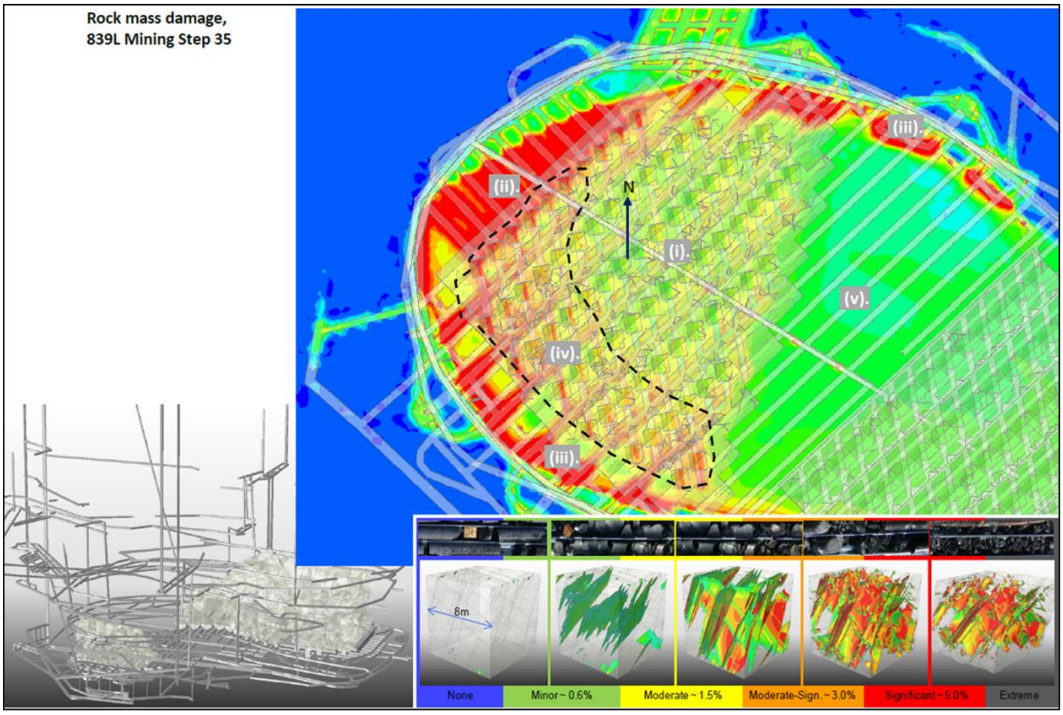


Figure 3.5: Rock mass damage on the extraction horizon at (75% undercutting)

Though Beck Engineering expected failure as a result of the kimberlite pipe geometry relative to the boundary of the pipe, the extent of the weakzone was unexpected and therefore not included in the initial geotechnical model. The infrastructure in the undercut level collapsed in the area described in chapter 1 subsection 1.5. The mine decided to use preconditioning by blast to recover this uncaved area affecting 3 tunnels in the extraction level.

4. CAVE INITIATION USING PRECONDITIONING AND RELATED UNDERGROUND MONITORING

A risk assessment team was formulated in order to put together a strategy that would see CDM recover the ore locked up as a result of the undercut failure. The following is discussed under this heading:

- Preconditioning: - The use of pre-conditioning as a tool to initiate the cave above the undercut level (824 m below surface), and to reduce stress concentrations around the drawpoints on the extraction level (839 m below surface). Once the shape of the drawbell was achieved, the drones were employed to determine visually whether the individual draw bells connected at the top above the major and minor apex.
- Drone Survey: - The drones were employed (through an external business partner) to determine visually whether the individual draw bells connected at the top after pre-conditioning, prior to initiating the cave. All interpretations are the researcher's own opinion.
- Borehole Camera: The borehole camera was used to the inspect the vertical boreholes to assess possibility the possibility of re-compaction.
- The PC/BC model was reviewed to check the height of draw, compare the radius of the drawzone interaction between the drawbells spaced 16 m and 24 m apart. The width of the drawzone originally used as an input into the model will be evaluated to check

validity when drawpoints and consequently drawbells are spaced 24 m apart (increased spacing).

- Zeb Laser Scanner: - The laser scanner was used to measure deformation on the walls of the extraction tunnels (before and after pre-conditioning), which was later used to verify the numerical modelling results.

4.1 Preconditioning

Preconditioning using explosives (emulsion) was the method employed at CDM in order to break the pillar left at the undercut horizon. This involved drilling blast holes with lengths ranging from 20 m - 40 m (instead of the 10 m that would have been drilled at the undercut level) depending on the orientation. These holes were drilled from the extraction level with closely monitored drilling accuracy (Figure 4.1). This accuracy was essential since the holes intersected each other and future draw bell holes.

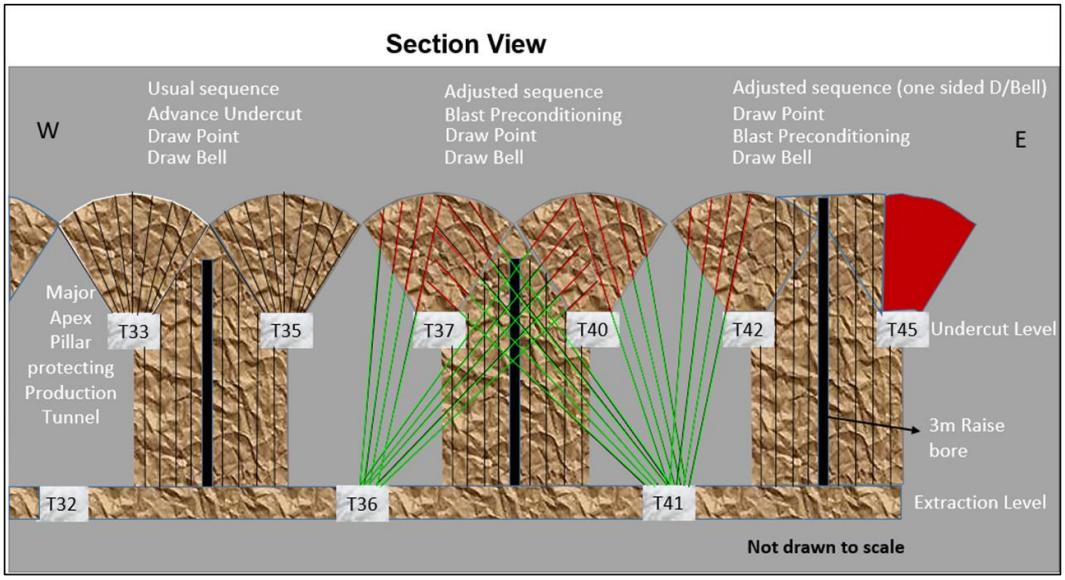


Figure 4.1: Section view showing drilled holes and sequence of mining (Courtesy of the Drill & Blast Engineering team, 2021)

Stemming (using cement grout) of the holes was deemed essential to maintain the integrity of the extraction level by keeping the major apex stable. Stemming was done shortly after charging the intended toe of the hole (the position of the undercut level) but before the holes went off.

In Figure 4.1, the red lines show the charged length while the green show the grouted remainder of the hole. Far east is the red solid ground that could not be recovered due to the existence of Tunnel 42 (T42) implying that the preconditioning hole could not be drilled past. The vertical thin black lines represent rings/ drill holes intended to create a drawbell while the thick black line represent a 3 m diameter raise bore. From the left between Tunnel 32 (T32) and Tunnel 36 (T36) of the extraction level, the normal sequence would have the advanced undercut pass a distance at least 15 m (45º rule) from the draw bell below it, followed by the draw point and eventually the raise boring and blasting of the draw bell (refer to Figure 1.10).

The pillar left in the undercut as a result of the localized undercut failure led to a change in the sequence. The adjusted sequence meant that preconditioning takes precedence followed by break-aways for draw points and eventually the opening of draw bells. In a few instances, where the draw bells were one sided, the sequence was changed to draw point breakaways, preconditioning and finally the blasting of draw bells. This was necessary to avoid uncontrolled intersection of holes such that the extraction level stability is compromised by the preconditioning itself. Shown in Figure 4.2

is an example of the grout holes with charge fuses as described above. The ring holes were spaced 2 m apart.



Figure 4.2: Depicting the grout holes during the precondition process

In Figure 4.3, the two levels in relation to each other (undercut and extraction level) and the extent of the pillar are shown. It is important to note that each draw bell receives ore material from two undercut tunnels (e.g., a draw bell between T32 and T36 of the extraction level would receive some of the material from T33 and some from T35 of the undercut level).

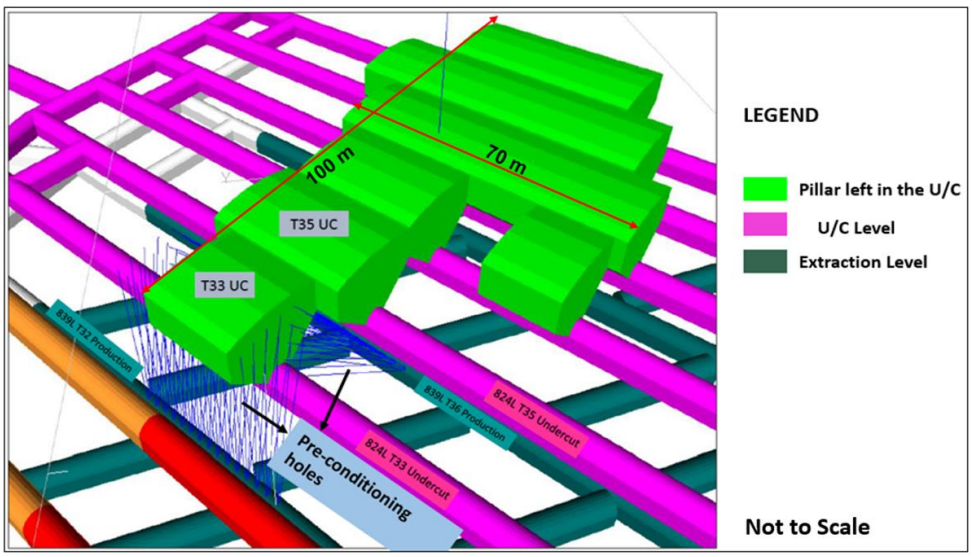


Figure 4.3: Isometric view illustrating the pillar left in the undercut in relation to the extraction level with drilled holes depicted

The overall picture of the events that took place at the Northeast corner which is where the 1060 PG kimberlite was intersected (weak zone) are depicted in Figure 4.4. The cave propagation thus cave back is clearly shown around matured draw points in the South-Westerly (SW) direction while the pillar is shown in the NE corner. In the PC/BC modelling which is a custodian of the resident Geologist at CDM (Phahla, 2021 via email), the zone above each of the DP acts as a separate draw column, which in time may increase in size laterally resulting in interaction between the adjacent draw columns, depending on the rate of draw and whether drawbells were designed to connect from the construction phase. Preconditioning of the pillar is also depicted in the position where the undercut would have been extracted. The monetary consequences of leaving the pillar unmined are shown in (Appendix A)

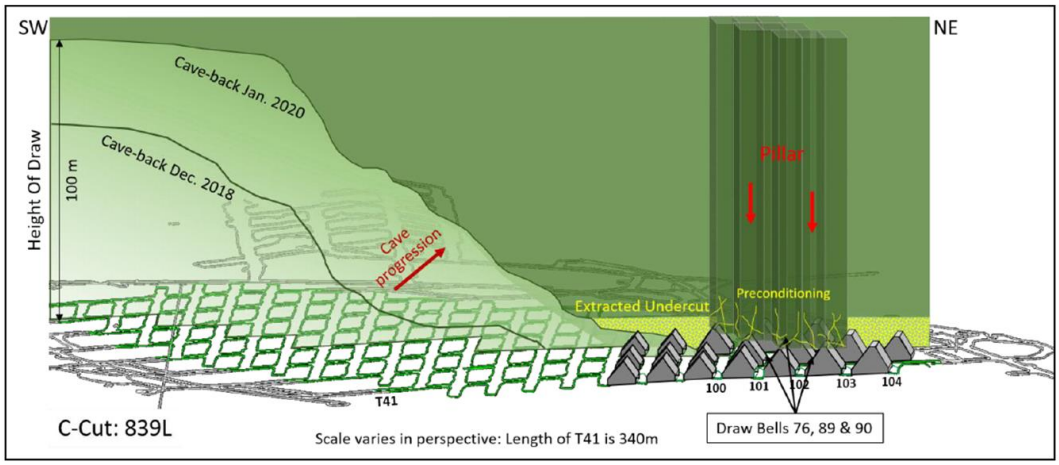


Figure 4.4: Schematic illustration of the cave back and the blast conditioned section of the undercut (Holder *et al.*, 2020)

To ensure maximum ore recovery, drill rings were designed to target the unbroken rock material and attempt to increase the chances of drawpoints connecting. This avoided any ore locked up in pillars and point loading on to the extraction level. The ring designs are shown in Figure 4.5 and more illustrations in Appendix B.

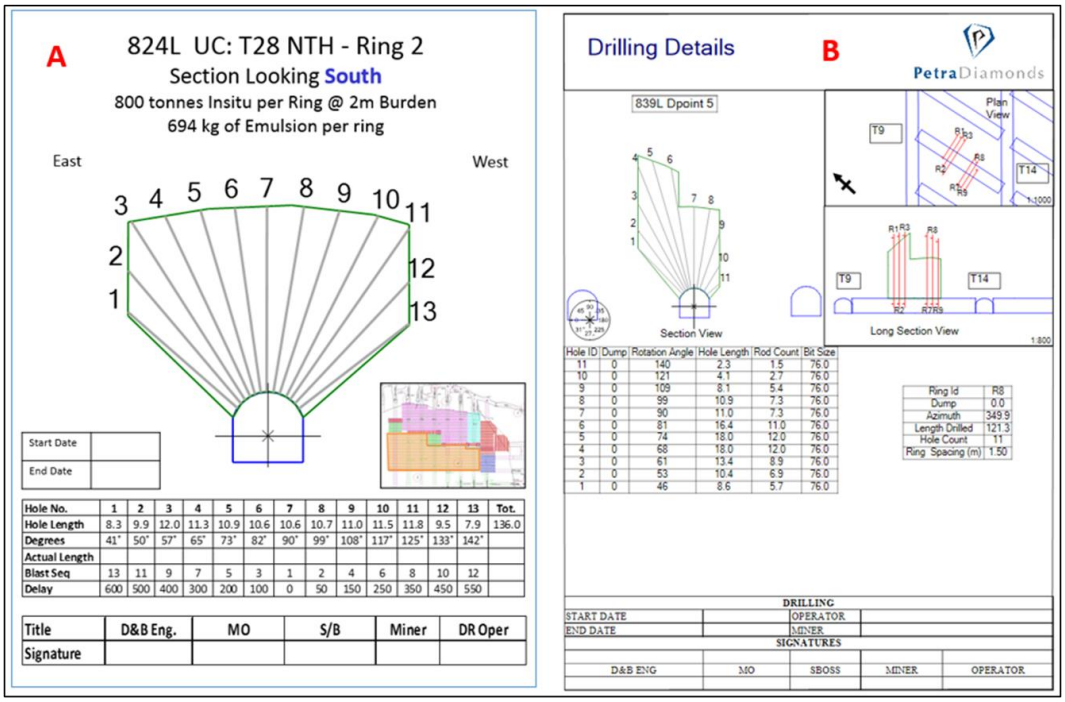


Figure 4.5: Illustrating the ring designs (a) 824L Undercut (b) 839L Extraction horizon (courtesy of the drill & balst Engineering team)

4.1.1 Drone Footage

Drone footage was undertaken at CDM shortly after the Capital expenditure (CAPEX) tonnes were loaded out at the weak zone drawpoints. At this stage, no ore was reporting to the drawpoints except a few oversized boulders. This lack of material was believed to be resulting from a lack of

interconnectivity at the top of the adjacent drawbells. A series of scans were done using a drone which confirmed large voids within the drawbell (Figure 4.6 and 4.7).

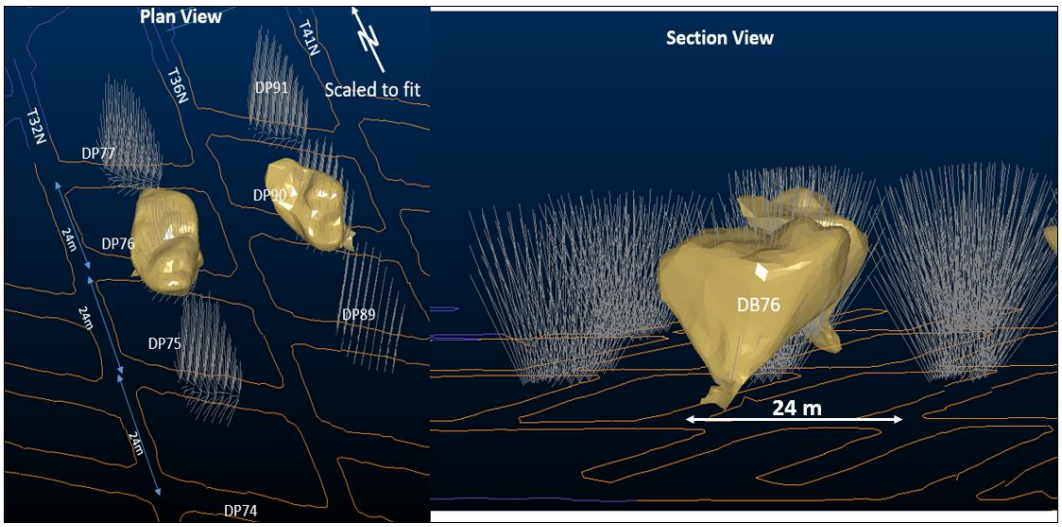


Figure 4.6: View of draw bell void scans showing a lack of interaction across the major apex (courtesy of the drill & blast Engineering team, 2021)

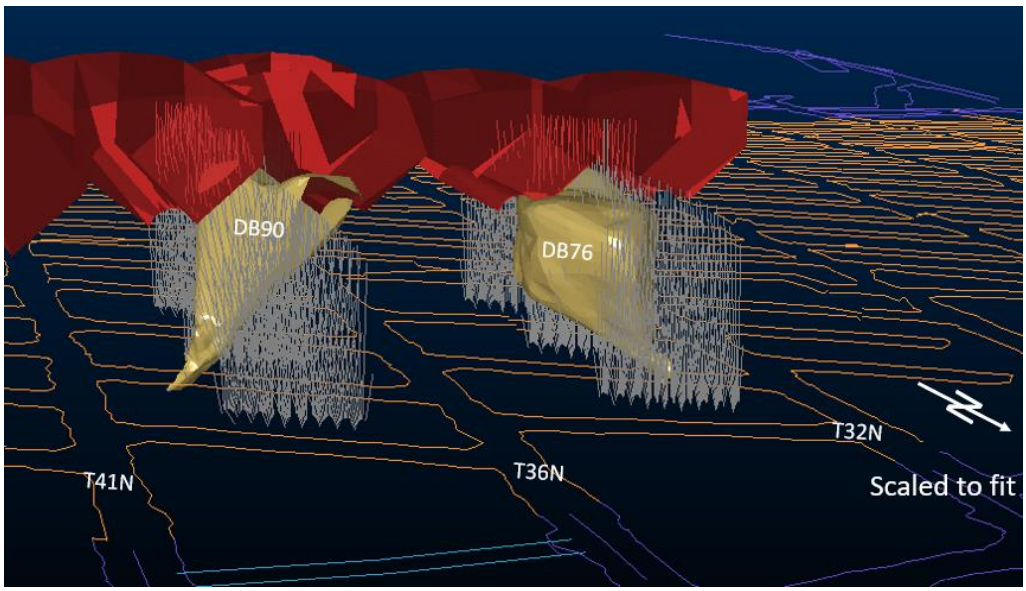


Figure 4.7: View of draw bell void scans showing a lack of interaction across the minor apex (between DB90 & DB77)

The purpose of the drone was to verify whether adjacent drawbells were connected as per best practice as far as ideal draw column interaction is concerned. The value this data provided allowed for underbroken areas to be targeted for recovery drilling to ensure connection between adjacent drawbells. Depending on the position of the underbreak and ultimately lack of connection between adjacent drawbells, the drill rigs were positioned such that the oversized boulders and uncaved material were targeted in an attempt to initiate caving. From the drone footage, it was also noted that the slope at which the major and minor apices were formed was gentle when DPs were spaced 24 m apart compared to the original design.

4.1.2 Review of the PC/BC Input Parameters

The PC/BC model as utilised at CDM is based on Laubscher's empirical work. It states that for drawzone interaction to occur, the spacing of drawpoints must be 1.5 times the width of the draw zone (Laubscher, 1994). The design drawzone width for CDM that was input into the model is 14 m. At any given time, the PC/BC model assumes that drawpoints overlap and interact with each other. Figure 4.8 is an example of a comparison of the size of the overlap between matured drawpoints (spaced 16 m apart) and those spaced 24 m apart centre to centre.

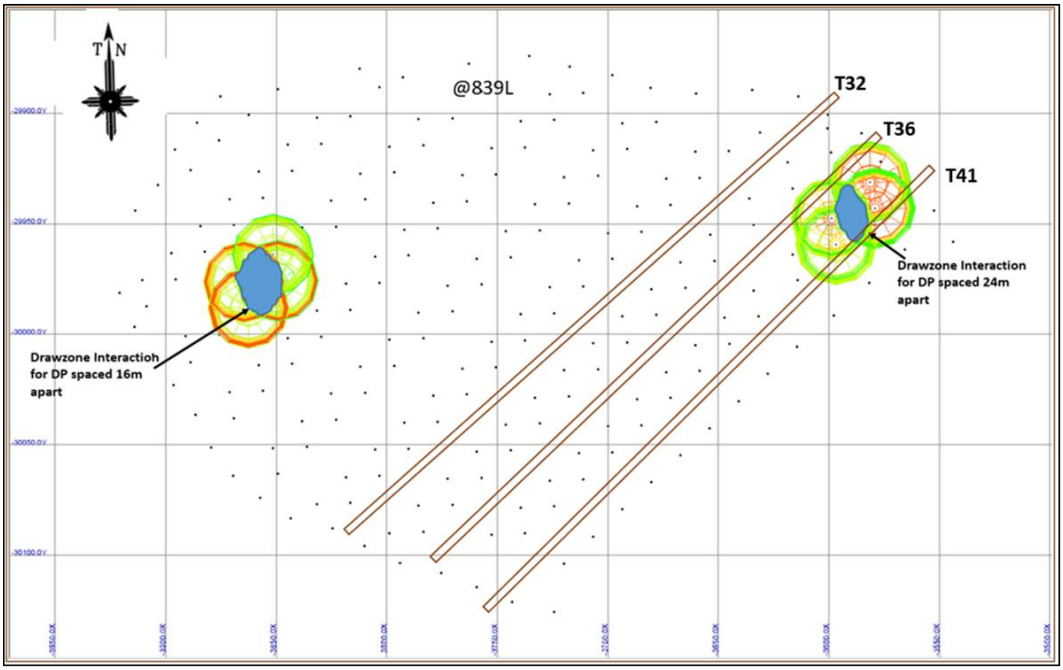


Figure 4.8: An example comparison of drawzone interaction size between DP spaced 16 m and those spaced 24 m (after Phahla, 2021)

It is evident that the increased spacing of drawpoints reduced the size of the overlapping drawzones though the PC/BC model does not explicitly predict any lack of interaction. The drawpoints/drawbells showed a reduced area (on plan) of overlap which equates to a reduced chance of drawzone interaction.

Attempts to draw as much as possible (as much as allowable on the model) in the weak zone were effected late 2019/early 2020. Despite these attempts, challenges such as uncaved material in the form of very high hang-ups, rapid rock mass deterioration and open voids were experienced.

Figure 4.9 shows the height of draw at the Northeast corner as well as the tonnages extracted on the whole footprint.

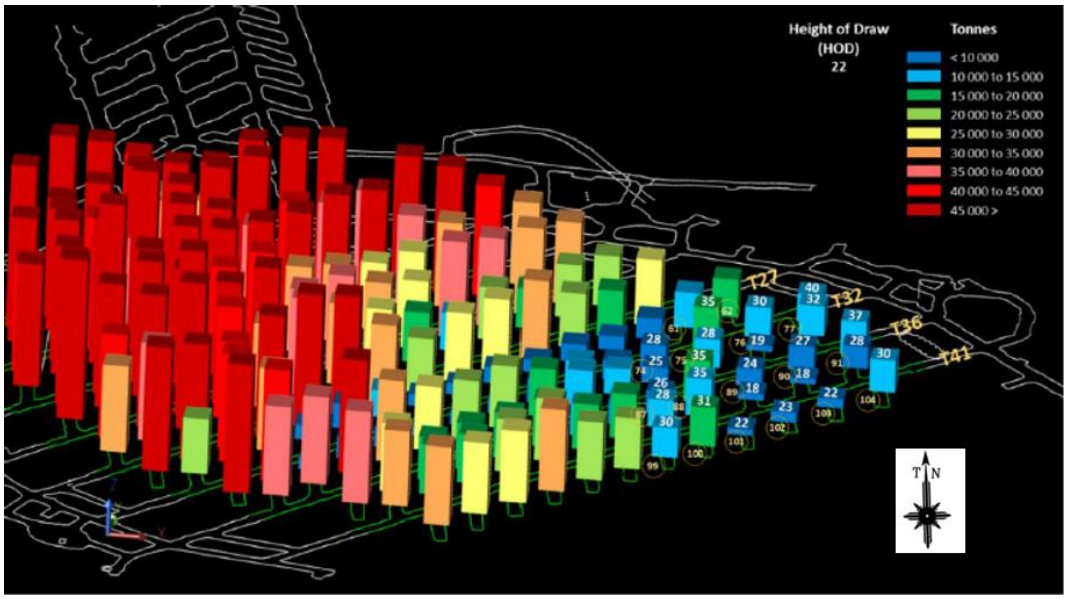


Figure 4.9: Illustrating the tonnes extracted at the C-Cut footprint and the HOD achieved at the NE corner (after Phahla, 2021)

It is evident that the Northeast corner still has a lot of ore reserves locked up with the majority of drawpoints averaging less than 10 000 tonnes. This equates to a height of draw of 22 m on average as opposed to a height of 60 m which would have enabled drawzone interaction (as per mine design). Laubscher suggested that DP must not be spaced more than 1.5 times the drawzone width (Laubscher, 1994). For CDM the design width is 14 m suggesting that the maximum spacing for DP was to be capped at 21 m.

4.1.3 Recompaction at the Weakzone

To confirm the re-compaction theory, boreholes were drilled 45^0 in a westerly direction and along the major apex for a total length of 20 m from the affected area at the extraction horizon targeting the undercut. These holes were drilled 10 months after preconditioning work commenced. The positions of the holes drilled are indicated in Figure 4.10. The drill holes were expected to intersect broken material at about 15 m into the rock mass. In two of the holes this was not the case while in one (T36), broken material was intersected at 17 m.

Re-compaction influences the stress state at extraction horizon. This means that the attempts to initiate caving were not realised and at this specific weak zone, uncaved material would exert pressure on the extraction level and related tunnels and/crosscuts. This would be exacerbated by the cave front and related abutment stresses.

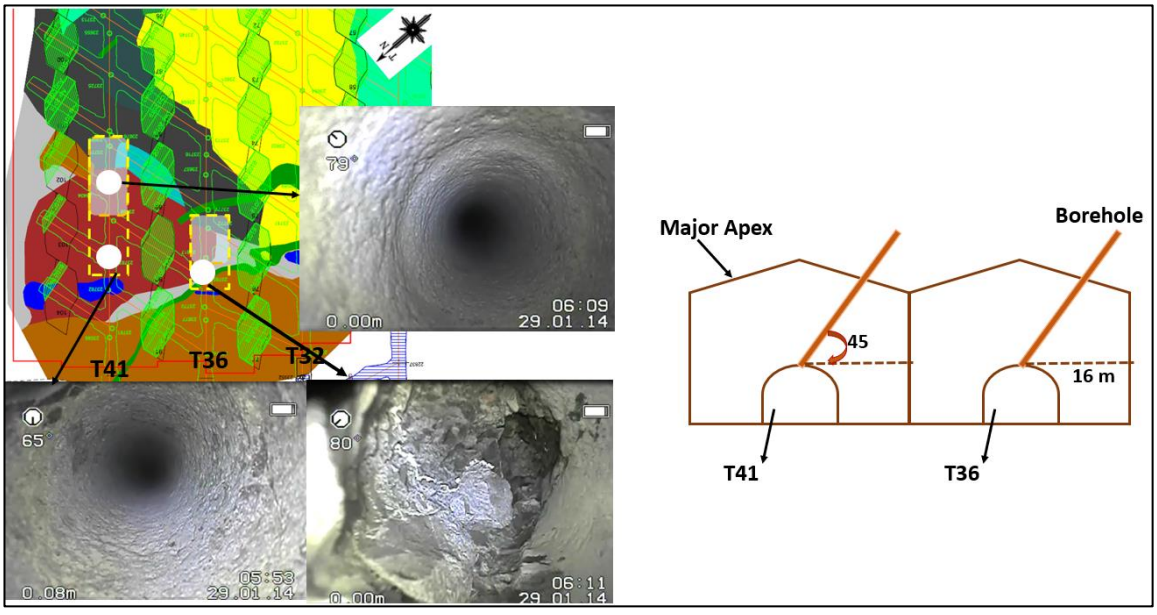


Figure 4.10: Illustrating drilled borehole positions and related footage

The aim was to drill holes to intersect the blasted ore at the undercut level and with the use of a borehole camera to check if the pre-conditioning was indeed effective. The results from the borehole camera investigation showed that re-compaction had in fact taken place in two out of the three holes drilled. The borehole camera footage, coupled with ten months delay in construction of the draw points and the low initial draw-down rate in the affected area supports the re-compaction.

4.2 Zeb Laser Scanner Results

Monitoring was done by the author using the ZEB-HORIZON 3D mobile scanner in conjunction with manual measurements using laser technology (Distomats). The Geoslam Zeb-Horizon scanner (shown in Figure 4.11) does not make use of the co-ordinate system, and all processing was done in point cloud. It is important to note that scanning of the area commenced after some movement had already taken place but before any development of crosscuts to drawbells and preconditioning. Monitoring of the main tunnels continued throughout the preconditioning activities, development of drawpoints/crosscuts and drawbells until total failure of the 3 tunnels was recorded.



Figure 4.11: Geoslam Zeb Horizon 3D Instrumentation

Scans were initially done over a period of 4 months when pillar blasting for preconditioning commenced, and minimal tunnel contraction was recorded as shown in Figure 4.12.

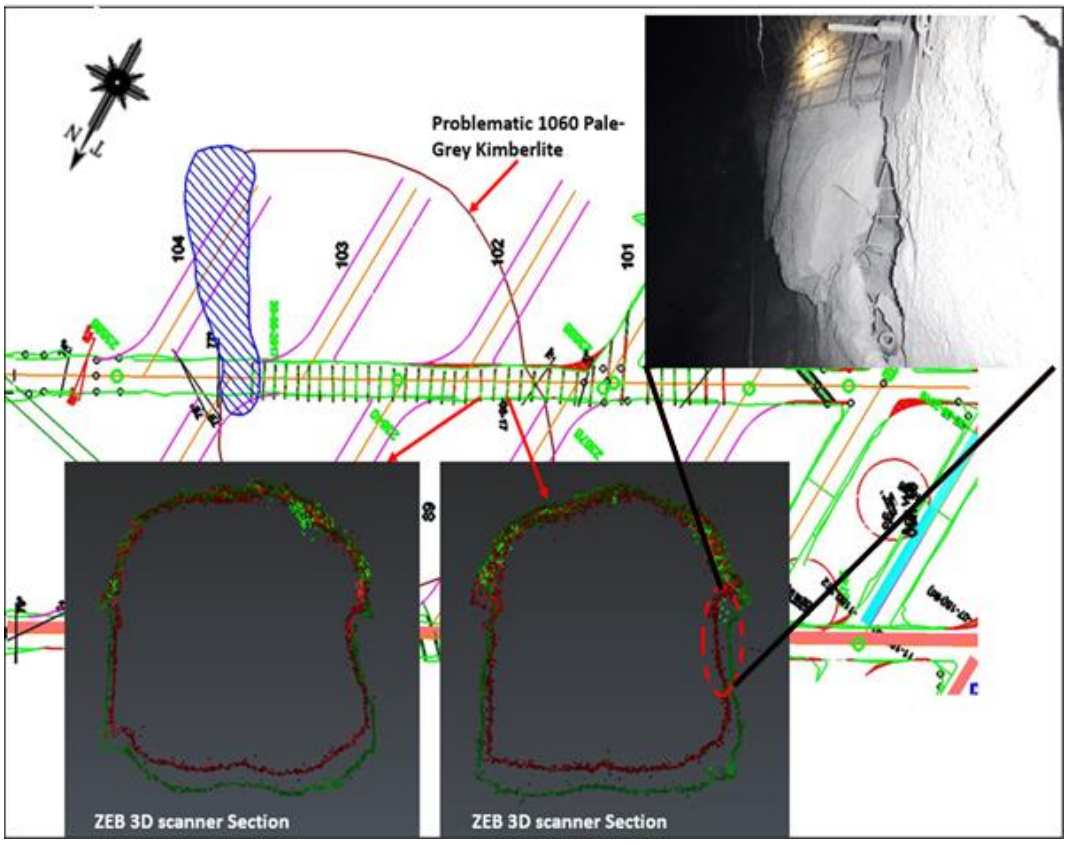


Figure 4.12: Sections showing sidewall bulging from the Mobile scanner and Images taken underground around the Pillar/1060 Grey Kimberlite area

It was later decided to continue monitoring whether the major and minor pillars would be able to maintain the load once the crosscut breakaways were open for the formation of drawpoints. Tunnel convergence ranging from 0.2 m to over 0.5 m was recorded in the period ending January 2020. This contraction was observed to be more prominent on the sidewalls especially where there were no bird cage anchors installed. Slabbing of shotcrete was the first sign of deformation followed by resin bolts and bird cage anchors being swallowed into the rock.

The scanner is limited to readings in the range of 0 – 0.5 m whether in contraction or scaling of the tunnels. This range is depicted in Figure 4.13 and 4.14. Also shown in these figures is the severe deformation experienced in T41 and T36 at the end of January 2020. This deterioration was rapid within days to a few weeks only.

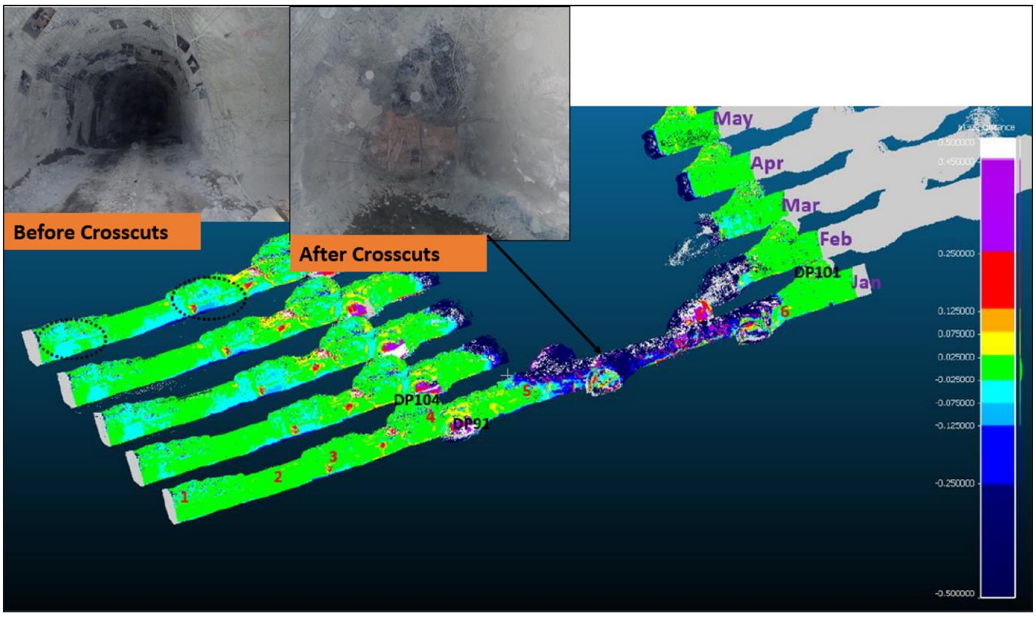


Figure 4.13: Showing T41 rock mass damage as measured by the Zeb Horizon scanner and underground observations

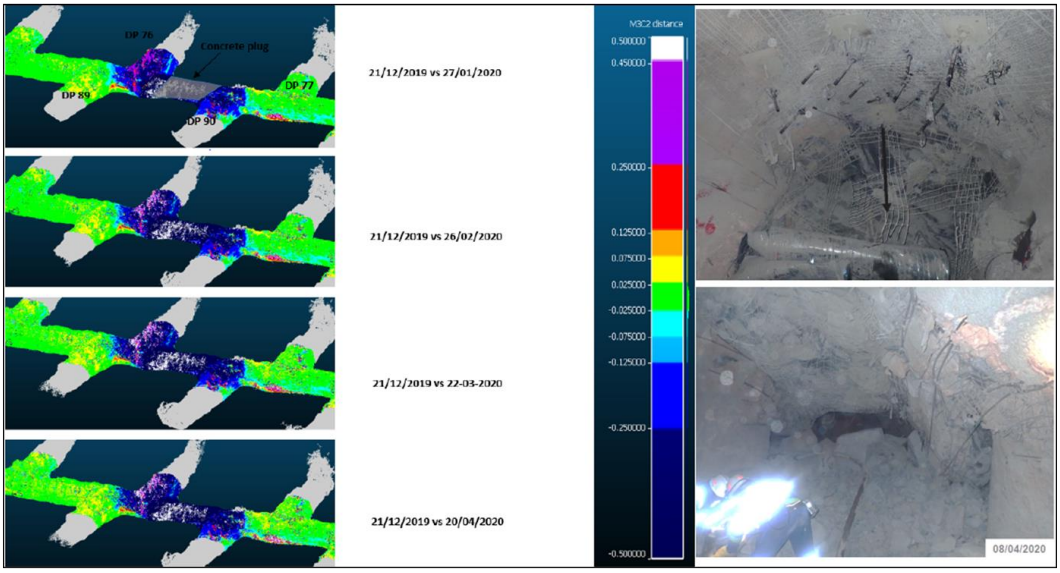


Figure 4.14: Showing T36 rock mass damage and underground tunnel closure

An example of an individual scan showing closure between DP89 and DP103 is depicted in Figure 4.15. It can be deduced that very minimal closure was recorded during this period of a week. The tunnel deformation took place rapidly at the end of December 2019 to the end of January 2020. The tunnel conditions were severe such that concrete filling the weak zone area was deemed the best solution. Monitoring at this area continued for another 4 months to ensure the effectiveness of the concrete.

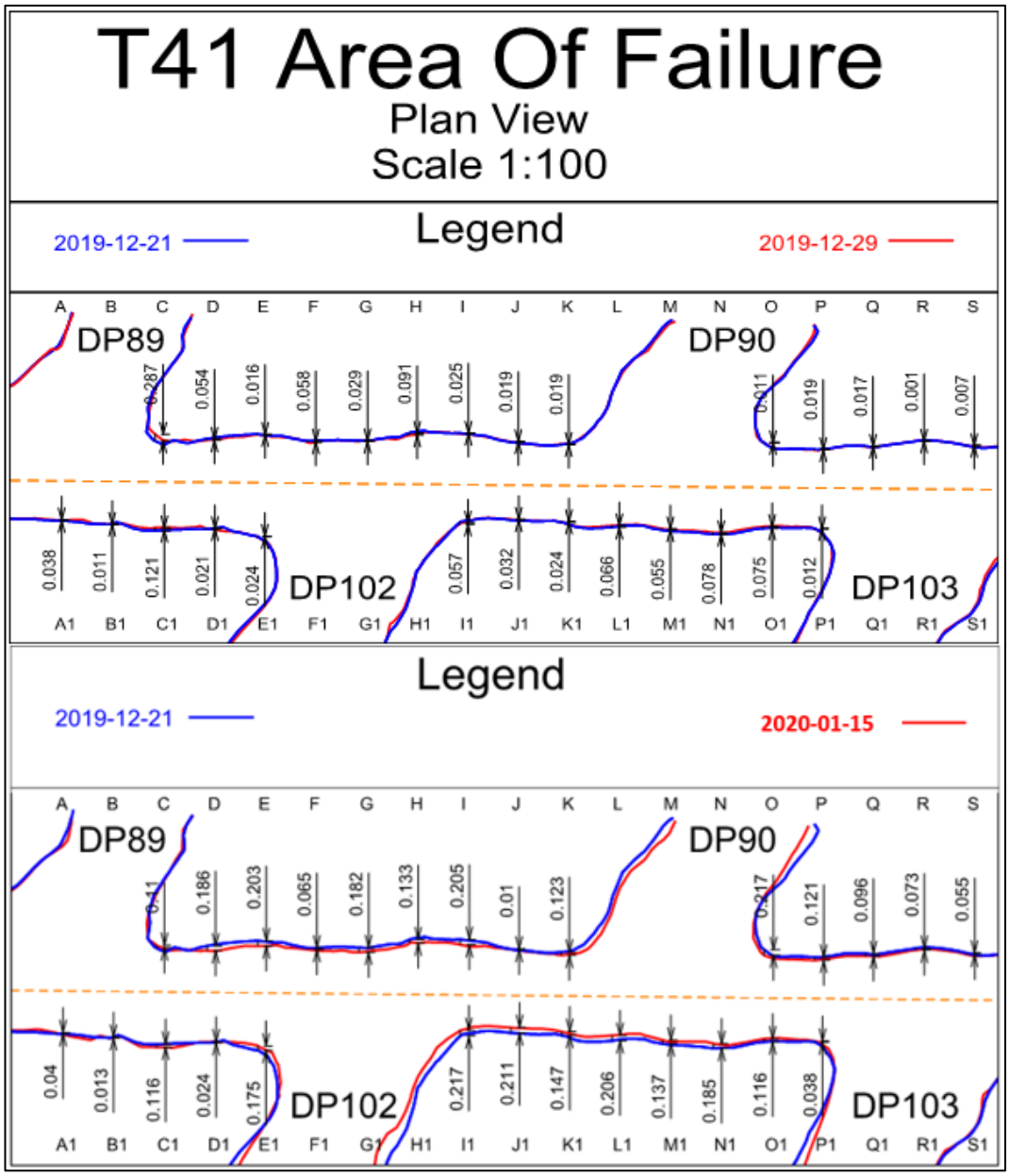


Figure 4.15: An example of the weekly scans conducted at the weak zone

Partial tunnel closure of T36 took place end of 2019 making this tunnel the first to be concrete filled. This was exacerbated by the presence of major geological structures such as dykes and the presence of water. The timelines and activities taking place in the tunnels are presented in Figure 4.16 and 4.17 with the measured displacement.

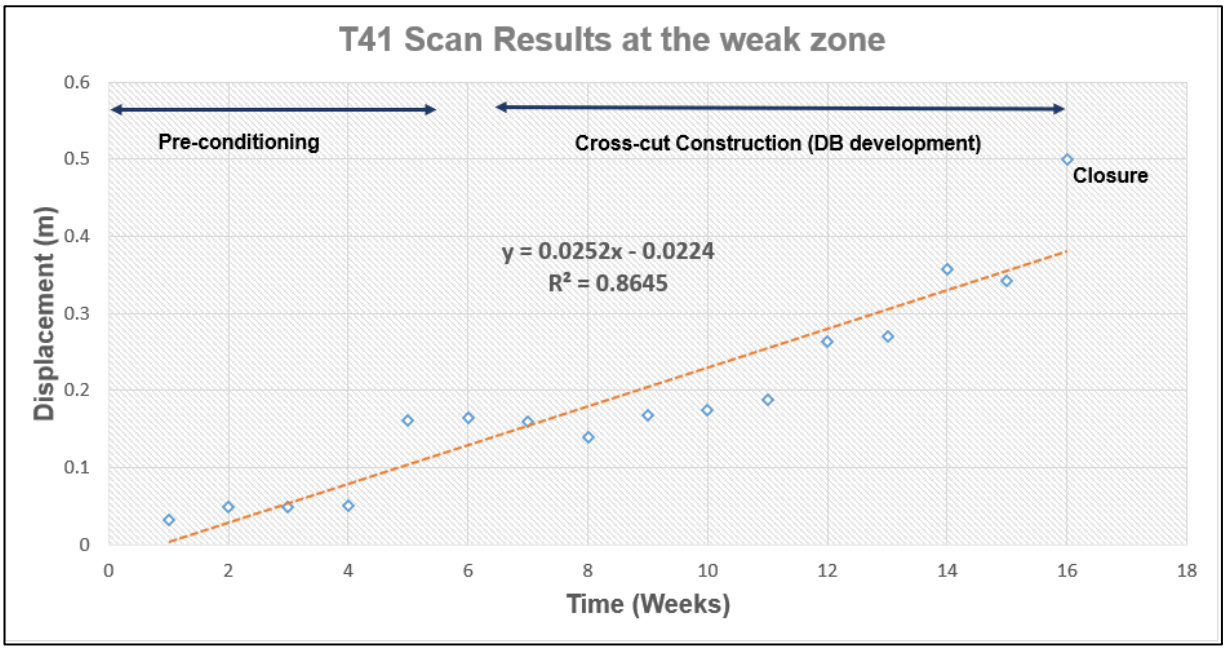


Figure 4.16: Depicting tunnel convergence at T41 and the correlation to the activity taking place

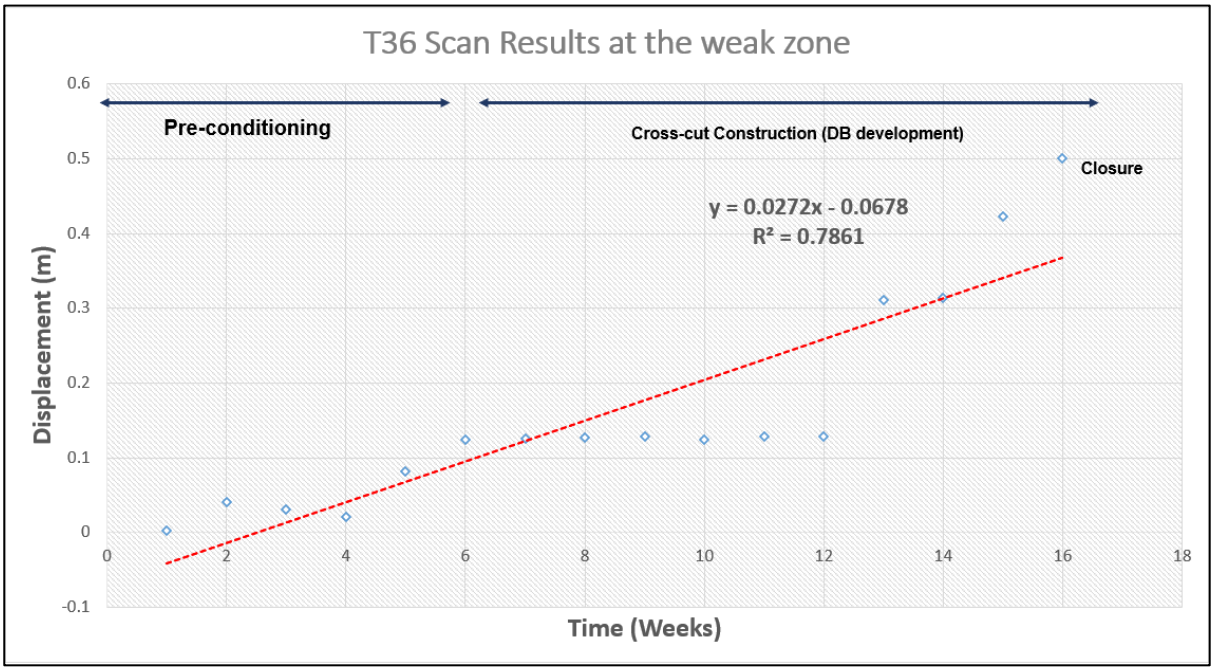


Figure 4.17: Depicting tunnel convergence at T36 and the correlation to the activity taking place

Manual laser Distomat readings were taken at 2m intervals underground bi-weekly (due to labour resource constraints) measuring both the hanging wall and sidewalls. These results are tabulated in Appendix C. The results correlate with the scan results showing a total deformation of 0.6 m sidewall to sidewall over a period of 4 months. Deformation was evident in the vertical direction, but because of the continual sliping of the footwall measurements were not possible. However, in one location where measurements were possible, 1.4 m deformation was measured between the hangingwall and footwall. The lateral deformation could not be correlated to any one side. Both sides were assumed to be equally bulging into the tunnel. Figure 4.18 shows the comparison between the scanner and laser technology.

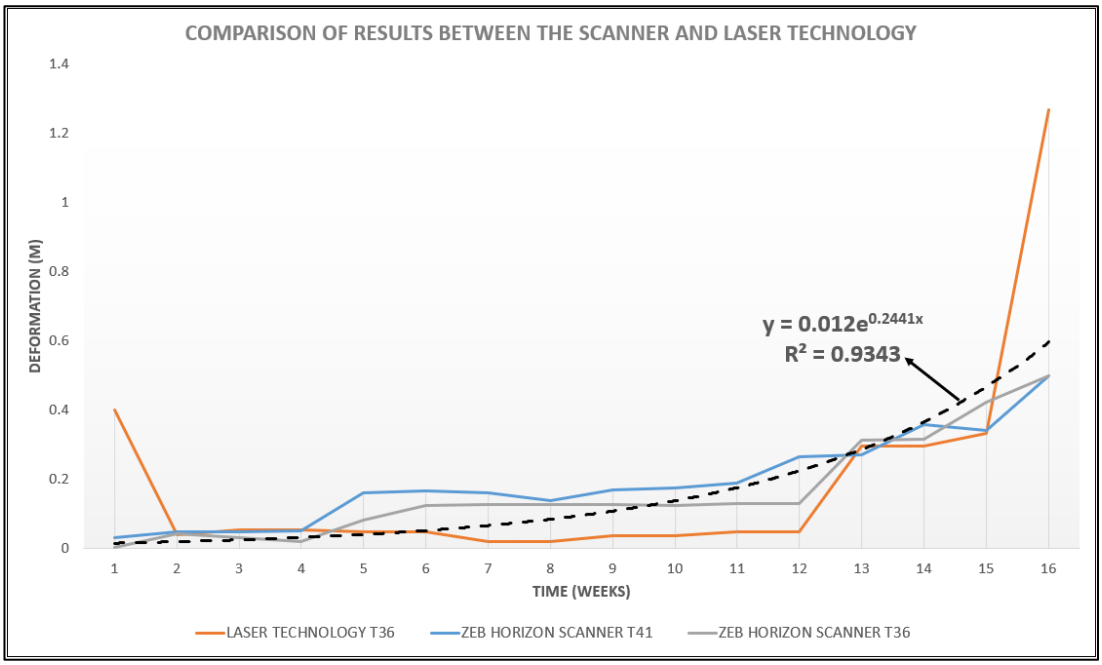


Figure 4.18: Comparison between the Zeb Horizon Scanner and Laser Technology

5. STABILITY ASSESSMENT USING THE FLAC3D NUMERICAL MODELLING SOFTWARE

FLAC3D utilises an explicit finite difference software package which deals with volume formulation. It captures the complex behaviours of several stages, and is able to show large displacements and strains, exhibit non-linear material behaviour, or even total collapses. The C-Cut block cave exhibits complex geometry with large displacements anticipated, and for this reason FLAC3D was chosen to be suitable for this research. The input parameters used in the model are tabulated below (Table 5.1). Input parameters were adopted from the internal reports of Beck Engineering (2016), and were used during the global geotechnical modelling for the C-Cut block cave. The input parameters for the different rock types are attached in Appendix F.

Table 5.1: FLAC3D input parameters

Rock Material	UCS (Average)	Density (Average)	Rock Mass Modulus (Average)	Poisson's ratio (Average)	Average Bulk Modulus	Average Shear Modulus	Average Cohesion	Average Friction Angle	Rock Mass Rating (RMR)
	(MPa)	(kg/m^3)	(GPa)		(GPa)	(GPa)	(MPa)	(deg)	
Metasediment (Host rock)	120	2900	32	0.26	14	10	2.5	45	55
1060 Pale Grey Kimberlite (1060 PGK)	60	2400	24	0.21	13.7	8.5	1.6	35	40
Hypabyssal Black kimberlite (BLK)	110	2700	30	0.21	17.2	10.6	1.9	36	60
Brown Kimberlite (BK)	60	2400	24	0.21	13.7	8.5	1.6	35	40
Grey Kimberlite (GK)	100	2700	16	0.27	11.6	6.3	1.3	35	45

5.1 Strength Criterion

The constitutive models for both the Hoek-Brown and Mohr-Coulomb (M-C) strength criteria are available in FLAC3D. The former does not follow a traditional/typical constitutive model thus takes significantly longer to solve than the latter (Saiang et al., 2014). For this reason, the M-C strength criterion was used for this research. The shear strength of a rock mass is usually described by a Coulomb criterion with two strength components: a constant cohesion and a normal-stress-dependent friction component. An elasto-plastic, perfectly plastic material behaviour was applied to the model.

5.2 Failure Criterion

The failure criterion utilised in this report is the strain criterion where the onset of fracturing occurs at 1.5% strain and total failure occurs at 5% strain. This was calibrated using data from upper levels (as utilised by the Beck Engineering in the regional model).

5.3 Model set-up

The extrude command was used in this model to obtain the third dimension from the plan view. According to the FLAC3D manual (Itasca, 2021), An extrusion is a 2D geometric description of a model, which can be extruded in the third dimension, specified by an extrusion vector, to create FLAC3D zones.

Points are created in space, connected by edges, which are themselves connected into blocks. Edges are either linear or curved, in which case they follow a path given by control points. Blocks of two types can be created using the ‘Extrude’ function: blocks with structured mesh referred to as “regular blocks” (these are typically 4 sided blocks) and blocks with unstructured mesh referred to as irregular blocks. These blocks may have a convex or concave boundary and may be multiply connected and/or contain nested blocks. Both structured and unstructured meshes consist of triangular and/or quadrilateral elements. Upon extrusion, a single zone (brick or wedge) will be created from each element of the mesh. Figure 5.1 shows the 2D geometry created to develop the 3D model using the ‘extrude’ function.

Number of zones and their ratio can be assigned for every edge and propagate automatically across all regular blocks attached to the edge. However, these parameters are unique for every edge in an irregular block; upon any changes of the edge parameters, including vertex locations, the unstructured mesh must be re-created.

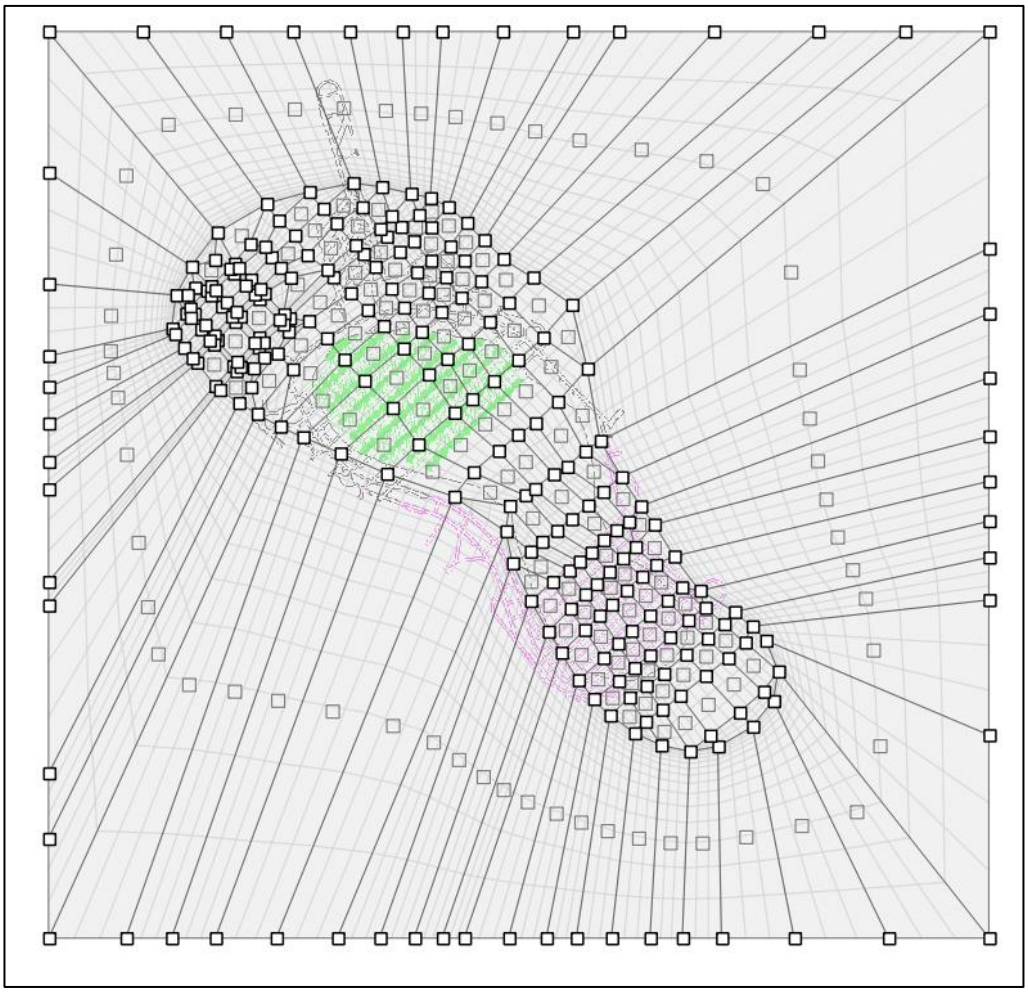


Figure 5.1: Snapshot from the FLAC3D Software illustrating an example of the Extrude file

The following describes the layout as modelled in FLAC3D:

- The boundaries of the model were placed/fixed sufficiently far such that they do not impact the results. For example, the boundaries were placed at least 2 times the width of the pipe at the elevation of interest.
- The Z component is fixed at -1240m. The X component is fixed at 225 and -804 while the Y component is fixed at 737 and -254 depicted in Figure 5.2.

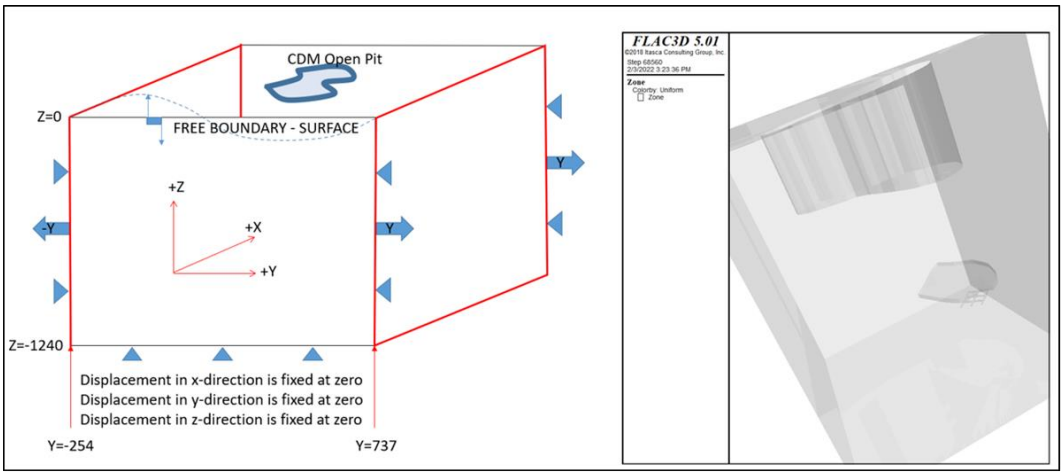


Figure 5.2*:* Showing the schematic diagram of the boundary conditions and model set up - note that the open pit excavation was included in the model and was simulated as a separate mining step between the pre-mining phase, and the underground development phase

- The tunnels where 1060 PG kimberlite is present are situated 839m below surface (extraction level) while the undercut level is situated 824 mbs.
- The zone sizes were reduced to 0.5 m around the three tunnels simulated in the 1060 Pale Grey kimberlite, which resulted in many zones (considered to be a large model) resulting in a rather slow solving process. To reduce the overall number of zones in the model, the ratio command in FLAC3D was used to discretise the zones around the North-East (N-E) corner of the extraction level. This command allows smaller zones to be created around the area of interest (in this case the N-E extraction level tunnels in the 1060 Pale Grey kimberlite), with larger zones created progressively away from the area of interest.

- The Metasediment host rock and the different kimberlite facies (Black Kimberlite, Grey Kimberlite, Brown Kimberlite and 1060 Pale Grey Kimberlite) was included in the FLAC3D model, as per the updated geological model received via email from the Geology Department (Figure 1.7) and presented in the model as per Figure 5.3.

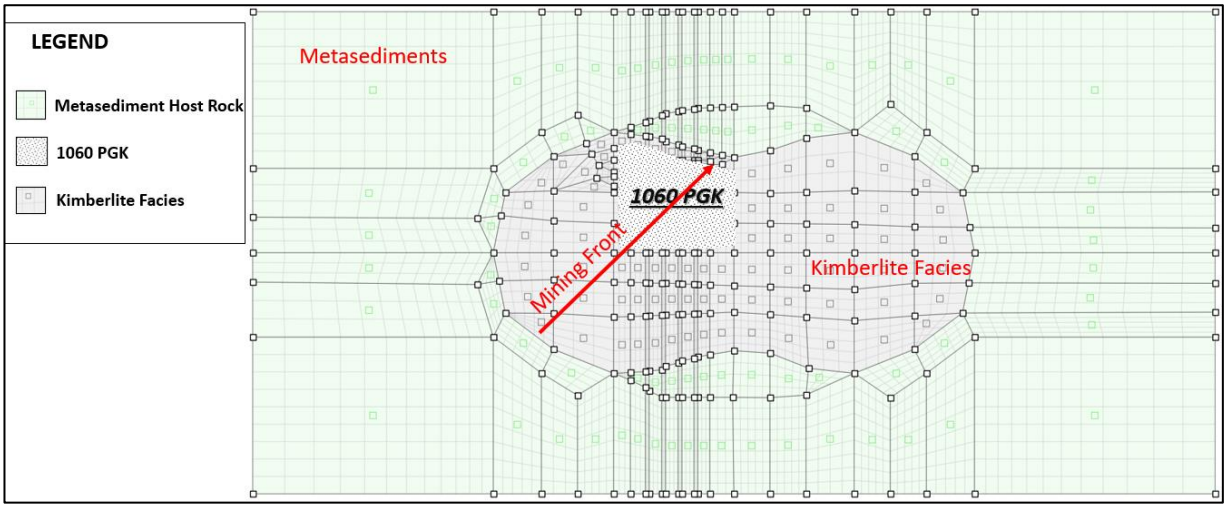


Figure 5.3: Showing an Illustration of the Hosting Rock and different Kimberlite Facies

- Simulations were done for DP spaced 24m apart (a layout change to cater for the weak kimberlite) which did not form part of the regional modelling initially done for the feasibility study of the C-Cut block.
- Critical steps to the 1060 PGK analysis at the extraction level were as follows and shown in Figure 5.4:
    - Mining Step 0: putting tunnels across the footprint (only 3 tunnels were considered for this study).
    - Mining Step 1: 10% undercutting through Grey Kimberlite
    - Mining Step 2:
    - Mining Step 3: 30% undercutting

- Mining Step 4: 45% undercutting (still following the mining front)
- Mining Step 5: 60% undercutting
- Mining Step 6: Current undercut face at 75% undercutting (loss of the undercut tunnels resulting in uncaved material)
- Mining Step 7: 90% undercutting

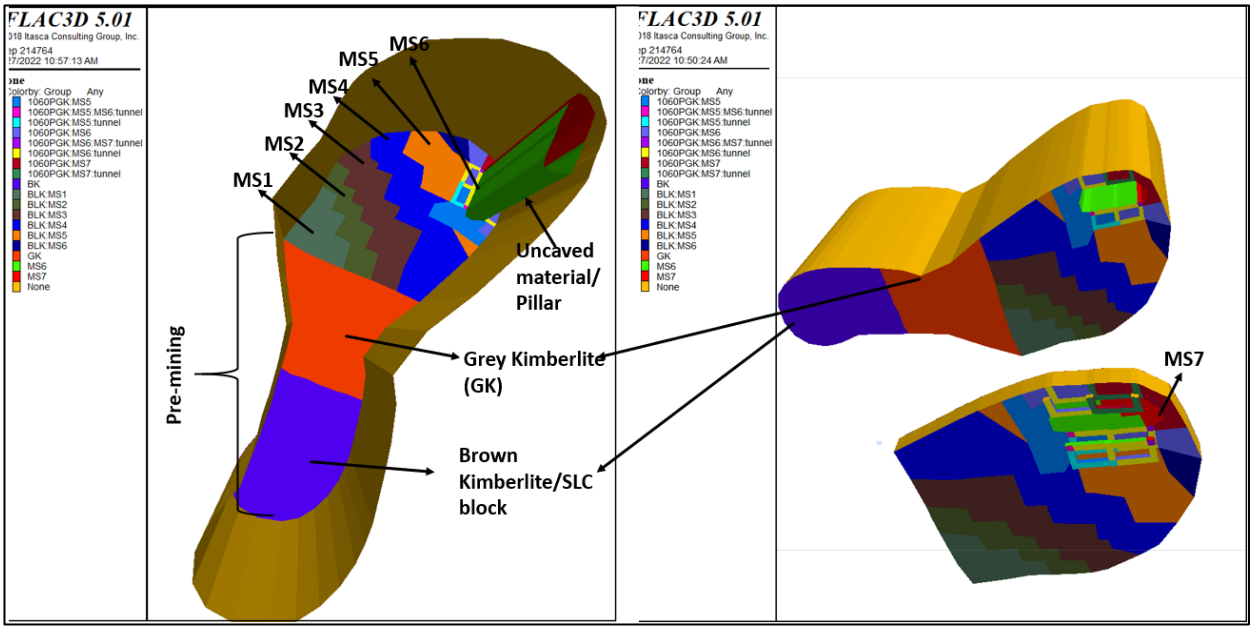


Figure 5.4: Illustrating Sequencing of the Weakzone

Restrictions / limitations of this model:

- The sub-level caving in the Brown Kimberlite were included as part of the current mining, however the zones sizes were larger as it was outside the area of interest (1060 Pale Grey). The model, although complete in extents, may therefore not be used to interpret the rock mass response in the sub-level cave area.
- The drawbells have not been explicitly included in this model, however it should be noted that the last 25% footprint of the undercut

level was lost, and the draw bells were not yet completed by then although deformation was already evident.

- The modelling approach is to evaluate the impact of the retreating cave front on the tunnel excavations (which would impact the drawbells in a similar manner). Even if the draw-bells are included in the model explicitly, the stresses due the retreating cave completely dominate the potential local stress interaction (local stress interaction between the development excavations is noticeable during the development phase, however it is less substantial compared to the stress changes as a result of the retreating cave front).
- No discontinuities were simulated as part of this study.
- No support elements have been simulated in this study.
- Figure 5.5 is an illustration of the mining sequence as simulated in FLAC3D with the sequencing done in a total of 18 steps going through the different facies.

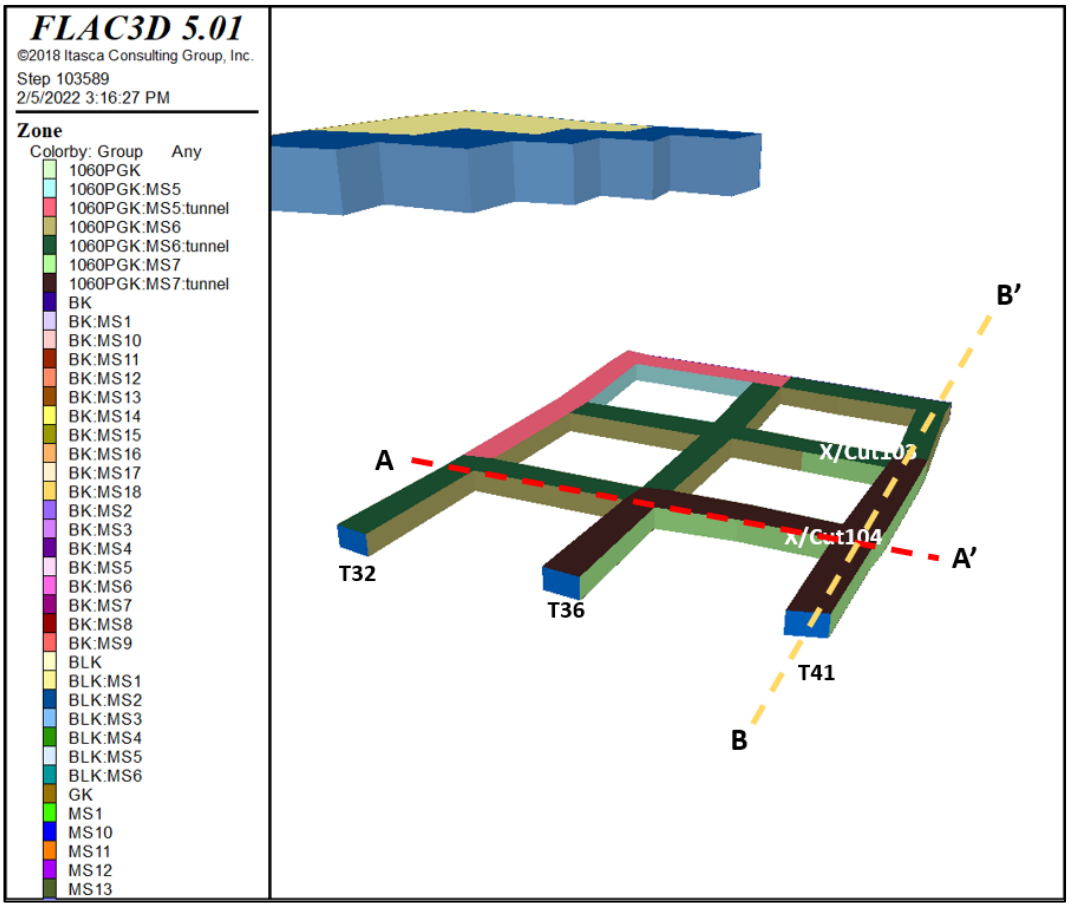


Figure 5.5: Snapshot from FLAC3D model showing excavations relative to each other and relative to the undercut – note that 18 mining steps were scheduled in the FLAC3D model to simulate the development sequence and cave retreat

5.4 FLAC3D Results and Analysis

In all mining engineering projects, there is an in-situ state of stress in the ground before any excavation is opened. In FLAC3D, an attempt is made to reproduce this in-situ state by setting initial conditions as shown in Figure 5.6. Ideally, information about the initial state comes from field measurements. But, when these are not available, the model can be run for a range of possible conditions.

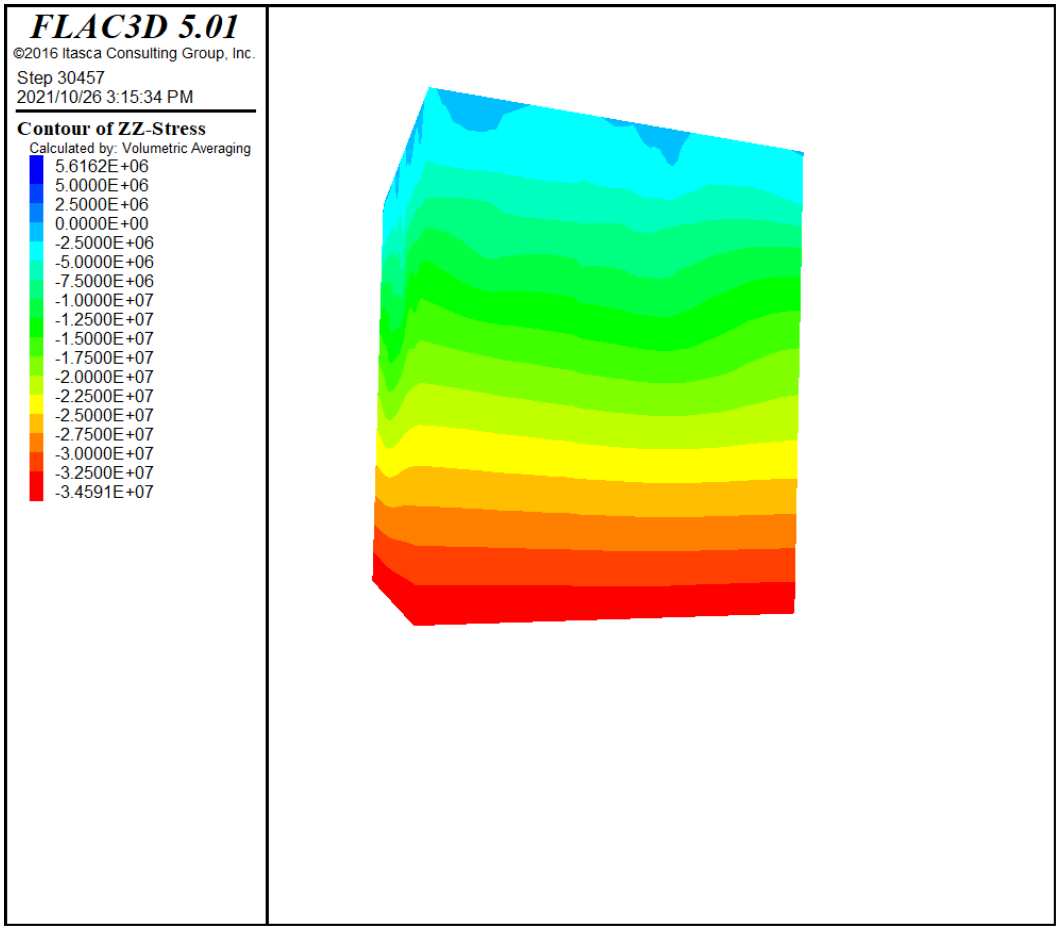


Figure 5.6: showing increasing stress with depth

As mentioned before, the criterion used in the model was derived from work initially conducted by an Australian based company during the feasibility study of the C-Cut block cave (Beck, 2016). The strain criteria suggest that an onset of fracturing will occur at 1.5% while serious damages will occur at 5% strain. The same 5% was also adopted in the analysis for this research. The cave propagation is illustrated in Figures 5.7 to 5.9 with significant excavation failure only at mining step (MS) 6 which translates to 75% undercutting.

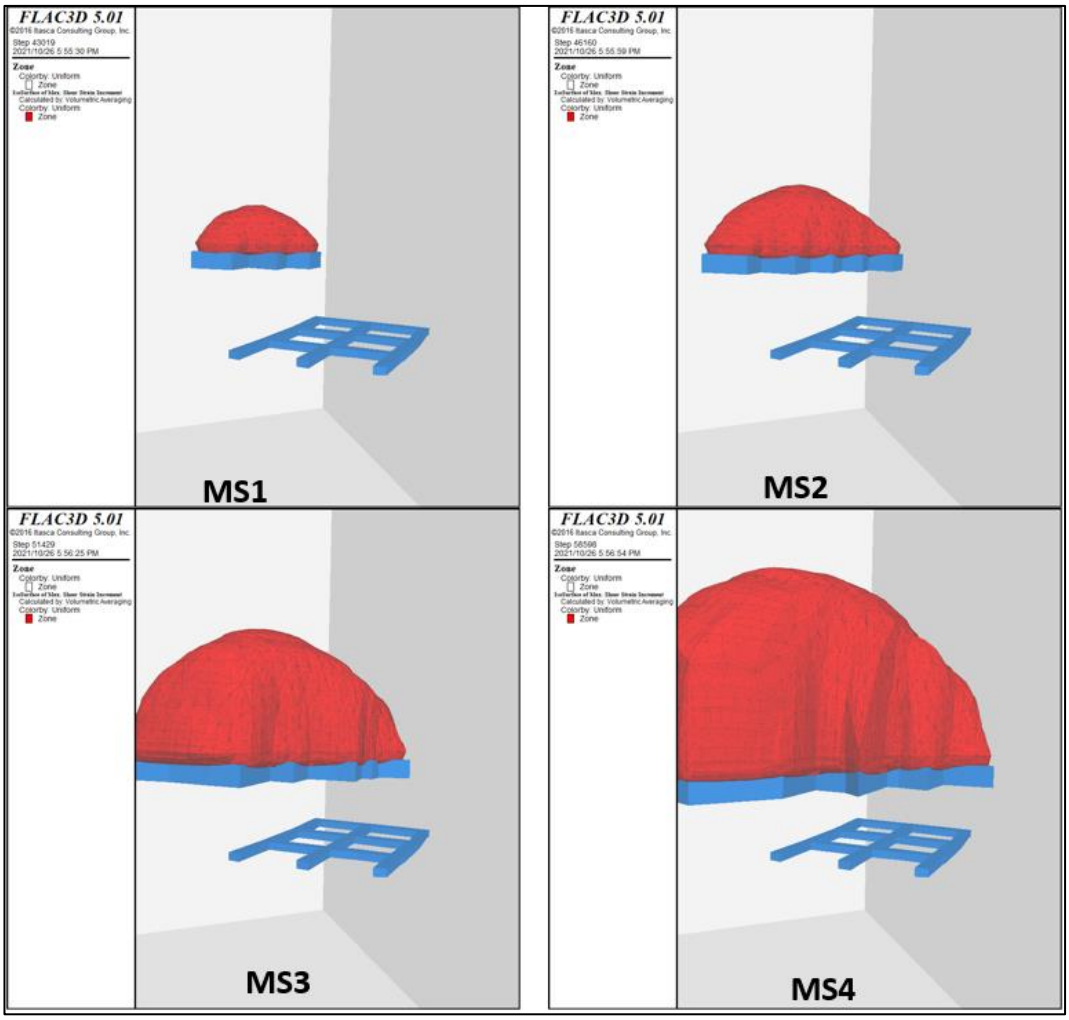


Figure 5.7: Illustrating mining steps and an increasing cave propagation with each step (ideal/strong kimberlite throughout the footprint of the C-Cut block cave)

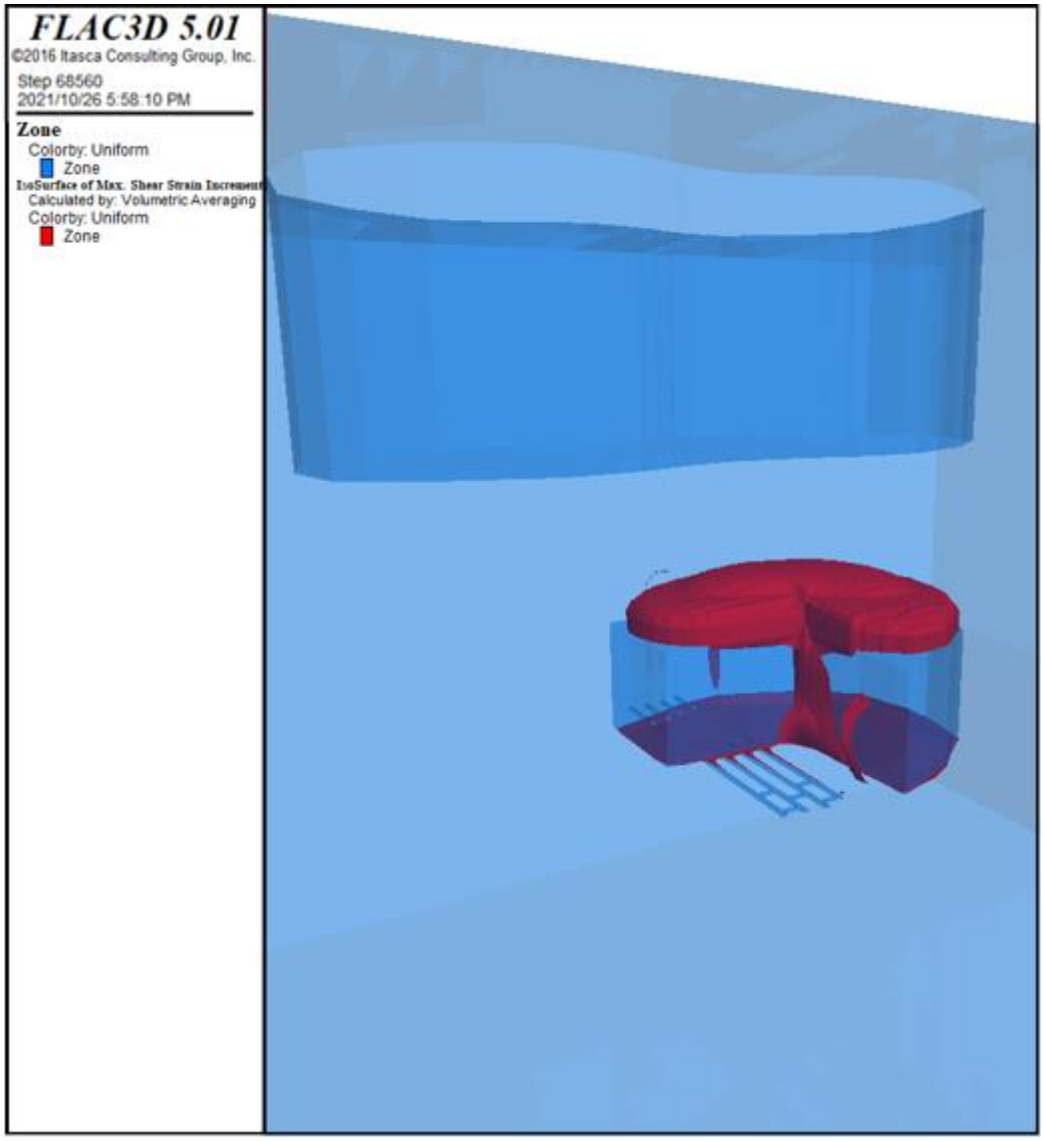


Figure 5.8: Illustrating damage at the weakzone (mining step 5 of the C-Cut cave still on strong/Black kimberlite)

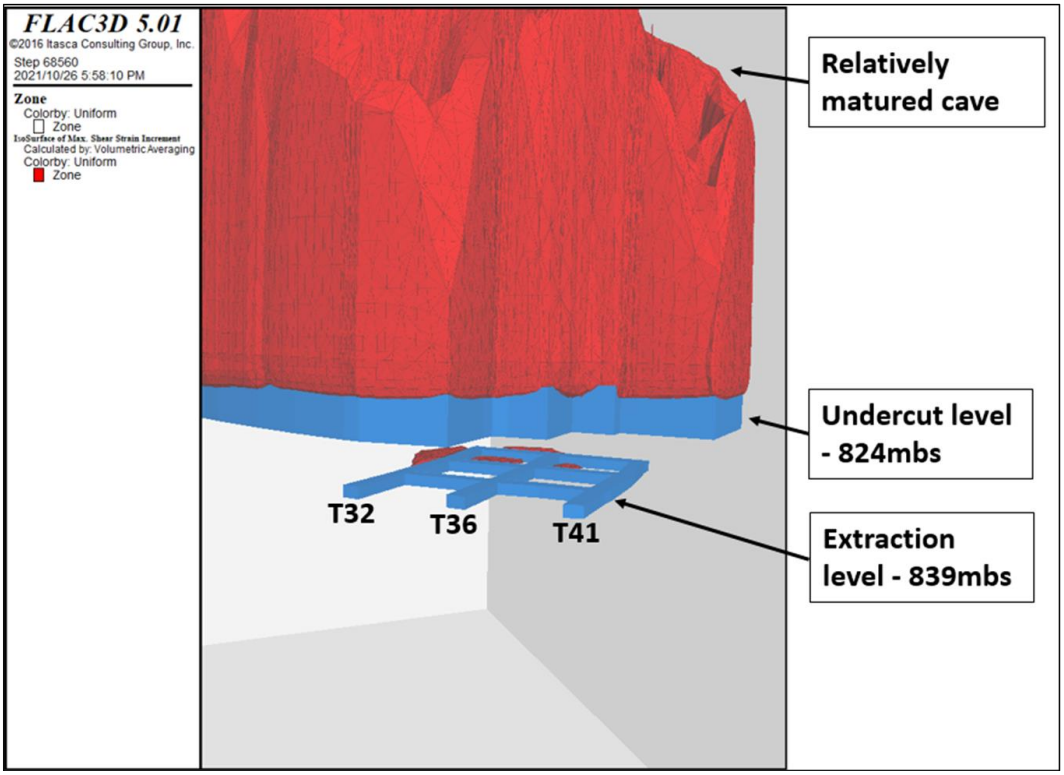


Figure 5.9: Showing shear failure on the extraction level at 75% undercutting (MS6)

An unbalanced force plot was determined to check the reliability of the model. Each grid point is connected to zones that contribute forces to the grid point. At equilibrium, the algebraic sum of these forces is almost zero (i.e., the forces acting on one side of the grid point nearly balance those acting on the other). If the unbalanced forces approach a constant non-zero value, this indicates that failure and plastic flow are occurring within the model. A rule of thumb is that an average force ratio of 1e-5, a local force rat 1e-4, or a convergence of 1.0 mm all indicate overall convergence. For this model, the unbalanced force plots are presented in Figure 5.10 and Figure 5.11 for mining steps 1-4 and 5-7, respectively.

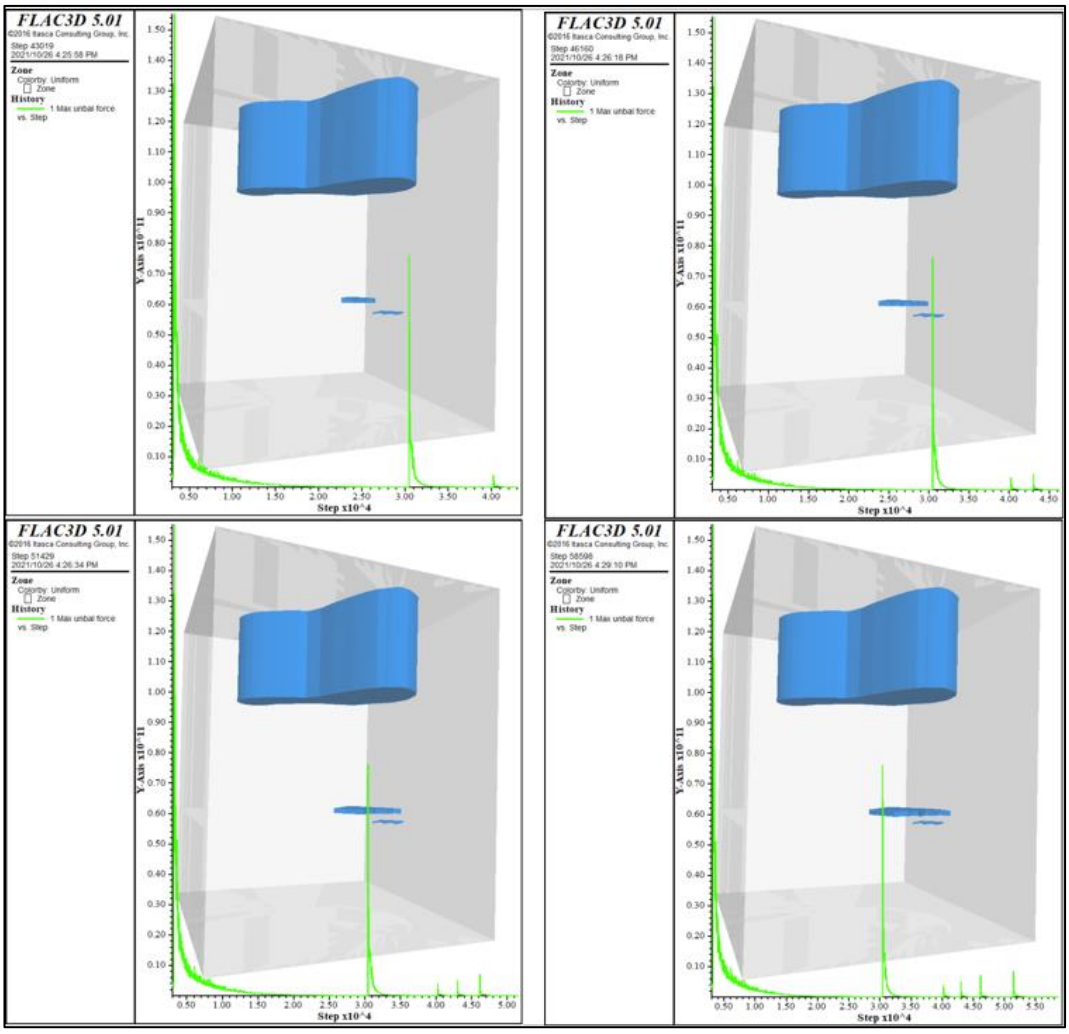


Figure 5.10: Illustrating and unbalanced force for MS1 to MS4

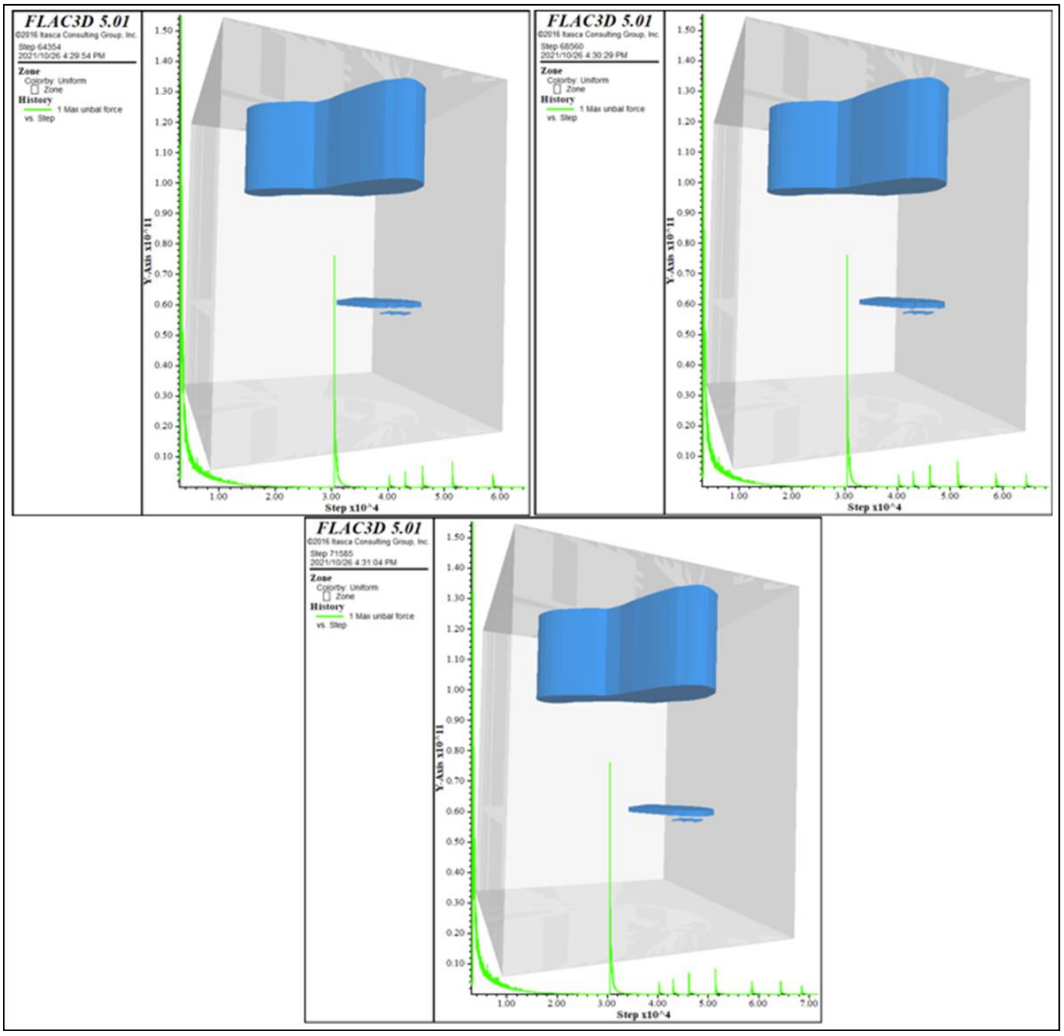


Figure 5.11: Illustrating unbalanced forces for MS5 to MS7

The displacements determined by the model range from 0.045 m to 0.5 m which is in line with measurements taken underground using the mobile scanner and the laser technology discussed in detail in Chapter 4. The displacement increases as the abutment zone approaches the tunnels and crosscuts on the extraction horizon. MS 1 and MS2 recorded 0.045 m and 0.064 m respectively along line BB' in Figure 5.5. Line AA' is a section along X/Cut 77, 91 and 104 showing the three tunnels while the BB' line is a section along T41 showing X/Cut 89 opposite 102, 90 opposite 103 and 91 opposite 104. This increase in dispalcement is shown in Figure 5.12, and

these numbers are expected in this mining environment as stress changes often occur during the mining cycle.

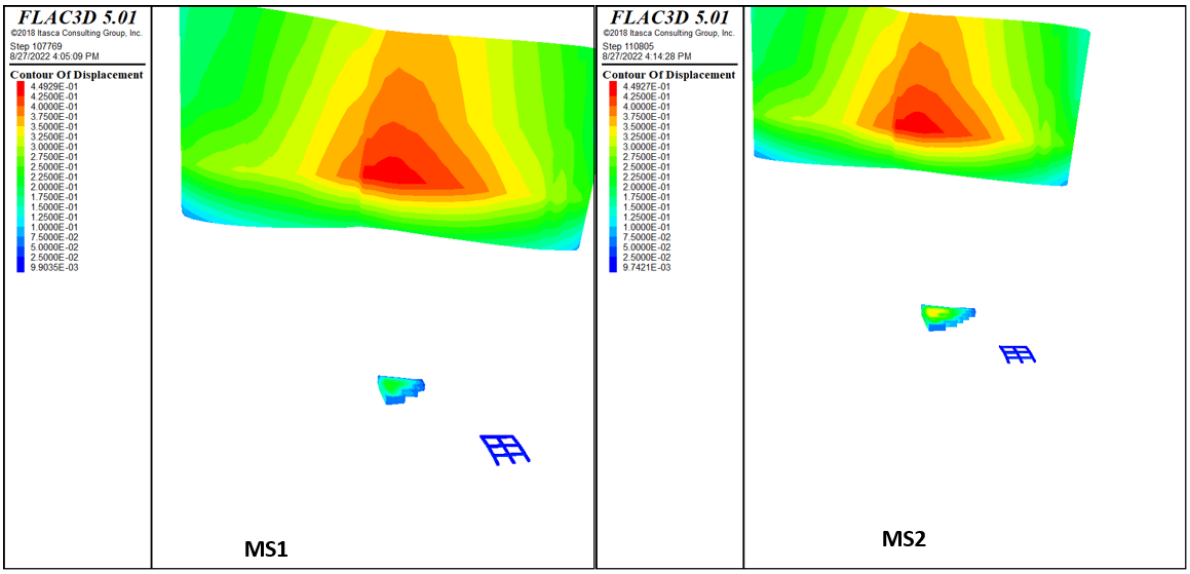


Figure 5.12: Displacement depicted at the weak zone for MS1 and MS2

As the mining front moves towards the NE corner, the weak zone starts to deform though not in large displacement values. At MS3 and MS4 the displacement values for both the tunnels and crosscuts were 0.082 m and 0.145 m respectively. This phenomenon is depicted in Figure 5.13.

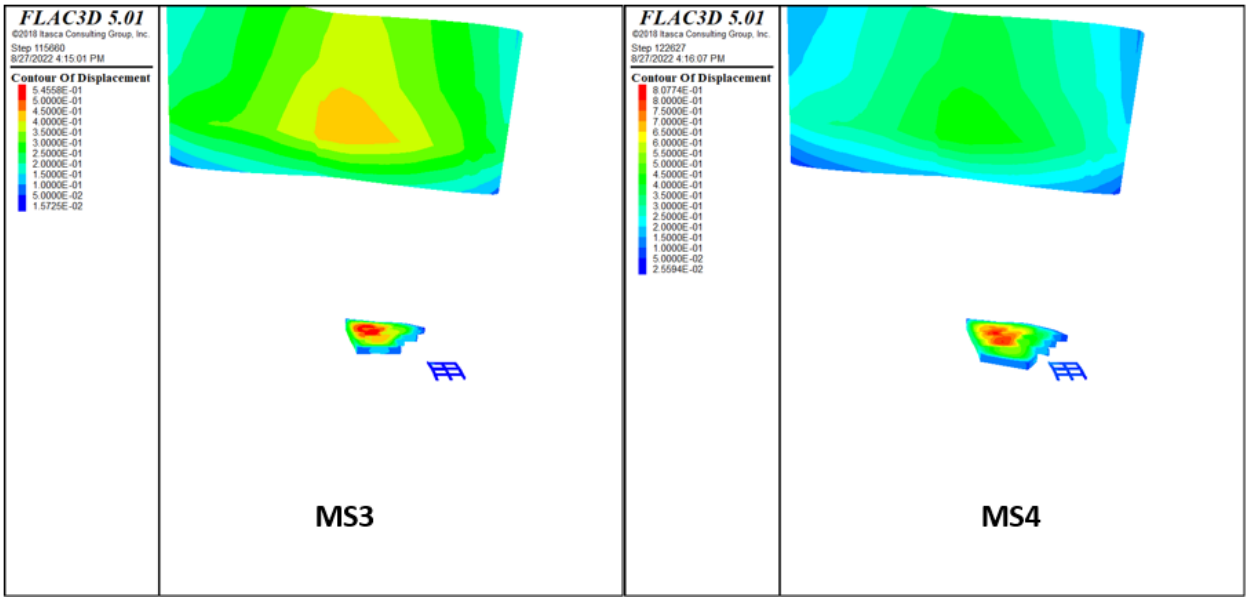


Figure 5.13: Showing contours of displacement for MS3 and MS4 for the weak zone

Similar trends were observed at MS5 where the displacement was predicted to be 0.27 m. The major rock mass instability occurred at MS6 with displacement as high as 0.42 m. This is in line with underground measurements discussed above. Figure 5.14 shows the displacement at the end construction phase of the undercut or 75% undercutting.

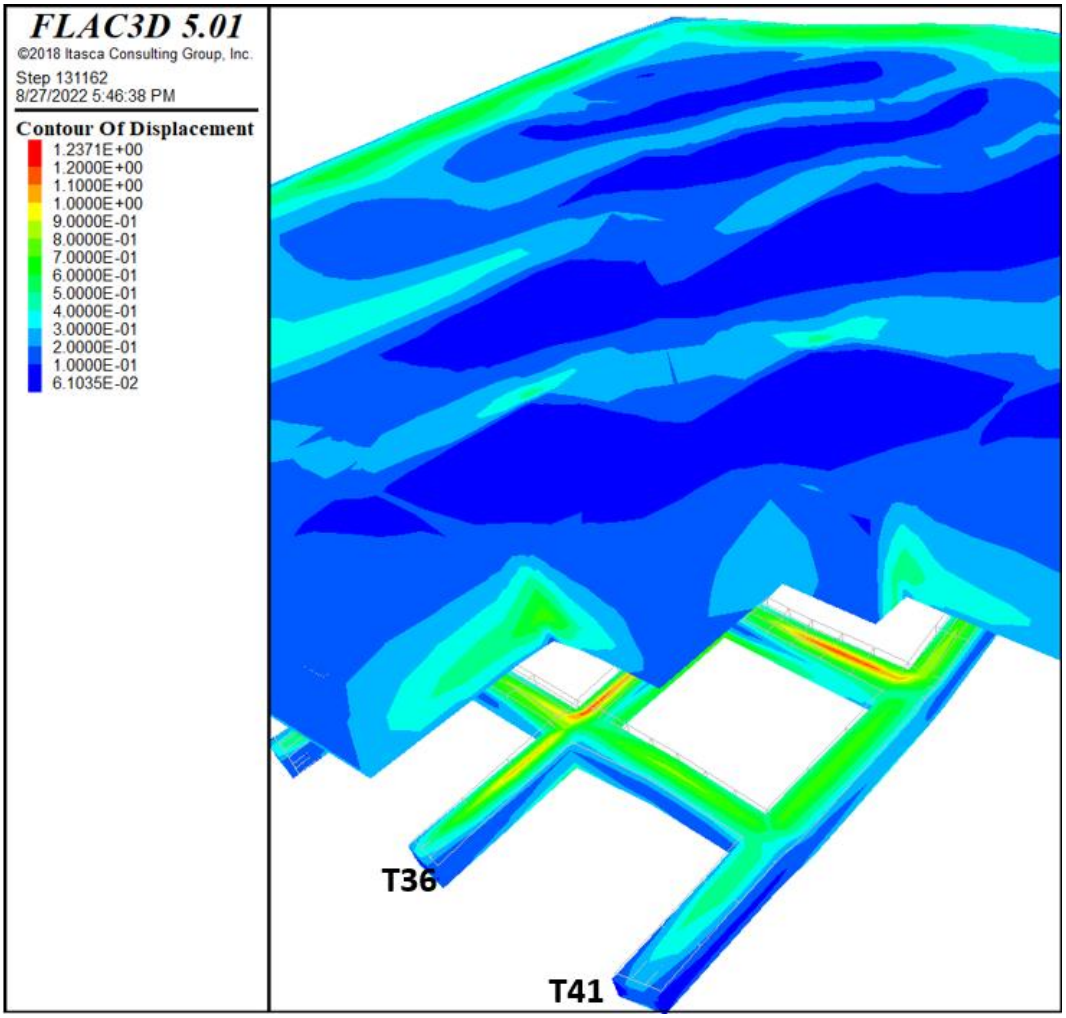


Figure 5.14: High displacement at the end construction phase (MS6)

Sections were taken in two directions along T41 (outer most tunnel) to understand the state of the individual cross cuts. This is shown from Figure 5.15 to Figure 5.19.

As expected, minimal displacement was recorded at the excavations in the NE corner during the early stages of the mining block. This is also evident in Figure 5.16.

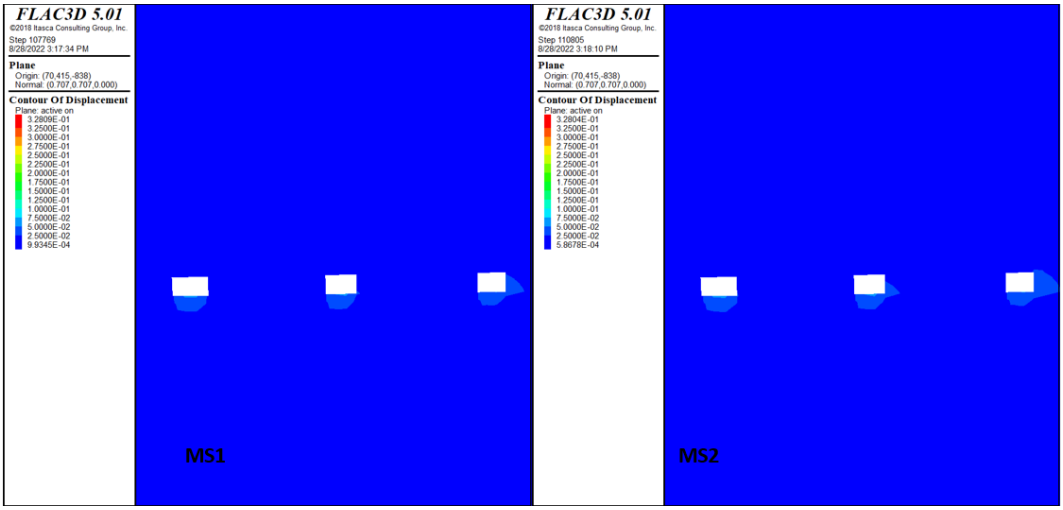


Figure 5.15*:* Contours of displacement – Long section along T41 Showing X/Cuts at the weak zone (MS1 and MS2)

At MS4 it can be deduced that the onset of failure was starting. The excavations are beginning to be affected by the undercut mining front. Practically, this was evident through the scaling/slabbing of shotcrete, opening up of existing geological structures, formation of new fractures and support units being swallowed into the rock while the rock mass around bulges into the tunnel.

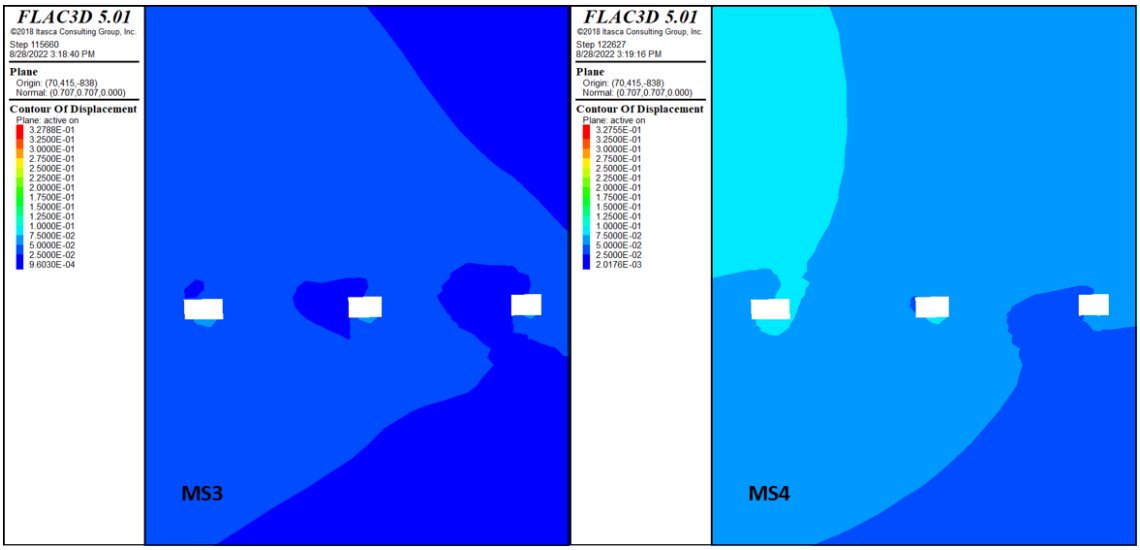


Figure 5.16: Contours of displacement Long section along T41 at the weak zone (MS3 and MS4)

Significant displacement was recorded at MS5. A close look at the affected crosscuts is presented in Figure 5.17. The affected crosscuts are (named after DP) DP102 in T41 and DP 89 also in T41. The following was noted from the model:

- Cross cuts are located right below the abutment zone of the undercut mining front.
- Footwall heave is predominant at this stage
- Sidewall closure is in the range of 0.24 - 0.25 m which is in line with underground measurements

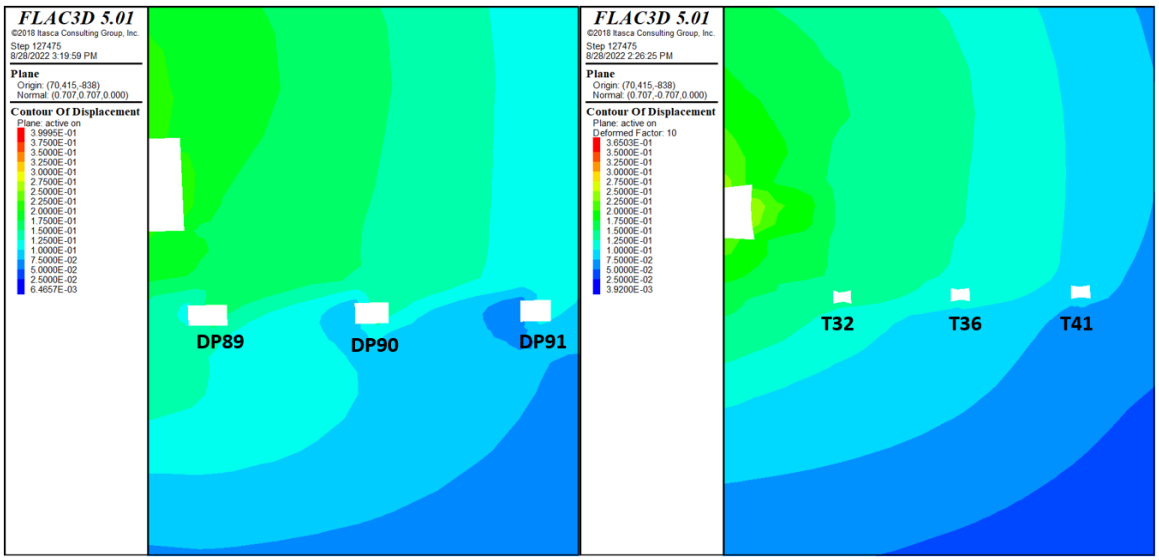


Figure 5.17: Contours of displacement (Left – Long section along T41 at the weak zone, Right – section along X/Cuts showing Tunnels)

Affected crosscuts at MS6 include DP90 and DP76 at T36 as well as DP103 and DP90 at T41. Summary of results (presented in Figure 5:18) as observed from the model are as follows:

- Crosscuts are within the abutment zone

- Footwall heave is prominent possibly due to the rock mass strength and this is presented in table 5.1 and 5.2.
- Sidewall closure is the range of 0.33 – 0.42 m depending on where the measurement is taken (Tunnels or X/Cuts) and this is in line with underground observations. High closure rates are representative of significant damage in pillar cores.
- The roof of the crosscuts also sags but only between 0.16 – 0.18 m which is the least closure compared to sidewalls and footwall heave.

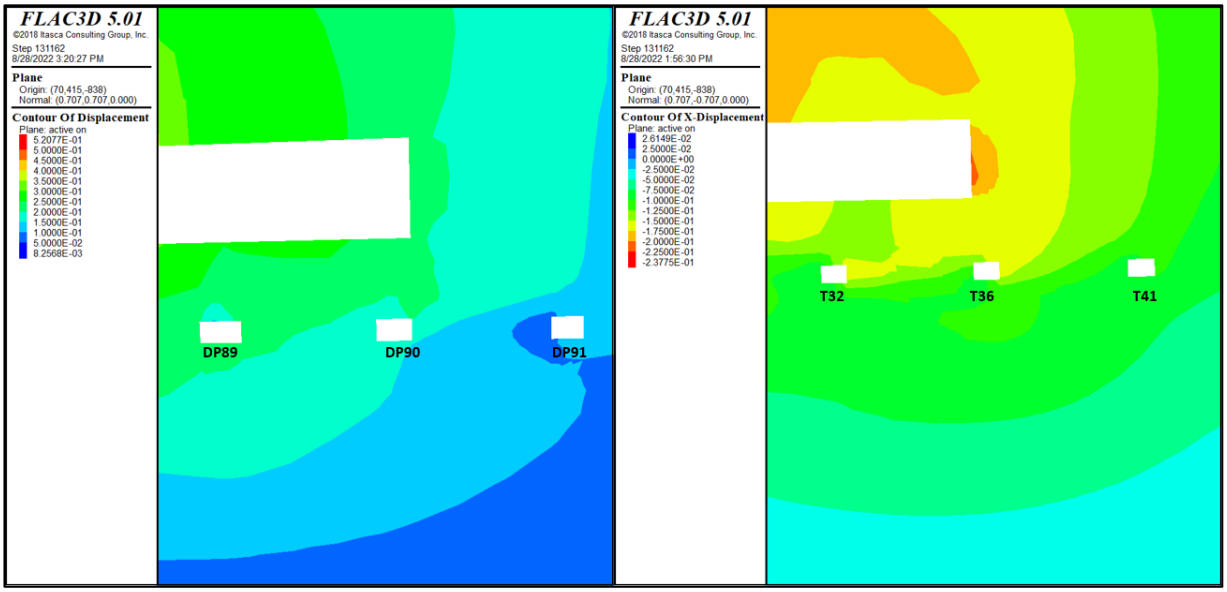


Figure 5.18: Depicting contours of displacement – Long section along T41 at MS6

Table 5.2: Section Along X/cuts Showing Tunnels (T32, T36 & T41 *)*

MINING STEP	HANGING WALL	FOOTWALL	LEFT SIDEWALL	RIGHT SIDEWALL	TOTAL SIDEWALL
MS1	0.019	0.052	0.027	0.032	0.059
MS2	0.02	0.053	0.029	0.035	0.064
MS3	0.029	0.059	0.036	0.046	0.082
MS4	0.06	0.083	0.065	0.08	0.145
MS5	0.11	0.12	0.11	0.13	0.24
MS6	0.16	0.17	0.17	0.16	0.33
MS7	0.17	0.24	0.23	0.21	0.43

Table 5.3*:* Section Along the T41 Showing X/Cuts (DP89, DP90 & T91)

MINING STEP	HANGING WALL	FOOTWALL	LEFT SIDEWALL	RIGHT SIDEWALL	TOTAL SIDEWALL
MS1	0.021	0.052	0.023	0.022	0.045
MS2	0.023	0.053	0.021	0.025	0.046
MS3	0.03	0.063	0.026	0.039	0.065
MS4	0.069	0.096	0.068	0.077	0.145
MS5	0.16	0.15	0.12	0.15	0.27
MS6	0.18	0.25	0.2	0.22	0.42
MS7	0.21	0.27	0.24	0.26	0.5

Affected crosscuts at MS7 (complete mining of the undercut) include DP91 and DP77 at T36 as well as DP104 and DP91 at T41. Summary of results (presented in Figure 5:19) as observed from the model are as follows:

- Outer most drawpoints situated close to the contact zone between kimberlite and the host rock (metasediment).
- Compared to adjacent DPs, these crosscuts experienced the most closure on sidewalls while footwall heave was still occuring.

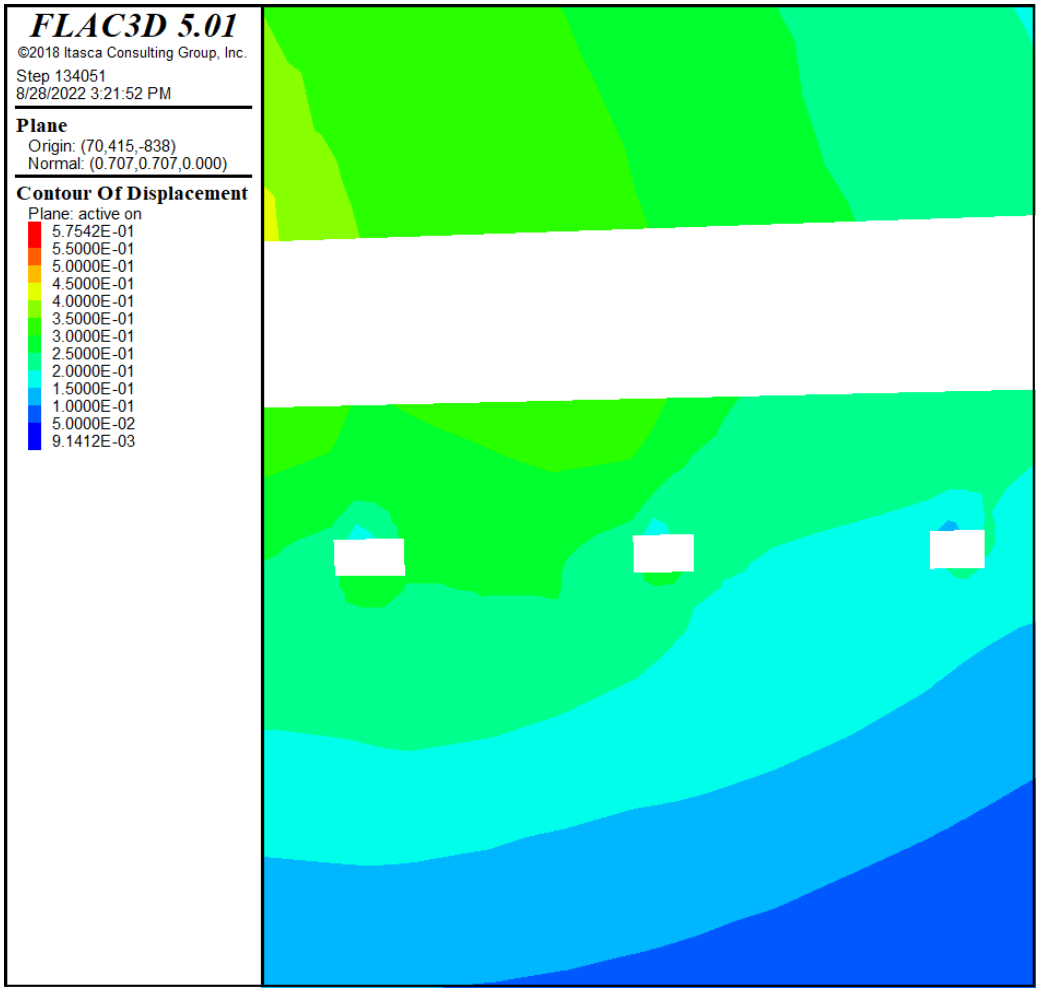


Figure 5.19: Depicting contour of displacement – Long section along T41 at MS7

Deformation as measured on FLAC3D is plotted in Figure 5.20. The relationship between the mining step and displacement is given by equation:

$$y = 0.0828x - 0.1181 \quad (9)$$

where the regression (R^2) = 0.909.

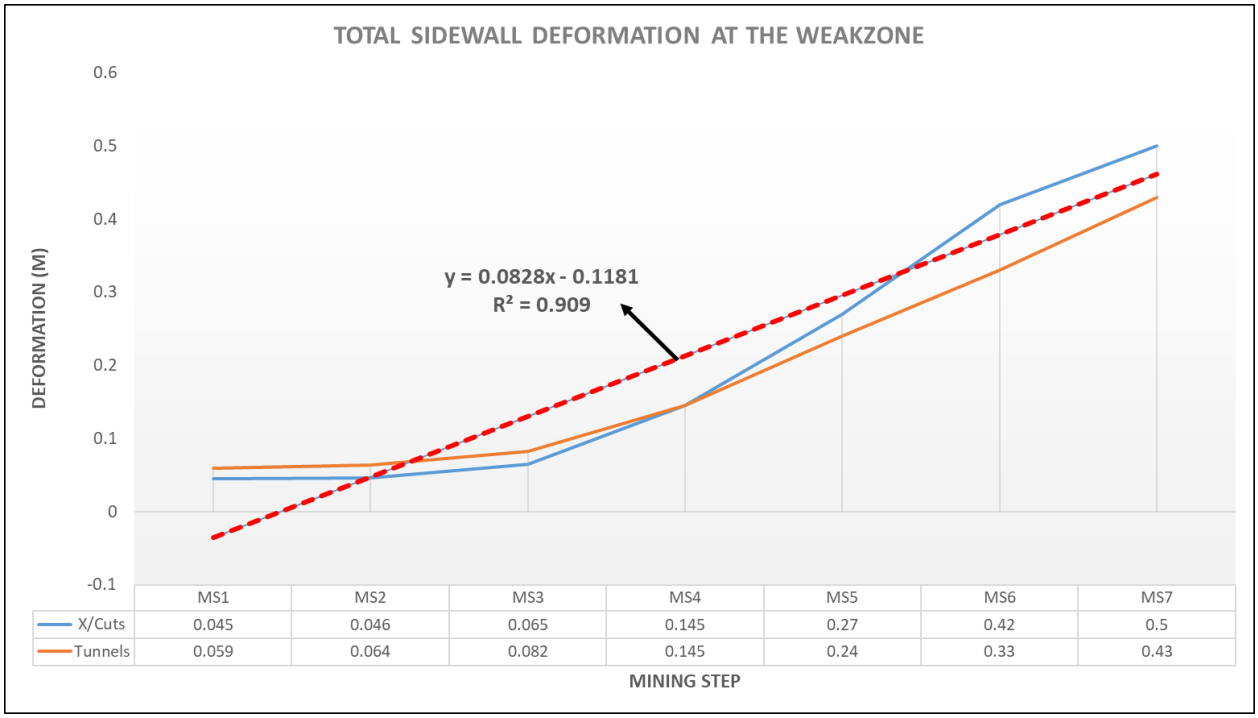


Figure 5.20: Deformation Measured using FLAC3D

6. DISCUSSION

The numerical modelling results using FLAC3D show considerable damage despite increasing the spacing of drawpoints at the weak zone. Beck Engineering predicted completion challenges brought about by the geometry of the pipe relative to the pipe boundary.

FLAC3D and cumulative underground results follow the same trend though the model underestimates the final result by at least 16% (Figure 6.1). The possible reasons for the variance in the underground vs the model results could be a combination of the fact that the presence of water as well as the effect of geological features was not included in the model. The cumulative total deformation variance in underground results is negligible and can be attributed to either the accuracy of the Scanner considering the use of point cloud as well as the shotcrete scaling that took place in between the scans and manual Distomats.

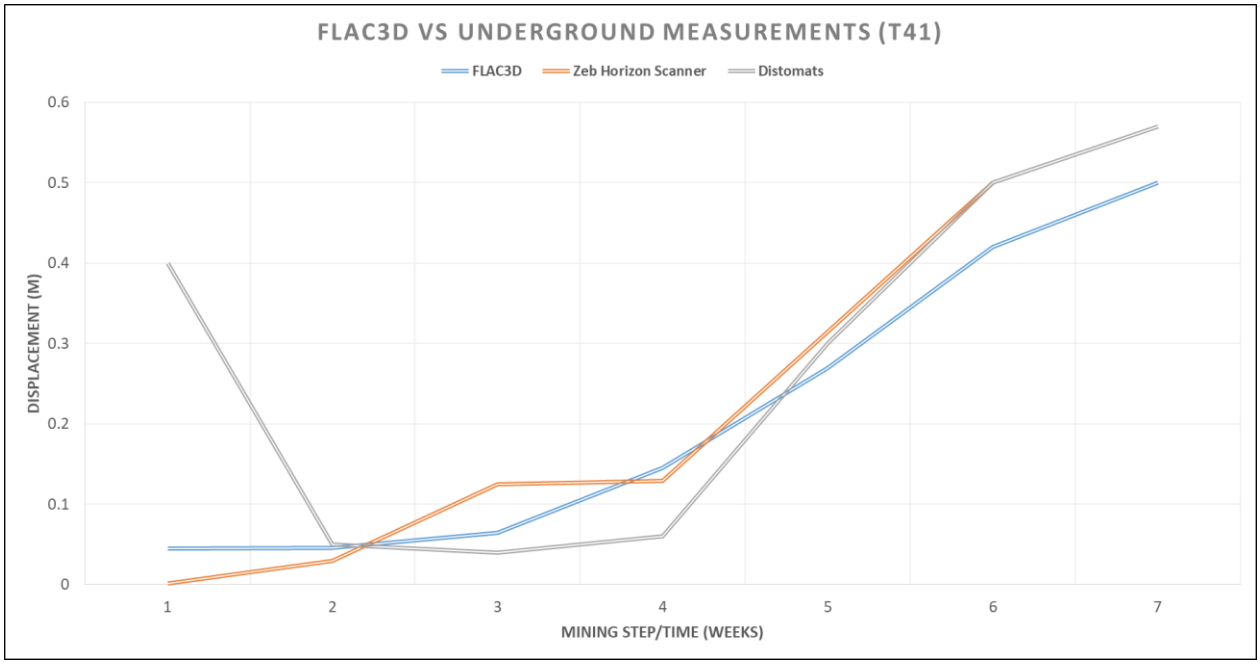


Figure 6.1: Deformation Results Comparing underground measurements and FLAC3D Results.

Block caving as a mining method comprises of complex mechanisms that contribute towards the overall stability and thus success of a block. It is important to understand each contributing factor, its limits and consequences should best practice not be followed. This is especially true at the C-Cut block. The increased drawpoint spacing meant to alleviate stability challenges at the weakzone, was the very factor that could have possibly contributed to the high deformation rates measured during the development of this area. This was evident through the drone footage which confirmed what Laubscher (1994) warned against. The initial struggles with adjacent drawpoints not connecting proved to have contributed significantly to the geotechnical challenges experience within the weak zone.

The possibility of recompaction after preconditioning in the weakzone was proven to be highly likely by the borehole camera holes drilled in the weakzone. The long period between preconditioning and the time the drawbells were opened and ready for production suggests that such compaction was entirely possible. It took more than 6 months, which is the maximum time suggested by the recompaction theory of a competent kimberlite (Tukker et al., 2016). This time frame could even be less for a weakzone especially in the presence of water.

The end stage construction of a block cave presents a phenomenon with high abutment stresses exerted on an already compromised pillar between the cave front and the kimberlite/waste rock contact zone. The existence of weak zones makes it even more difficult to maximise ore recovery in these areas.

7. CONCLUSION

In the introduction it was mentioned that one of the key objectives for a mining house is to maximise profit while doing so in a safe manner. The stability of underground workings is paramount to the existence of the mining industry. Unfortunately, this is not always achievable. Despite numerous attempts and recognisable dedication, localised rock mass failures occur. This type of failure occurred at CDM, hence the research was conducted to understand the drivers of the unstable conditions.

Block caving is a complex mining method. Often, when failure occurs it will be a combination of factors such as the influence of geological structures, presence of water, type of facies, cave management and sequencing of the undercut relative to the extraction horizon (effect of abutment stresses).

The literature review showed clearly that drawzone interaction cannot be compromised, as doing so can be detrimental to the overall business. The profitability of the block was affected as the ore was locked up in the region of the limit ellipsoid and not reporting to the ellipsoid of motion. Consequently, the material would therefore not report to the drawpoint. A detailed study is essential before changing layouts that are significantly different from those presented during a feasibility study.

The research aimed to evaluate drawzone interaction. The combined use of drone footage to assess the voids in the DB, the borehole camera to assess the possibility of recompaction, empirical methods and the detailed evaluation of the PC/BC model suggest that there was little to no drawzone

interaction in the region of the weak material. It is clear from the size of the interactive zone that once DP are spaced further than the limit suggested by empirical methods, instability may prevail. These empirical methods (Laubscher, 1994) suggest isolated drawzones once the spacing is increased from 16 m. The question of whether preconditioning was effective as a fracture initiation tool has not been properly investigated. It is highly likely that recompaction took place before the drawbells were completed.

From this study, it was found that high deformation rates occurred because of the geometry of the CDM pipe, the weak 1060 PG kimberlite and point loading from the uncaved material/ pillar directly above this zone. The result was total closure of the affected tunnels. Even more significant was the effect of the abutment stresses as the undercut mining front advanced towards the weak zone.

In the prediction model created by Beck Engineering (2016) the cave induced stresses in the NE corner (area of the 1060 PG kimberlite) were already high due to pipe geometry and a reducing pillar. In the FLAC3D model, additional induced stresses were observed due to the weak zone. The unstable area in the FLAC3D model followed the same trend as was measured underground, but the deformation in the model was slightly lower. At 75% undercutting, the extraction horizon production drifts (tunnels) proved to be taking excessive strain, which worsened once the crosscuts were developed. Very little time was available to rehabilitate the area. FLAC3D results showed that the abutment stresses far exceed the rock mass strength in the weak zone area. The closure from the FLAC3D model

and measurements underground imply that the major and minor apices took strain as the abutment stresses were approaching. Failure took place as soon as the crosscuts were developed, because of the decreased sizes of the pillars on the extraction horizon.

In an attempt to maintain stability, the spacings of DPs were increased. This decision was detrimental to stability because of the interactive draw requirement of block caving. The support strategy that was employed also proved to have some shortcomings. In hindsight, a sacrificial (secondary) initiation level (undercut) in the weak zone area may have worked to destress the actual undercut.

8. RECOMMENDATIONS

Too little was known about the existing weak zone at the site. It is recommended that a more comprehensive geotechnical evaluation should have been made at pre-feasibility stage. Where weak zones are found, a change in mining method should be considered, possibly with a change in the support strategy.

When a new block is planned, extensive and detailed geological/geotechnical studies need to be undertaken in an attempt to make informed decisions regarding longevity and success of a block.

9. SUGGESTIONS FOR FURTHER WORK

Future work following this research could focus on the following:

- The question of whether preconditioning is effective as a fracture initiation tool in this mining environment remains an interesting area of study. The effectiveness of preconditioning by blast, in environments where recompaction is prevalent, could be beneficial for future mining blocks.
- A more detailed numerical model that considers the effect of geological structures, as well as the presence of water, on closure in a weak Kimberlite may provide some useful information for future BC design.

REFERENCES

Anhaeusser, C.R. and Burger, A.J., 1982 An Interpretation of U-Pb Zircon ages for Archaean tonalitic Gneisses from the Johannesburg-Pretoria granite dome. Trans. Geol. Soc. S. Afr., Vol. 85, pp.111 - 116

Bartlett P.J, 1998, Planning a mechanised cave with coarse fragmentation in Kimberlite, *University of Pretoria*: Research output, pg. 15-25 https://repository.up.ac.za/handle/2263/51828 [Accessed: 02/10/2021]

Bartlett, P.J., 1998 Premier Mine. *Seventh International Kimberlite Conference* — Large Mines Field Excursion, Cape Town, 7IKC Organizing Committee, pp. 39–49.

Beck, D., 2009, Medium Term Stability and Deformation, Unpublished consulting report.

Beck, D., 2016, Assessment of stability of proposed designs for CCut Phase 1 and 2, Unpublished consulting report.

Brady, BHG. and Brown, ET., 2004, Rock Mechanics for Underground Mining, Rock Strength and Deformability, pp. 106, Kluwer Academic Publishers, Dordrecht.

Brown, E T., 2003, Block Caving Geomechanics, Undercutting Strategies, pp. 192-196, Julius Kruttschnitt Mineral Research Centre, The University of Queensland.

Butcher, R.J., 1999, Design Rules for Avoiding Draw Horizon Damage in Deep Level Block Caves, *The Journal of the South African Institute of Mining & Metallurgy,* vol.99, pp.151 - 156.

Butcher, R.J., 2000a, Block cave undercutting – aims, strategies, methods, and management. Proceedings MassMin 2000, Brisbane, (Ed: G Chitombo), *Australasian Institute of Mining and Metallurgy: Melbourne pp.* 405 - 411.

Castro, R. and Halim, A., 2008, Study of multiple drawzone interaction in block caving mines by means of a large 3D physical model, International Journal of Rock Mechanics and Mining Science, vol.45, pp.1044 – 1051.

Castro, R L., Vargas, R. and de la Huerta, F., 2012, Determination of Drawpoint Spacing in Panel Caving: A Case Study at The El Teniente Mine, *The Journal of The Southern African Institute of Mining and Metallurgy, vol. 112, pp.871 -876.*

Castro, R., Arancibia, L., Guzman, D. and Henriquez, J P., 2018, Experiments & Simulation of Gravity Flow in Block Caving through FlowSim, *Proceeding of the Fourth International Symposium on Block & Sublevel Caving, Australian Centre for Geomechanics, Perth, pp. 312 – 322.*

Castro, R., 2006, Study of the Mechanisms of Gravity Flow for Block Caving, *PhD thesis, The University of Queensland, Brisbane.*

Cordova, E., Gottreux, I., Anani A., Ferada, A., and Contreras J S., 2021 Blasting and preconditioning modelling in underground cave mines under

high stress conditions, *Journal of the Southern African Institute of Mining & Metallurgy*, Vol. 121 no. 2, pp. 71-80.

CDM, 2005, Cullinan Diamond Mine BA West & Decline, Study Report Phase 1, Mining Technical Report, Unpublished Archives.

CODE OF PRACTICE, 2019, Cullinan Diamond Mine Mandatory Code of Practice to Combat Rock mass Failure Accidents in Massive Mining Operations, Geological Setting, Vol. 13, pp. 10-13

Diering, T., 2000, PC-BC: A block cave design and draw control system, *Proceedings of MassMin 2000, Brisbane, October-November 2000*, ed. G Chitombo, AusIMM, Carlton, Victoria, Australia, pp. 469-484.

Drill & Blast Engineering team, 2021, Cullinan Diamond Mine, Drone Scan and Drill design, Email communication.

Ferjani, M., 2003, An investigation of the plug/funnel-flow model, Master's thesis, University of Minnesota.

Halim, A., 2006, Study of the Influence of interactive draw upon drawpoint spacing in block and sublevel caving mines (PhD Thesis), University of Queensland.

Hoek, E., and Brown ET, 1980, Empirical strength criterion for rock masses, Journal of the Geotechnical Engineering Division, Vol.106, pp 1013-1035

Hoek, E., 1994, Strength of rocks and rock masses, International Society for Rock Mechanics and Rock Engineering, Vol.2, pp 4-16.

Hoek, E., Brown ET, 2018, The Hoek-Brown failure criterion and GSI – 2018 edition, Journal of Rock Mechanics and Geotechnical Engineering, Vol.11, pp 445 – 463.

Hoek, E., Kaiser PK, Bawden WF, 1995, Support of underground excavations in hard rock, Rotterdam: AA, Balkema, pp 97 – 102

Hoek, E., Carranza-Torres, C., Corkum, B., 2002, Hoek-Brown failure Criterion – 2002 edition, *Proceedings of the 5th North American Rock Mechanics Symposium and the 17th Tunnelling Association of Canada Conference: NARMS-TAC 2002, Toronto, Ontario, Canada, 7-10 July 2002,* Vol.1, pp. 267 – 273.

Holder, A., Wolmarans, A., Mzimela, B., Beck, D., Tukker, H., Boshoff, P., Matoba, T., Phahla, T., 2020, A block cave construction process realigned to minimize the extent of predicted deformation within a weak mining zone, MassMin Proceedings.

Itasca Consulting Group, 2021, FLAC3D User-Guide Manual, Extrude Command. [Online] Available at: http://docs.itascacg.com/flac3d700/flac3d/docproject/source/elements/extrude/extrude.html [Accessed 29/10/2021]

Just, GD., 1981. The Significance of Material Flow in Mine Design and Production. Design and Operation of Caving and Sublevel Stoping Mines, 715-728. Society of Mining Engineers of AIME: New York.

Kvapil, R., 1992. Sublevel caving. *SME Mining Engineering Handbook, 2nd edition, (Ed: HL Hartman), 2: 1789-1814. Society for Mining, Metallurgy and Exploration: Littleton, Colorado.*

Labuz, JF. and Zang, A., 2012, Mohr-Coulomb Failure Criterion, International Society for Rock Mechanics and Rock Engineering, vol.45, pp 975 – 979.

Laubscher, D.H., 1994, Cave Mining - The State of the Art, the Journal of the Southern African Institute for Mining and Metallurgy, Vol.94, Pg.279 – 293.

Nedderman, R.M., 1995, The use of the kinematic model to predict the development of the stagnant zone boundary in the batch discharge of a bunker, Chemical Engineering Science, Vol. 50, pp. 959–965.

Phahla, T., 2021, Head of Geology – Cullinan Diamond Mine, Draw Control Analysis, Email Communication.

Pierce, M.E., 2010, A Model for Gravity Flow of Fragmented Rock in Block Caving Mines, *PhD Thesis, The University of Queensland*, pp7-9.

Richardson PM., 1981, Area of Draw influence and Drawpoint Spacing for Block Caving Mines, The American Institute of Mining, Metallurgy, and Petroleum Engineers

Rustan, A., 2000, Gravity Flow of Broken Rock – What is Known and Unknown. *Proceedings MassMin 2000, Brisbane, (Ed: G Chitombo), 557-567.* Australian Institute of Mining and Metallurgy: Melbourne

Saiang, D., Gwynn, X. and Marshall, N., 2014, Hoek-Brown vs Mohr-Coulomb – Results from a Three Dimensional Open-pit/Underground Interaction Model, SRK Consulting (UK)

Steward, C.A., Allman, A. and Hall, B.E., 2010, Block cave optimisation - a value-driven approach. In Potvin, Y., ed. Second International Symposium on Block and Sublevel Caving. Perth, Australia, 2010. *Australian Centre for Geomechanics.*

Tukker, H., Holder, A., Swarts, B., van Strijp, T. and Grobler, E., 2016, The CCUT block cave design for Cullinan Diamond Mine, Journal of the Southern African Institute of Mining and Metallurgy, Vol.116, pp. 715 - 722

Ugarte, E., Pourrahimian, Y. and Boisvert, JB., 2017, Determination of optimum drawpoint layout in block caving using sequential Gaussian simulation, *Underground Mining Technology, Sudbury, Canada.*

Van As, A., 2017, Investor Presentation, Oyu Tolgoi: Advancing value - creating options. [Online] Available at: Microsoft PowerPoint - Investor Presentation August 2017_1 Aug 2017 FINAL.pptx (q4cdn.com)

[Accessed: 27/11/2021]

Van As, A. and Van Hout, G.J., 2008, Implications of widely spaced drawpoints. MassMin2008. Proceedings of the 5th International Conference and Exhibition on Mass Mining, Schunnesson, H. and Nordlund, E. (eds.). Lulea University of Technology, Sweden. pp. 147-154.

Woo, KS., Eberhardt, E., Elmo, D. and Stead, D., 2013, Empirical Investigation & Characterization of Surface Subsidence related to Block Cave Mining, *International Journal or Rock Mechanics & Mining Sciences*, Volume 61, Pg. 31 - 42

APPENDICES

Appendix A.

Table A-1: Revenue locked up in the weak zone drawpoints

DPTS	STATUS	TLIMIT	Loaded	Total lost tons	AVR. GRD	CRTS
839036076	CLOSED	231192	8116	175072	41.69	72994.11
839036090	CLOSED	220294	16568	212629	35.84	76211.18
839041089	ClOSED	228677	7302	140255	58.49	82029.27
839041090	ClOSED	232082	7020	211316	38.52	81390.31
839041091	CLOSED	207502	23607	218197	29.45	64258.76
839041102	CLOSED	364340	14969	317297	49.09	155763.74
839041103	CLOSED	355244	12386	370356	35.79	132533.43
839041104	CLOSED	305970	38879	327966	30.45	99858.80
			TOT	**1 973 088**	**38.77**	**765 040**
			$\CRT	99$/C		
			R\$ EXCH	14.2		
			Total lost revenue in $	$ 84 154 356.20		
			Total lost revenue in R	ZAR 1 194 991 858		

Appendix B.

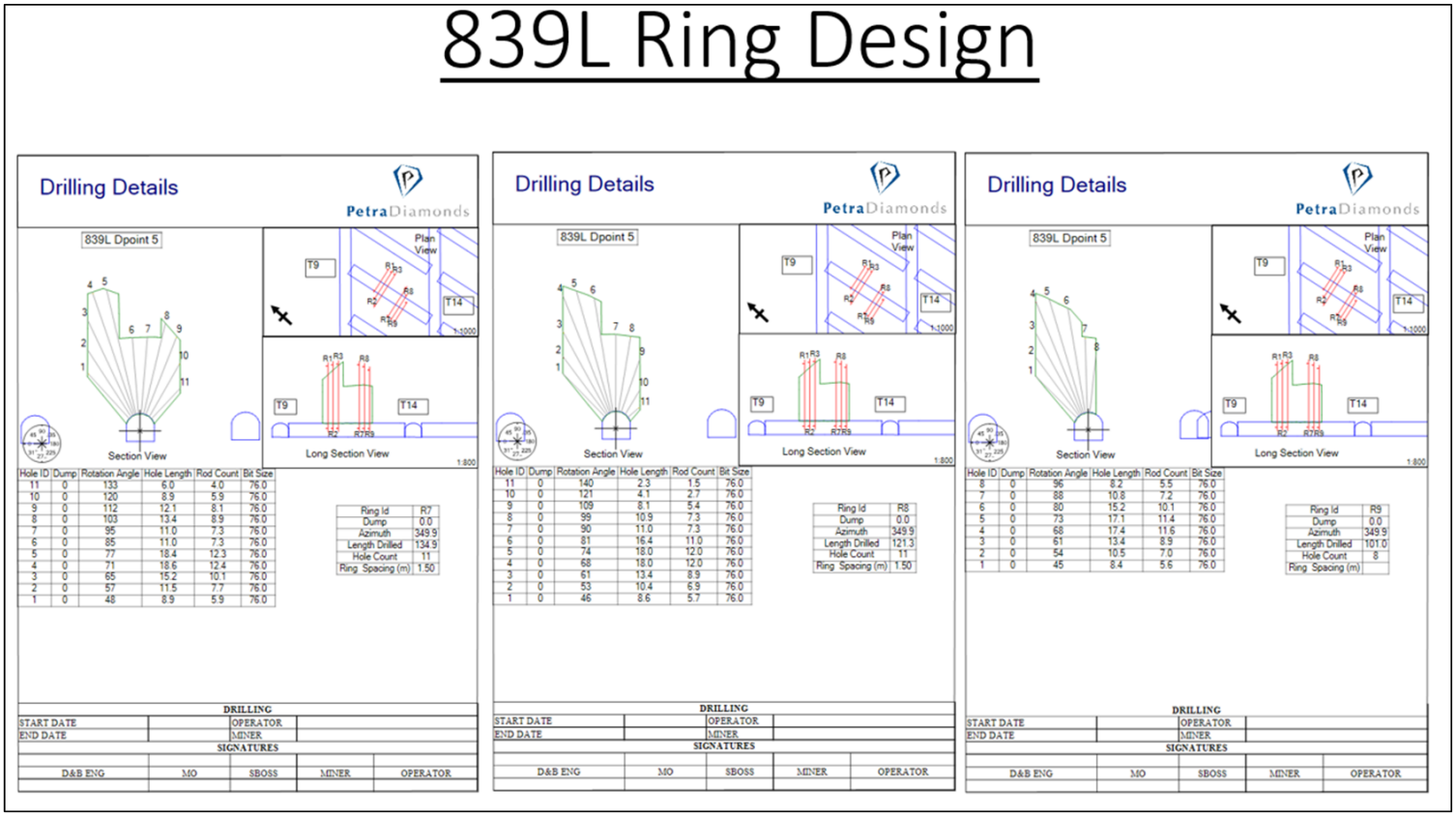


Figure B-1: Ring Designs for the extraction horizon weak zone

Appendix C.

Table C-1: Manual Laser technology results for T41

1060 Pale Grey Kimberlite Area | NB: Height is not a reliable measure

Tunnel	Position (Using Anchor Lines)	Week1		Week 3		Week 5		Week 7		Week 9		Week 11		Week 13		Week 15	
		Width	Height	Width	Height	Width	Height	Width	Height	Width	Height	Width	Height	Width	Height	Width	Height
41	L1	4.2	3.9	4.2	3.9	4.2	3.9	4.2	3.6	4.2	3.6	4.1	3.8	4.1	3.8	4.1	3.6
	L2	4	4.2	4	4.2	4.8	4.3	4.4	3.6	4.4	3.6	4.4	3.8	4.4	3.8	4.4	3.8
	L3	4	4.2	4	4.2	4	4.2	4.3	4.5	4.3	4.5	4	4.4	4	4.4	4	4.3
	L4	3.7	4.2	3.7	4.2	3.7	4.5	3.8	4.4	3.8	4.4	3.7	4.2	3.7	4.1	3.7	4.2
	L5	3.7	4.2	3.7	4.2	3.7	3.8	3.6	3.8	3.6	3.8	3.6	3.6	3.6	3.6	3.6	3.6
	L6	3.8	4.1	3.8	4.1	3.7	3.5	3.6	3.4	3.6	3.4	3.6	3.4	3.6	3.5	3.6	3.4
	L7	3.9	4	3.9	4	3.9	3.6	4.2	3.5	4.2	3.5	4.2	3.4	4.2	3.4	4.2	3.4
	L8	3.7	3.9	3.7	3.9	3.6	3.6	3.9	3.5	3.9	3.5	3.7	3.5	3.7	3.5	3.7	3.6
	L9	4.1	3.6	4.1	3.6	4.1	3.9	3.6	3.9	3.6	3.9	3.9	3.7	3.9	3.7	3.9	3.8
	L10	3.8	3.5	3.8	3.5	4	3.5	3.6	3.6	3.6	3.6	3.6	3.5	3.6	3.5	3.6	3.8
	L11	3.5	3.2	3.5	3.2	3.4	3.5	3.4	3.6	3.4	3.6	3.4	3.2	3.4	3.2	3.4	3.7
	L12	3.5	3.2	3.5	3.2	3.7	3.5	3.7	3.7	3.7	3.7	3.6	3.5	3.6	3.5	3.6	3.7
	L13	3.7	3.4	3.7	3.4	4	3.9	4.1	3.7	4.1	3.7	4	3.5	4	3.5	4	3.5
	L14	3.9	3.5	3.9	3.5	3.5	3.5	3.9	3.7	3.9	3.7	3.8	3.5	3.8	3.5	3.8	3.5
	L15	3.9	3.5	3.9	3.5	3.8	3.8	3.5	3.5	3.5	3.5	3.5	3.2	3.5	3.3	3.5	3.2
	L16	3.9	3.6	3.9	3.6	3.7	4	3.9	3.6	3.9	3.6	3.8	3.3	3.8	3.5	3.8	3.3
	L17	3.9	3.6	3.9	3.6	3.8	4.7	3.7	3.8	3.7	3.8	3.7	4.1	3.7	4.1	3.7	4.1
	L18	3.9	3.7	3.9	3.7	3.7	5.1	3.7	4.3	3.7	4.3	3.7	3.9	3.7	3.9	3.7	3.9
	L19	3.9	3.7	3.9	3.7	4.2	5	3.8	4.4	3.8	4.4	3.7	4.3	3.7	4.3	3.7	4.3
	L20	3.9	3.7	3.9	3.7	3.9	4.9	4.2	4.7	4.2	4.7	4.1	4.6	4.1	4.6	4.1	4.6
	L21	3.9	3.8	3.9	3.8	3.9	4.7	3.9	4.3	3.9	4.3	3.8	4.5	3.8	4.5	3.8	4.5
	L22	3.9	3.8	3.9	3.8	3.7	4.3	3.9	4.4	3.9	4.4	3.8	4.5	3.8	4.5	3.8	4.5
	L23	3.9	3.8	3.9	3.8	4	3.9	3.9	4.3	3.9	4.3	3.7	4.2	3.7	4.2	3.7	4.2
	L24	3.9	3.8	3.9	3.8	3.8	3.8	4.1	3.9	4.1	3.9	3.9	3.8	3.9	3.8	3.9	3.8
	L25	3.9	3.9	3.9	3.9	3.8	3.8	3.8	3.6	3.8	3.6	3.7	3.6	3.7	3.6	3.7	3.6
	L26	3.9	3.8	3.9	3.8	3.7	3.9	3.6	3.9	3.6	3.9	3.6	3.5	3.6	3.5	3.6	3.5
	L27	3.7	3.8	3.7	3.8	3.7	3.8	3.6	3.7	3.6	3.7	3.5	3.6	3.4	3.6	3.4	3.6
	L28	3.3	3.8	3.3	3.8	3.3	3.5	3.2	3.7	3.1	3.5	3.1	3.4	3.1	3.4	2.9	3.4
	L29	3.3	3.7	3.3	3.7	3.3	3.7	3.2	3.5	3.2	3.4	3.2	3.4	3.2	3.4	3.1	3.4
	L30	3.4	3.6	3.4	3.6	3.4	3.6	3.4	3.6	3.4	3.7	3.3	3.5	3.3	3.5	3	3.5
	L31	3.5	3.3	3.4	3.3	3.2	3.6	3.2	3.5	3.1	3.7	3	3.6	3	3.6	2.9	3.6
	L32	3.4	3.1	3.3	3.1	3.2	3.6	3.2	3.5	3	3.3	2.9	3.3	2.9	3.3	2.9	3.3
	L33	3.5	3	3.5	3	3.4	3.6	3.3	3.2	3	3.2	3	3.2	3	3.2	2.8	3.2
	L34	3	2.9	3	2.9	2.9	3.6	2.9	3.4	2.9	3.3	2.9	3.3	2.9	3.3	2.9	3.3
	L35	3.1	3.3	3.1	3.3	3.1	3.6	3	3.6	3	3.6	3	3.6	3	3.6	2.8	3.6
	L36	3.1	3.5	3.1	3.5	3.1	3.7	3.1	3.6	3	3.6	3	3.4	3	3.4	2.9	3.4
	L37	3.4	3.8	3.4	3.8	3.4	3.8	3.4	3.9	3.4	3.4	3.4	3.4	3.4	3.4	3.1	3.2
	L38	3.6	3.9	3.6	3.9	3.6	3.9	3.5	3.7	3.5	3.7	3.5	3.5	3.5	3.5	3.4	3.5

Table C-2: Manual Laser technology cumulative results for T41

Week 1	Week 3	Week 5	Week 7	Week 9	Week 11	Week 13	Week 15	Cumulative
0.3	0	0	0.1	0	0.1	0.1	0	0.6417
0.7	0	0	0.1	0.1	0	0	0.2	0.6583
0.7	0	0	0.1	0	0	0	0.1	0.7000
0.6	0	0	0	0	0.1	0	0.3	0.7500
0.5	0.1	0.2	0	0.1	0.1	0	0.1	0.8167
0.6	0.1	0.1	0	0.2	0.1	0	0	0.8500
0.5	0	0.1	0.1	0.3	0	0	0.2	0.8583
1	0	0.1	0	0	0	0	0	0.9917
0.9	0	0	0.1	0	0	0	0.2	
0.9	0	0	0	0.1	0	0	0.1	
0.6	0	0	0	0	0	0	0.3	
0.4	0	0	0.1	0	0	0	0.1	
0.0257	**0.0167**	**0.0417**	**0.0500**	**0.0667**	**0.0333**	**0.0083**	**0.1333**	**0.9917**

Table C-3: Manual Laser technology results for T36

Tunnel	Position	Week 1		Week 3		Week 5		Week 7		Week 9		Week 11		Week 13		Week 15	
		Width	Height	Width	Height	Width	Height	Width	Height	Width	Height	Width	Height	Width	Height	Width	Height
T36	R92 T37	3.6	4	3.6	4	3.5	4	3.5	3.6	3.5	3.4	3.5	3.8	3.3	3.8	3.1	3.8
	R93 T37	4.1	4.1	4	4.1	4.1	4.1	4.1	3.6	4	4.1	4	4.1	3.7	4.1	3.4	4.1
	R94 T37	4.2	4.2	4.1	4.2	4	4.2	4	3.8	3.9	3.9	3.9	3.9	3.8	3.9	3.5	3.9
	R95 T37	4	4	4	4	3.9	4	3.8	3.8	3.8	3.6	3.6	4	3.1	4	3	4
	R96 T37	4	4	3.9	4	4	4	4	3.4	4	3.4	4	3.7	3.8	3.7	3.6	3.7
	R97 T37	3.7	4	3.6	4	3.6	4	3.5	3.4	3.5	3.4	3.5	3.6	3.2	3.6	3	3.6
	R98	4	4	4	4	3.9	4	3.9	3.6	3.7	3.8	3.7	3.8	3.2	3.8	2.9	3.8
	R99	4	4	4	4	3.9	4	3.8	3.8	3.8	4.1	3.7	3.6	3	3.6	2.8	3.6
	R100 T37	3.9	3.3	3.8	3.3	3.8	3.9	3.8	3.7	3.8	3.8	3.7	3.5	3.6	3.5	3	3.5
	R101 T37	3.5	3.1	3.5	3.1	3.4	3.1	3.4	3.6	3.4	3.6	3.4	3.7	3.1	3.7	2.9	3.7
	R102 T37	3.3	3.3	3.3	3.3	3.3	3.3	3.3	3.9	3.3	3.9	3.2	3.9	3.1	3.9	2.8	3.9
	R103 T37	3.4	3.6	3.3	3.6	3.3	3.5	3.3	4.2	3.3	4.1	3.2	3.8	3.2	3.8	2.8	3.8
	R104 T37	3.9	3.5	3.8	3.5	3.7	3.5	3.7	3.8	3.5	3.8	3.5	3.8	3.3	3.8	2.9	3.8
	R105 T37	3.9	3.5	3.8	3.5	3.7	3.7	3.7	3.4	3.7	3.4	3.6	3.7	3.4	3.7	3	3.7
	R106 T37	3.9	3.5	3.8	3.5	3.7	3.9	3.6	3.9	3.6	3.9	3.6	3.5	3.5	3.5	2.8	3.5
	R107 T37	3.7	3.5	3.7	3.5	3.7	3.5	3.7	3.7	3.7	3.4	3.6	3.7	3.1	3.7	2.7	3.7
	R108 T37	3.7	3.5	3.7	3.5	3.6	3.5	3.6	3.7	3.6	3.4	3.5	3.4	3	3.4	2.7	3.4
	R109 T37	3.6	3.5	3.6	3.5	3.6	3.5	3.6	3.5	3.6	3.5	3.6	3.5	2.9	3.5	2.6	3.5
	R110 T37	3.8	3.8	3.7	3.8	3.6	3.7	3.6	4	3.5	4.1	3.5	4	3.4	4	2.9	4

Table C-4: Manual Laser technology cumulative results for T36

Week 1	Week 3	Week 5	Week 7	Week 9	Week 11	Week 13	Week 15	Cumulative
0.6	0	0.1	0	0	0	0.2	0.2	0.4
0.1	0.1	-0.1	0	0.1	0	0.3	0.3	0.45263158
0	0.1	0.1	0	0.1	0	0.1	0.3	0.5
0.2	0	0.1	0.1	0	0.2	0.5	0.1	0.52105263
0.2	0.1	-0.1	0	0	0	0.2	0.2	0.55789474
0.5	0.1	0	0.1	0	0	0.3	0.2	0.59473684
0.2	0	0.1	0	0.2	0	0.5	0.3	0.64210526
0.2	0	0.1	0.1	0	0.1	0.7	0.2	0.93684211
0.3	0.1	0	0	0	0.1	0.1	0.6	1.26842105
0.7	0	0.1	0	0	0	0.3	0.2	
0.9	0	0	0	0	0.1	0.1	0.3	
0.8	0.1	0	0	0	0.1	0	0.4	
0.3	0.1	0.1	0	0.2	0	0.2	0.4	
0.3	0.1	0.1	0	0	0.1	0.2	0.4	
0.3	0.1	0.1	0.1	0	0	0.1	0.7	
0.5	0	0	0	0	0.1	0.5	0.4	
0.5	0	0.1	0	0	0.1	0.5	0.3	
0.6	0	0	0	0	0	0.7	0.3	
0.4	0.1	0.1	0	0.1	0	0.1	0.5	
0.4	0.052632	0.047368	0.021053	0.036842	0.047368	0.294737	0.331579	1.268

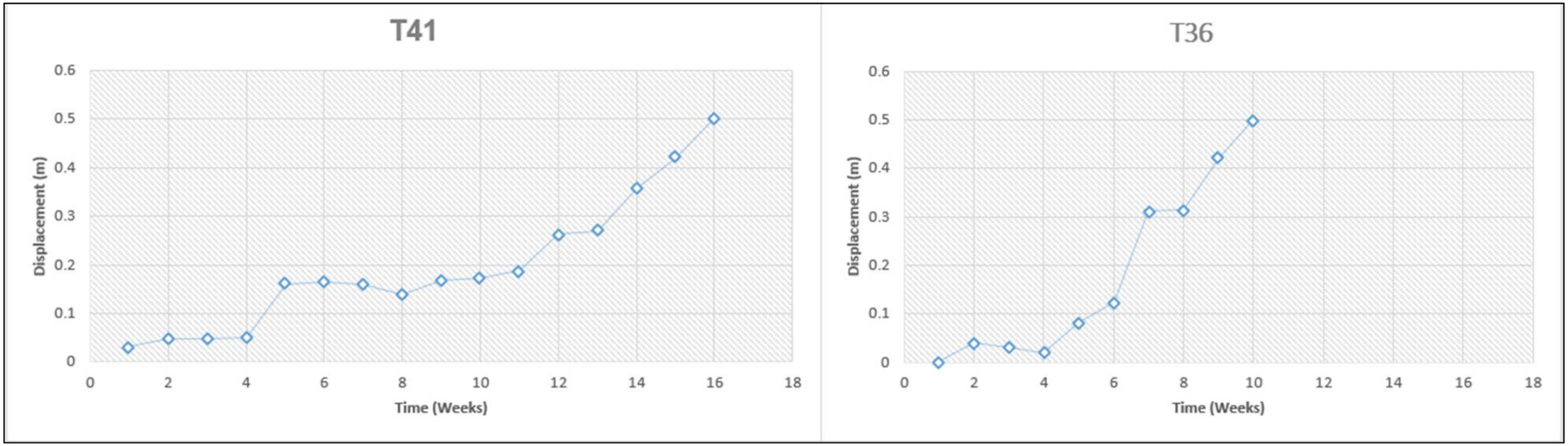


Figure C-1: Scan Results for Individual Tunnels

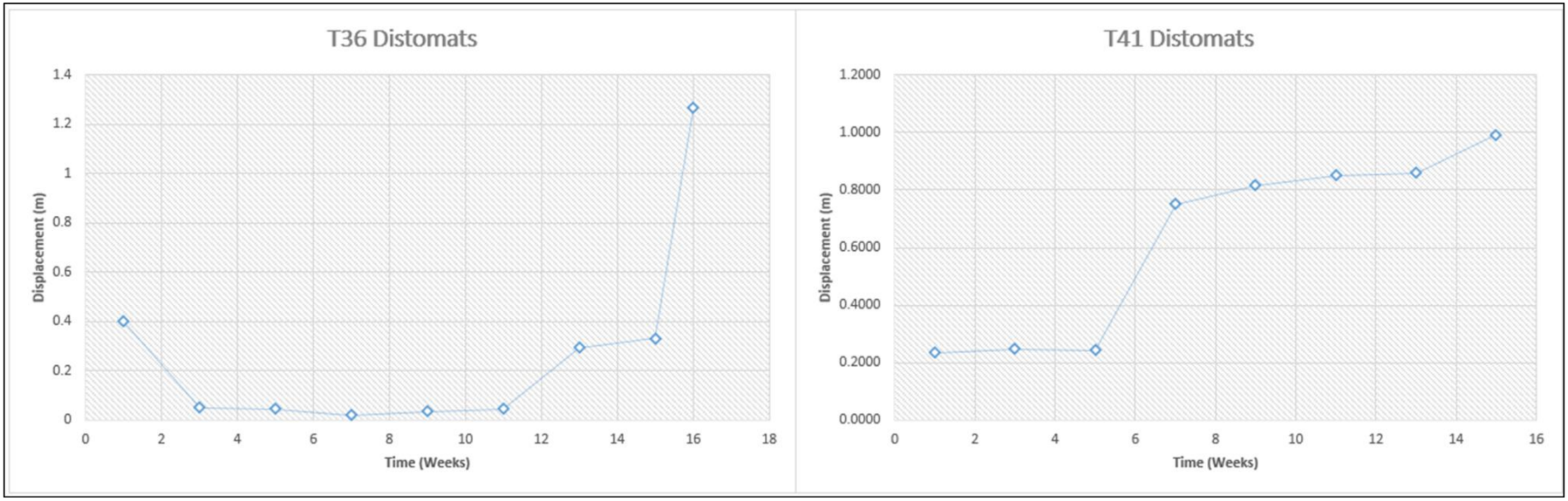


Figure C-2: Laser technology results for individual tunnels

Appendix D.

Table D-1: CDM RMR Database

				CDM Rock Mass Rating											
				D	A	B	E	F	G	H	I	J			
Level	Access	Tunnel	DP	Blasting Practice	No. of Joint Sets	Joint Spacing	Joint Dip	Joint Orientation	Roughness & Planarity	Infilling	Water	Major Structures (sills/faults/shear zone/ dyke/bedding planes etc)	Result	RMR	
				P Banjwa											
824	North	37	0	b Avarage drill&blast	c (2)	e (<0.1 m)	a (60-90 deg)	c (Oblique to face)	b (smooth)	b (<1 mm)	a (dry)	a (none)	54,4	poor	
824	North	35	0	b Avarage drill&blast	c (2)	c (0.5-1 m)	b (45-60 deg)	b (Dip into drive face)	b (smooth)	b (<1 mm)	a (dry)	b (perpendicular)	40,4	very poor	
824	North	40	0	a Smoot wall blasting	c (2)	e (<0.1 m)	a (60-90 deg)	c (Oblique to face)	b (smooth)	b (<1 mm)	a (dry)	a (none)	48,3	very poor	
824	North	42	0	b Avarage drill&blast	d (3)	c (0.5-1 m)	d (<25 deg)	c (Oblique to face)	a (rough)	d (3-5 mm)	a (dry)	a (none)	37,5	very poor	
824	North	40	0	a Smoot wall blasting	c (2)	c (0.5-1 m)	a (60-90 deg)	b (Dip into drive face)	b (smooth)	c (1-3 mm)	a (dry)	b (perpendicular)	41,1	very poor	
824	North	45	0	b Avarage drill&blast	d (3)	c (0.5-1 m)	c (25-45 deg)	b (Dip into drive face)	b (smooth)	d (3-5 mm)	a (dry)	b (perpendicular)	31,4	very poor	
824	North	37	0	c Poor drill&blast	c (2)	c (0.5-1 m)	c (25-45 deg)	b (Dip into drive face)	b (smooth)	d (3-5 mm)	a (dry)	a (none)	31,9	very poor	
824	North	40	0	b Avarage drill&blast	b (1)	b (1-2 m)	a (60-90 deg)	a (Dip out of drive face)	b (smooth)	c (1-3 mm)	a (dry)	a (none)	53,7	poor	
839	North	41	0	b Avarage drill&blast	c (2)	e (<0.1 m)	a (60-90 deg)	b (Dip into drive face)	b (smooth)	d (3-5 mm)	a (dry)	a (none)	36,2	very poor	
839	North	36	0	a Smoot wall blasting	d (3)	d (0.1-0.5 m)	a (60-90 deg)	b (Dip into drive face)	b (smooth)	c (1-3 mm)	c (dripping)	b (perpendicular)	30,9	very poor	
839	North	36	0	a Smoot wall blasting	b (1)	e (<0.1 m)	a (60-90 deg)	b (Dip into drive face)	b (smooth)	b (<1 mm)	a (dry)	c (oblique)	41,8	very poor	
839	North	41	0	c Poor drill&blast	d (3)	c (0.5-1 m)	a (60-90 deg)	b (Dip into drive face)	a (rough)	a (none)	a (dry)	a (none)	49,4	very poor	
839	North	36	0	c Poor drill&blast	c (2)	b (1-2 m)	a (60-90 deg)	a (Dip out of drive face)	a (rough)	c (1-3 mm)	a (dry)	a (none)	52,1	poor	
839	North	36	0	b Avarage drill&blast	d (3)	c (0.5-1 m)	a (60-90 deg)	b (Dip into drive face)	a (rough)	d (3-5 mm)	a (dry)	c (oblique)	35,4	very poor	
839	North	32	0	c Poor drill&blast	e (4)	e (<0.1 m)	a (60-90 deg)	b (Dip into drive face)	b (smooth)	b (<1 mm)	a (dry)	a (none)	34,2	very poor	
839	North	32	0	b Avarage drill&blast	e (4)	e (<0.1 m)	a (60-90 deg)	b (Dip into drive face)	b (smooth)	b (<1 mm)	a (dry)	a (none)	38,5	very poor	
839	North	41	0	c Poor drill&blast	d (3)	d (0.1-0.5 m)	b (45-60 deg)	b (Dip into drive face)	b (smooth)	b (<1 mm)	a (dry)	c (oblique)	31,9	very poor	
839	North	32	0	c Poor drill&blast	e (4)	d (0.1-0.5 m)	d (<25 deg)	b (Dip into drive face)	a (rough)	b (<1 mm)	a (dry)	a (none)	35,1	very poor	
839	North	36	0	c Poor drill&blast	d (3)	b (1-2 m)	a (60-90 deg)	b (Dip into drive face)	a (rough)	e (5-10 mm)	a (dry)	a (none)	32,9	very poor	
839	North	36	0	a Smoot wall blasting	c (2)	d (0.1-0.5 m)	a (60-90 deg)	a (Dip out of drive face)	b (smooth)	c (1-3 mm)	a (dry)	c (oblique)	46,9	very poor	
839	North	36	0	a Smoot wall blasting	d (3)	c (0.5-1 m)	a (60-90 deg)	b (Dip into drive face)	a (rough)	d (3-5 mm)	a (dry)	c (oblique)	39,4	very poor	
839	North	41	0	b Avarage drill&blast	b (1)	e (<0.1 m)	a (60-90 deg)	b (Dip into drive face)	b (smooth)	b (<1 mm)	a (dry)	a (none)	44,3	very poor	
839	North	32	0	b Avarage drill&blast	c (2)	c (0.5-1 m)	b (45-60 deg)	b (Dip into drive face)	b (smooth)	d (3-5 mm)	a (dry)	b (perpendicular)	33,7	very poor	
839	North	41	0	b Avarage drill&blast	b (1)	e (<0.1 m)	a (60-90 deg)	b (Dip into drive face)	b (smooth)	b (<1 mm)	a (dry)	b (perpendicular)	39,8	very poor	
839	North	32	0	c Poor drill&blast	c (2)	e (<0.1 m)	a (60-90 deg)	b (Dip into drive face)	b (smooth)	b (<1 mm)	a (dry)	b (perpendicular)	34,8	very poor	
839	North	32	0	a Smoot wall blasting	e (4)	d (0.1-0.5 m)	a (60-90 deg)	b (Dip into drive face)	b (smooth)	c (1-3 mm)	a (dry)	a (none)	39,1	very poor	
839	North	41	0	c Poor drill&blast	d (3)	c (0.5-1 m)	a (60-90 deg)	a (Dip out of drive face)	b (smooth)	b (<1 mm)	a (dry)	a (none)	50,0	poor	

Appendix E.



Figure E-1: Presence of water at the weak zone

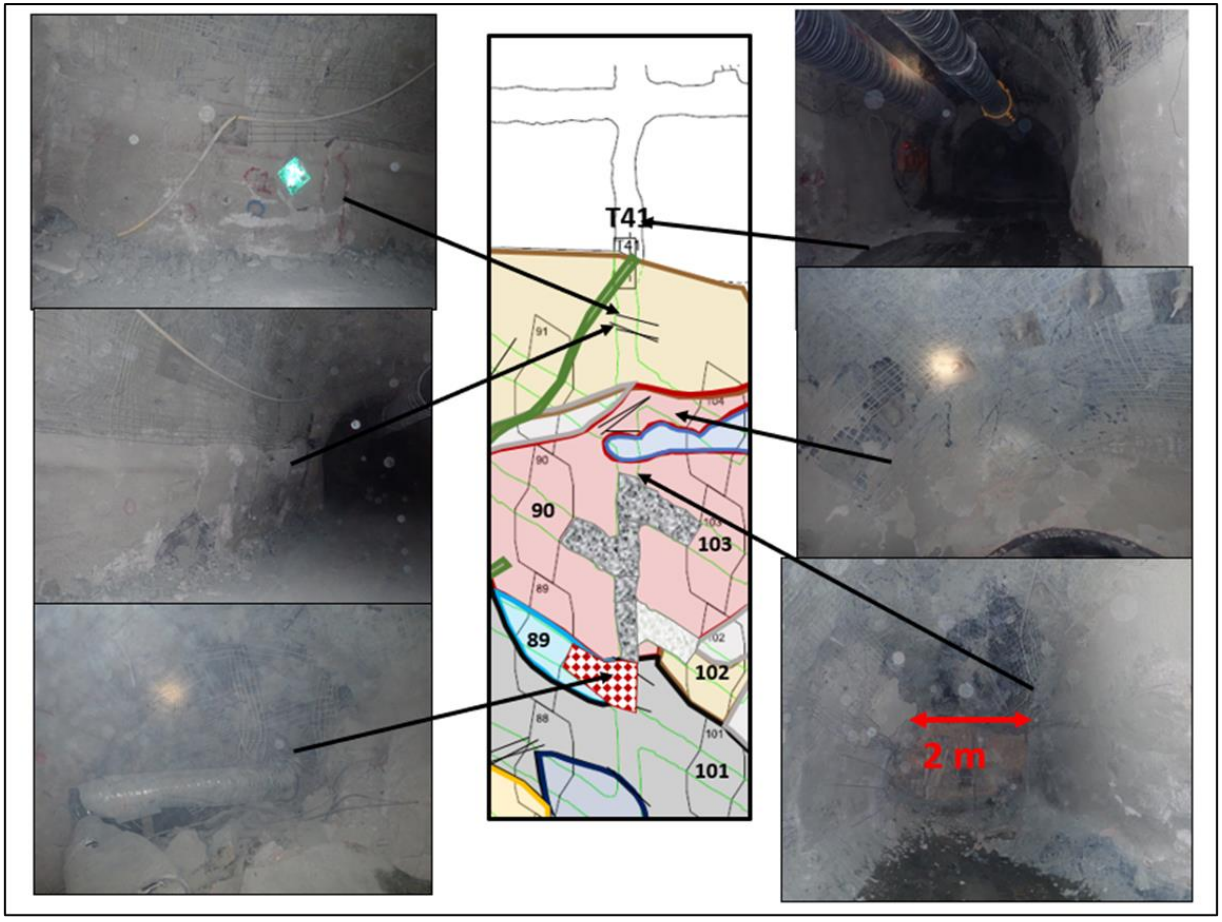


Figure E-2:Tunnel conditions showing extensive localized closure

Appendix F. Beck Engineering Input Parameters as used in the Regional Geotechnical Model.

Table F-1 : Grey Kimberlite

Material Name	Comment
GREY	*from Bartlett paper*

Elastic Properties	*E [Pa]*	*ν*
	1.60E+10	0.27

Density	*ρ [kg/m3]*
	2700

LR Model	Shape	*K [0.778-1]*
Drucker Prager		1

Variables	Delete Flag
14	10

Bulk Material			
Friction Angle [Deg]	*Cohesion Pa*	*Plastic Strain*	*Dilation (constant)*
35.2	1.40E+06	0	10
35.2	1.40E+06	0.005	
32.4	1.05E+06	0.02	

Joint	NOT USED	
Friction Angle [Deg]	*Cohesion Yield [MPa]*	*Dilation Angle [Deg]*
~~15.0~~	~~1.00E+11~~	~~8.0~~
Orientation (normal vector)		
~~[0,0,1]~~		

Fill		
E [Pa]	*ν*	*Ratio*
1.00E+08	0.25	1.0
Friction Angle [Deg]	*Cohesion Yield [MPa]*	*Plastic Strain*
30.0	1.00E+10	0

Cave
Stiffness
0.0001

Equivalent Mohr Coulomb Parameters			
	Friction Angle [Deg]	*Cohesion Yield [MPa]*	*Dilation Angle [Deg]*
Peak			
Residual			

Table F-2 : Brown Kimberlite

Material Name	Comment
BROWN	*from 2006 MC*

Elastic Properties	*E [Pa]*	*ν*
	2.40E+10	0.21

Density	*ρ [kg/m3]*
	2700

LR Model	Shape	*K [0.778-1]*
Drucker Prager		1

Variables	Delete Flag
14	10

Bulk Material			
Friction Angle [Deg]	*Cohesion Pa*	*Plastic Strain*	*Dilation (constant)*
35.2	1.60E+06	0	10
35.2	1.60E+06	0.005	
32.4	1.28E+06	0.02	

Joint	NOT USED	
Friction Angle [Deg]	*Cohesion Yield [MPa]*	*Dilation Angle [Deg]*
~~15.0~~	~~1.00E+11~~	~~8.0~~
Orientation (normal vector)		
~~[0,0,1]~~		

Fill		
E [Pa]	*ν*	*Ratio*
1.00E+08	0.25	1.0
Friction Angle [Deg]	*Cohesion Yield [MPa]*	*Plastic Strain*
30.0	1.00E+10	0

Cave
Stiffness
0.0001

Equivalent Mohr Coulomb Parameters			
	Friction Angle [Deg]	*Cohesion Yield [MPa]*	*Dilation Angle [Deg]*
Peak			
Residual			

Table F-3 : Metasediment Host Rock

Material Name	Comment
VOLCANIC	*from 2006 MC*

Elastic Properties	*E [Pa]*	*ν*
	3.20E+10	0.26

Density	*ρ [kg/m3]*
	2900

LR Model	Shape	*K [0.778-1]*
Drucker Prager		1

Variables	Delete Flag
14	10

Bulk Material			
Friction Angle [Deg]	*Cohesion Pa*	*Plastic Strain*	*Dilation (constant)*
44	2.46E+06	0	12
44	2.46E+06	0.005	
40	2.12E+06	0.01	

Joint	NOT USED	
Friction Angle [Deg]	*Cohesion Yield [MPa]*	*Dilation Angle [Deg]*
~~15.0~~	~~1.00E+11~~	~~8.0~~
Orientation (normal vector)		
~~{0,0,1}~~		

Fill		
E [Pa]	*ν*	*Ratio*
1.00E+08	0.25	1.0
Friction Angle [Deg]	*Cohesion Yield [MPa]*	*Plastic Strain*
30.0	1.00E+10	0

Cave
Stiffness
0.0001

Equivalent Mohr Coulomb Parameters			
	Friction Angle [Deg]	*Cohesion Yield [MPa]*	*Dilation Angle [Deg]*
Peak			
Residual			

Table F-4: Black Kimberlite

Material Name	Comment
BLACK	*from 2006 MC*

Elastic Properties	*E [Pa]*	*ν*
	3.00E+10	0.21

Density	*ρ [kg/m3]*
	2700

LR Model	Shape	*K [0.778-1]*
Drucker Prager		1

Variables	Delete Flag
14	10

Bulk Material			
Friction Angle [Deg]	*Cohesion Pa*	*Plastic Strain*	*Dilation (constant)*
37.1	1.90E+06	0	10
37.1	1.90E+06	0.005	
34.8	1.52E+06	0.02	

Joint	NOT USED	
Friction Angle [Deg]	*Cohesion Yield [MPa]*	*Dilation Angle [Deg]*
~~15.0~~	~~1.00E+11~~	~~8.0~~
Orientation (normal vector)		
~~[0,0,1]~~		

Fill		
E [Pa]	*ν*	*Ratio*
1.00E+08	0.25	1.0
Friction Angle [Deg]	*Cohesion Yield [MPa]*	*Plastic Strain*
30.0	1.00E+10	0

Cave
Stiffness
0.0001

Equivalent Mohr Coulomb Parameters			
	Friction Angle [Deg]	*Cohesion Yield [MPa]*	*Dilation Angle [Deg]*
Peak			
Residual			